DOE/BC/15190-3
(OSTI ID: 800797)

FOSSIL ENERGY

3-D RESERVOIR AND STOCHASTIC FRACTURE NETWORK MODELING FOR ENHANCED OIL RECOVERY, CIRCLE RIDGE PHOSPHORIA/TENSLEEP RESERVOIR, WIND RIVER RESERVATION, ARAPAHO AND SHOSHONE TRIBES, WYOMING

Semi-Annual Report
May 1, 2001-November 30, 2001

By:
Paul R. La Pointe[1]
Robert Parney[1]
Thorsten Eiben[1]
Mike Dunleavy[2]
John Whitney[3]
Darrel Eubanks[3]

Date Published: September 2002

Work Performed Under Contract No. DE-FG26-00BC15190

Golder Associates, Inc.
Redmond, Washington

National Energy Technology Laboratory
National Petroleum Technology Office
U.S. DEPARTMENT OF ENERGY
Tulsa, Oklahoma

DOE/BC/15190-3
Distribution Category UC-122

3-D Reservoir and Stochastic Fracture Network Modeling for Enhanced Oil Recovery, Circle Ridge Phosphoria/Tensleep Reservoir, Wind River Reservation, Arapaho and Shoshone Tribes, Wyoming

By
Paul R. La Pointe[1]
Robert Parney[1]
Thorsten Eiben[1]
Mike Dunleavy[2]
John Whitney[3]
Darrel Eubanks[3]

September 2002

Work Performed Under DE-FG26-00BC15190

Prepared for
U.S. Department of Energy
Assistant Secretary for Fossil Energy

Virginia Weyland, Project Manager
U.S. Department of Energy
National Energy Technology Laboratory
National Petroleum Technology Office
One West Third Street, Suite 1400
Tulsa, OK 74103

Prepared by
[1]Golder Associates Inc.
18300 NE Union Hill Road, Suite 200
Redmond, WA 98052

[2]Marathon Oil Company
Rocky Mountain Region
1501 Stampede Ave.
Cody, WY 82414

[3]Marathon Oil Company
5555 San Felipe
Houston, TX 77056

Table of Contents

1 INTRODUCTION 1
2 EXPERIMENTAL WORK 5
2.1 Overview 5
2.2 Experimental Techniques for Analysis of Subsurface Well Data 5
2.2.1 Fracture Image Logs 5
2.2.2 Dynamic Flow Logs 5
2.2.3 Single Well Pressure Build-Up or Fall Off Tests 6
2.2.4 Injected Tracer Studies 6
2.2.5 Analysis of Well Tests Using DFN Models 6
2.3 Experimental Techniques For Comparison of Strain Values Calculated from 3D Palinspastic Reconstruction with Fracture Orientations and Intensity in Outcrop 8
2.4 Experimental Techniques for Validation of DFN Model Geometry and Connectivity Using Subsurface Fracture Geometry and Flow Data 11
2.5 Integration of the Matrix and Fault Block Architecture into a Single Numerical Reservoir Model 12
2.6 Plans To Acquire Remaining Subsurface Flow And Fracture Data 13
2.6.1 Tracer Testing 13
2.6.2 FMI and Spinner Logging 13
2.6.3 Falloff and Multi-well Interference Testing: 13
3 RESULTS AND DISCUSSION 15
3.1 Overview 15
3.2 Task 2.6 – Generation of the DFN Model 15
3.2.1 Purpose of Task 15
3.2.2 Results of Comparison 16
3.3 Task 3.1 – DFN Flow Model Validation 27
3.3.2 Purpose Of Task 27
3.3.3 Comparison of Fracture Orientations and Intensity With Image Log Data 28
3.3.4 Derivation of Fracture Flow Parameter Values From Well Tests 36
3.3.5 High Resolution Injection Profile, Shoshone 65-37 49
3.3.6 Single Well Pressure Transient Testing 49
3.3.7 Comparison af Tracer Tests and Fracture Network Connectivity 51
3.4 Task 3.2 – Fault Block and Matrix Model Development 55
3.4.1 input data 55
3.5 Task 5.1 – Project Web Site 59
3.5.1 Web Site Development 59
3.5.2 Web Site Statistics 61
3.6 Marathons Contribution to this project to Date 62
4 CONCLUSIONS 63
4.1 Overview 63
4.2 Structural Controls on Reservoir Fracture Pattern 63
4.3 Validation of DFN Model 63
4.4 Determination of Properties for DFN Model 64
4.5 Construction of Integrated Matrix/Fault-Block/Fracture Model 64
REFERENCES 65

List of Graphical Materials

Figure 1-1. Horizontal map view of structural blocks defined for the Phosphoria Formation. Block definitions are very similar for the Tensleep Formation. 2
Figure 1-2. Stratigraphic column for the Circle Ridge Field (from Smith 2000). 3
Figure 2-1. Scanline used to measured fractures. Outcrop is of the Triassic Red Peak Member of the Chugwater Formation. 9
Figure 3-1. Map of principal extensional strain magnitude produced by folding. The contour map shows the approximate horizontal limits of the fault blocks used in the reconstruction. The location of the eleven scanline sites are shown on the map. The strains shown have been mapped on the present-day structural configuration of the Circle Ridge Field, and represent deformation in the Tensleep Formation. 17
Figure 3-2. Fracture orientations measured at scanlines 6 (red circle) and 5 (black circle). Black lines indicate trend of principal extension. Lines lengths are proportional to the magnitude of extension. 18
Figure 3-3. Plunge of principal direction of extension (contours) and trend of maximum extension direction. Plunge at Scanline 6 (red circle) is about 50^{o} to the northeast. Plunge at Scanline 5 (black circle) is similar. Black lines indicate trend of principal extension. Lines lengths are proportional to the magnitude of extension. 19
Figure 3-4. Comparison of extensional strain and fracture orientations measured at scanlines 7 (yellow circle), 8 (red circle) and 9 (violet circle). Black lines indicate trend of principal extension. Lines lengths are proportional to the magnitude of extension..... 20
Figure 3-5. Plunge of principal direction of extension (contours) and trend of maximum extension direction. Green shading indicates very shallow plunges. The three scanlines generally are in the vicinity of very shallow plunges, varying from -30^{o} to $+30^{o}$. This is consistent with the steep dips shown by all of the major joint sets in Scanlines 7, 8 and 9.Black lines indicate trend of principal extension. Lines lengths are proportional to the magnitude of extension. 21
Figure 3-6. Orientation of joints and principal extensional strain for Scanline 10 (Red Peak). The direction of strain is perpendicular to the dominant northeasterly-striking joint set. Black lines indicate trend of principal extension. Lines lengths are proportional to the magnitude of extension..... 22
Figure 3-7. Plunge of principal direction of extension (contours) and trend of maximum extension direction. The contours show the amount of plunge of the principal direction of extension. Green shading indicates very shallow plunges. Black lines indicate trend of principal extension. Lines lengths are proportional to the magnitude of extension. 23
Figure 3-8. Orientation of joints and principal extensional strain for Scanline 11 (Red Peak). The direction of strain is perpendicular to the dominant northeasterly-striking joint set. Black lines indicate trend of principal extension. Lines lengths are proportional to the magnitude of extension..... 24
Figure 3-9. Plunge of principal direction of extension (contours) and trend of maximum extension direction around Scanline 11. The contours show the amount of plunge of the principal direction of extension. Light blue shading indicates shallow plunges. Black lines indicate trend of principal extension. Lines lengths are proportional to the magnitude of extension. 25

Figure 3-10. Orientation of joints and principal extensional strain for Scanlines 1 and 2 (pink circle), Scanline 3 (red circle) and Scanline 4 (black circle). Black lines indicate trend of principal extension. Lines lengths are proportional to the magnitude of extension.....26
Figure 3-11. Plunge of principal direction of extension (contours) and trend of maximum extension direction around Scanlines 1, 2 (pink circle) 3 (red circle) and 4 (black circle). The contours show the amount of plunge of the principal direction of extension. Dark blue and orange/red shading indicates steep plunges. Black lines indicate trend of principal extension. Lines lengths are proportional to the magnitude of extension. 27
Figure 3-12. Dip and azimuth of fractures identified in image log from Shoshone 65-37. 29
Figure 3-13. Stereoplot of bedding plane orientations in Shoshone 65-37. 29
Figure 3-14. Cumulative fracture count with depth as a function of fracture type, Shoshone 65-37. 30
Figure 3-15. Stereoplots of fractures above and below 850 ft (259 m) measured depth in Shoshone 65-37. 31
Figure 3-16. Stereoplot of fractures as a function of pad count, Shoshone 65-37. 32
Figure 3-17. Comparison of principal extension trends and strain magnitudes with fractures interpreted from image logs in Shoshone 65-37. The principal extension vector typically plunges about 16°, making it almost perfectly orthogonal with the two, 4-pad sets. Also shown on the inset stereoplot are the three bedding planes.....33
Figure 3-18. Rosette of trend vectors of the direction of maximum extension due to folding in vicinity of Shoshone 65-37 based on palinspastic restoration. 34
Figure 3-19. Trend of principal extensional strain in the vicinity of Shoshone 66-07. Black lines indicate the trend of the extensional strain, while contours and line length indicate the magnitude. 35
Figure 3-20. Key well locations for nitrogen injection test.....37
Figure 3-21. Local scale DFN model for Shoshone 65-02. 38
Figure 3-22. Pressure snap shot at 100 hours. Color indicates change from initial reservoir conditions in red. 38
Figure 3-23. Build up test simulations for average fracture permeabilities of 1 to 1000 mD 39
Figure 3-24. Permeability thickness values based on late-time derivative curves.....40
Figure 3-25. Strain grid for development of regional scale model 41
Figure 3-26. Regional scale DFN model populated by strain perpendicular and strain parallel fracture sets. 41
Figure 3-27. Fracture intensity values (P_{32}) resulting from an average P_{32} value of 0.08 ..43
Figure 3-28. Pressure snapshot of injection in regional model with permeability ratio Set1:S 44
Figure 3-29. Pressure snapshot of injection in regional model permeability ratio Set1:Set2 = 10. This simulation shows earlier pressure breakthrough to the north-west and south-east rather than to the north-east set2 = 1.....44
Figure 3-30. Permeability ratio Set1:Set2 = 0.1.....45
Figure 3-31. Change in pressure for wells 52, 49 and 68. Pressure response is quicker for Shoshone 66-68 because it is closer to the injection in Shoshone 65-2.....45

Figure 3-32. Change in pressure for wells 65-52, 66-49 and 66-68. Pressure response is quicker for Shoshone 66-49 although Shoshone 66-68 is closer to the injection in Shoshone 65-2. 46
Figure 3-33. Breakthrough curves for all wells for varying the ratio of the fracture intensities between the T and L sets. 46
Figure 3-34. Relative breakthrough curves as a function of fracture length. 47
Figure 3-35. High-resolution spinner profile for Shoshone 65-37. 50
Figure 3-36. Fall-off curve for Shoshone 65-20. 51
Figure 3-37. Inferred dominant conductive fracture orientations and intensity throughout the region of the nitrogen injection test. Wells with bottom hole pressure data include 65-03, 66-08, 66-49, 66-68, 66-69 and 65-02, the injector (shown as a yellow filled circle). 53
Figure 3-38. Pattern of nitrogen breakthrough during nitrogen injection test. Yellow line on figure shows possible migration pathways for nitrogen. The two pathways generally parallel the dominant fracture trend (black lines) and follow or connect regions of ghier extensional strain. The two wells at the bottom of the diagram are not easily connected by any obvious fracture pathway leading from the injector. 54
Figure 3-39. Geo-Cellular Modeling Construction 56
Figure 3-40. Phosphoria horizon surfaces modeling using Petrel™ software. 57
Figure 3-41. Representation of fault surfaces. 58
Figure 3-42. Example of new first level option, WORKFLOW, added to project website. 60
Figure 3-43. Example of new first level option, RESULTS, added to project website. 60
Figure 3-44. Example of results available for the palinspastic reconstruction. 61
Figure 3-45. Web site activity, August 17, 2000 through December 4, 2001. 62

List of Tables

Table 3-1. Geometric inputs for local DFN model 39
Table 3-2. Input parameters for varying fracture intensities in T and L sets 47
Table 3-3. Input parameters for breakthrough test with variable fracture length 47
Table 3-4. First-level organization of project web site content. 59
Table 3-5. Updates to website content during period Nov. 1, 2000 to April 31, 2001. 61

ABSTRACT

This report describes the progress and results made in fulfillment of contract DE-FG26-00BC15190, "3-D Reservoir and Stochastic Fracture Network Modeling for Enhanced Oil Recovery, Circle Ridge Phosphoria/Tensleep Reservoir, Wind River Reservation, Arapaho and Shoshone Tribes, Wyoming" during the third 6-month period of the 2-year project. The goal of this project is to improve the recovery of oil from the Circle Ridge Oilfield, located on the Wind River Reservation in Wyoming, through an innovative integration of matrix characterization, structural reconstruction, and the characterization of the fracturing in the reservoir through the use of discrete fracture network models. Progress and results have been obtained during this period for several tasks: Task 2.6 – Generation of the DFN Model; Task 3.1 – DFN model flow validation; Task 3.2 – Fault-block & matrix model development; and Task 5.1 – Project Web Site.

A major achievement during this period has been the successful linkage of the 3D palinspastic reconstruction model to the present-day fracture orientations and intensity in the reservoir units. At the inception of this project, it was not known whether the strains calculated through the 3D structural reconstruction of the Field could be used to specify the orientations and intensity of fractures in the Tensleep and Phosphoria Formations. Analyses showed that the strain produced by the initial folding of the reservoir units prior to any major faulting probably produced most of the fractures important to secondary and tertiary recovery processes. In particular, the magnitude and orientation of the principal extension vector for the folding event correlates well with measured fracture orientations in outcrop and in the subsurface, as well as qualitatively with measured fractured intensity variations. A Decision Point in the project was whether the DFN model generated from the structural reconstruction strain fields would prove useful for modeling subsurface flow at the scale of secondary and tertiary recovery processes. Comparisons of the connectivity of fractures conditioned to the folding strain are reasonably consistent with nitrogen breakthrough data. Moreover, well-scale models based on the folding strain provide good matches to single and multiple well test data. Thus, a fracture model based on the extensional strain field produced during the initial folding should provide a useful basis for optimizing recovery from the reservoir units.

Also during this period, a new bromide tracer test was initiated in a subthrust structural block of the reservoir, and an additional image log and high-resolution spinner flow log were obtained and analyzed. The subsurface flow data has been analyzed to compute fluid flow parameter values for the DFN model. Not only will these parameter values be used to complete the final integrated reservoir model, but also the DFN simulations used to calculate these parameters show that it is possible to reproduce well-scale flow behavior using the DFN model conditioned to the strain due to the early folding of the Circle Ridge Field.

Another important accomplishment during this period has been the preliminary development of the integrated reservoir model, although the initial software system envisioned for this model was discarded in favor of others that could better portray the fault block geometry.

The project encountered a slight delay in the acquisition of the final subsurface data. This was due to two reasons: workover rig availability during the summer of 2001; and delays in permitting the final Na Br tracer experiment. This slight delay should not impact the final project deliverable schedule.

1 INTRODUCTION

The first six-month period of this project focused on data collection and preliminary analysis. This included petrophysical analysis and field data collection to support the construction of the 3D palinspastic reconstruction. During the next six-month period, the project's primary focus was the development of a fully three-dimensional structural reconstruction of the Circle Ridge Field.

The primary focus during the recently completed third six-month period has been generation and validation of the Discrete Fracture Network (DFN) model for the Field, and the completion of the preliminary integrated matrix/fault block reservoir model that will serve as the basis for planning optimization of recovery from the Field during the final six-month period and afterwards. The generation and validation of the DFN model involves several Tasks: Task 2.5 – Validation of cross-sections; Task 2.6 – Generation of the DFN model; and Task 3.1 – DFN flow model validation. From a technical standpoint, the generation and validation of the DFN model requires a comparison of numerous strain components calculated from the 3D palinspastic reconstruction presented in La Pointe and Hermanson (2001) with the fracture orientations and variations in intensity measured in outcrop (La Pointe and others, 2000; La Pointe and Hermanson, 2001). Once a preliminary hypothesis has been established as to what strain component(s) and structural event(s) might be useful for predicting fracture orientations and intensity from this analysis, the model is further validated by using it to predict subsurface image log fracture data obtained during the past twelve months. A final validation consists of comparing subsurface flow patterns in tracer experiments and single well test analyses to these models, to determine if the fracture patterns are consistent with the flow and transport data.

DFN models do not only portray the geometry of the reservoir-scale fractures, but also have fluid flow properties assigned to each fracture. In order to derive useful fluid flow values, it is necessary to analyze and model subsurface flow tests, such as single well, transient flow data. This was done during this six-month period, leading to the derivation of fluid flow parameters. This activity was carried out under Tasks 2.6 and 3.1.

A parallel effort during this phase of the project has been to generate the integrated matrix/fault block model that will serve as the basis for planning optimized recovery from the Field. The software system, RMS (Roxar), originally intended for this purpose, proved inadequate as it is difficult to accommodate some of the faulting complexities of the Circle Ridge Field. As a result, the integrated model of matrix and fault blocks (Task 3.2 – Fault block & matrix model development) is being carried out in parallel with both GoCad and Petrel modeling software to determine the best piece of software to be used for this project.

The original project scheduled called for all tasks through Task 3.2 to be completed by October 31, 2001. Nearly all of these tasks have been completed, although some refinement is expected in both the DFN model properties as the final subsurface data is

obtained and analyzed, and possibly in the integrated reservoir model as the refinements to the DFN model are incorporated into the integrated model.

The final completion of all scheduled tasks were slightly delayed due to unavoidable changes to the drilling and logging schedule. All Marathon data gathering was to be completed during the summer and fall of 2001. However, during the summer of 2001, there was a shortage of workover rigs and crews that met Marathon's stringent safety guidelines. This shortage resulted in a backlog of projects throughout Marathon's Rocky Mountain operations and deferred the data gathering at the Circle Ridge Field. Moreover, the final NaBr tracer test was delayed due to permitting issues until November 2001. Permission to inject the tracer was requested from the United States EPA in mid-July 2001, but was not obtained until late October.

These slight delays should not impact the timely completion of all deliverables for this project, and have not contributed to any unforeseen costs to the project.

Throughout this report, reference is made to the "overthrust block" and "subthrust block". In general, this nomenclature is used to distinguish between rock in the hanging wall of the main Red Gully Fault (overthrust) and rock in the footwall (subthrust). The actual structural geology is much more complex, as shown by the reconstruction results, but this terminology has been retained for ease of reference.

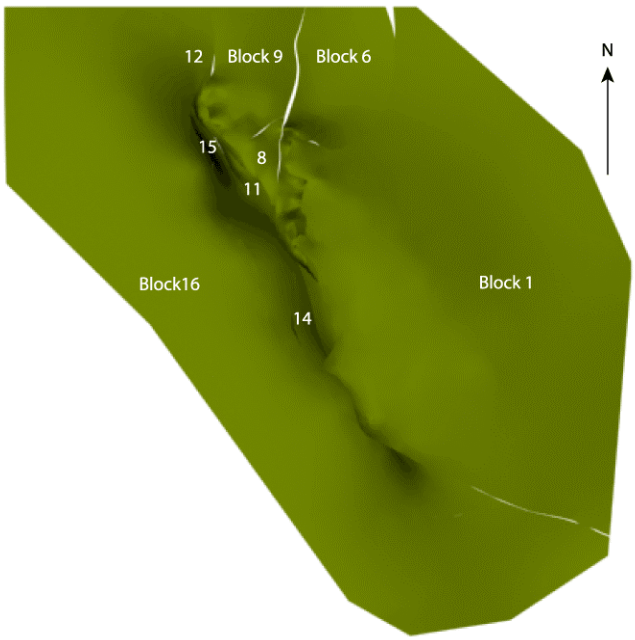

Figure 1-1. Horizontal map view of structural blocks defined for the Phosphoria Formation. Block definitions are very similar for the Tensleep Formation.

The field is further divided into several structural blocks (Figure 1-1), which are referred to in this report by their block number. Block 1 currently contributes most of the production.

For reference, the stratigraphic column for the Circle Ridge Field is given in Figure 1-2. Other geological details can be found in La Pointe and Hermanson (2001).

This report follows the outline mandated in Section 4.14 (Guidelines for Organization of Technical Reports (May 1999)) as specified in the contract. The discussion of the experimental work is organized by Task, as are the Results and Discussion section.

Era	Period	Unit		Symbol
Mesozoic	Cretaceous	Undifferentiated	Mowry Shale	Ku
			Thermopolis Shale	
		Cloverly Formation		Kcv
	Jurassic	Morrison Formation		Jm
		Sundance Formation		Js
		Gypsum Springs Formation		Jgs
		Nugget Sandstone		Jn
	Triassic	Chugwater Formation	Popo Agie Member	TRpa
			Crow Mountain Member	TRcm
			Red Peak Shale	TRrp
		Dinwoody Formation		TRd
Paleozoic	Permian	Phosphoria Formation		Pp
	Pennsylvanian	Tensleep Sandstone		
	Mississippian	Amsden Formation		
		Madison Limestone		
	Devonian	Darby Formation		
	Ordovician	Bighorn Dolomite		
	Cambrian	Gallatin Limestone		
		Gros Ventre Shale		
		Flathead Sandstone		
PRECAMBRIAN				

Figure 1-2. Stratigraphic column for the Circle Ridge Field (from Smith 2000).

2 EXPERIMENTAL WORK

2.1 Overview

Experimental work during the third six-month project period consisted primarily of:

1) the acquisition and processing of subsurface flow information;
2) the comparison of the strains calculated from the 3D palinspastic reconstruction with outcrop fracture data;
3) the validation of the DFN model geometry and connectivity using subsurface fracture geometry and flow data; and
4) the integration of the matrix, fault block and reservoir-scale fracture data into a single numerical reservoir model.

The sections that follow describe each one of these four areas in greater detail.

2.2 Experimental Techniques for Analysis of Subsurface Well Data

La Pointe and Hermanson (2001) have previously described many of the techniques used to acquire and analyze various types of subsurface well information. The subsurface data acquired and used in this project comprise both single well and multiwell tests. Many of these tests provide information that is used for several different purposes.

2.2.1 FRACTURE IMAGE LOGS

Three new fracture image logs were to be acquired as part of this project. Previously, a Fullbore Formation MicroImager™ (FMI - Schlumberger) log was obtained over an open-hole interval in Shoshone 66-07. During this project period, a second log was obtained using a Formation MicroScanner™ (FMS- Schlumberger) in Shoshone 65-37 over the interval 616 ft to 1230 ft (187.8 m to 374.9 m) MD. The open hole interval in this well contains Subthrust Block 6 Phosphoria Formation, Subthrust Block 6 Tensleep Formation, and Subthrust Block 6 basal Phosphoria and Tensleep Formations. The logs were interpreted by Marathon and resulted in a summary of fracture and bedding plane information.

2.2.2 DYNAMIC FLOW LOGS

In order to further understand which features provide the flow paths for fluid flow, high-resolution injection profiles were obtained for Shoshone 65-37. The flow logging was carried out using a Baker-Atlas spinner tool, and included a temperature log. The depth interval logged extended from the surface to a depth of 1220 ft (371.9 m).

2.2.3 SINGLE WELL PRESSURE BUILD-UP OR FALL OFF TESTS

A 44-hour Subthrust, Block 6, Phosphoria Formation falloff test was performed at Shoshone 65-20. This test was matched using commercial software and a uniform flux fractured well model in a radial composite reservoir. The analysis made it possible to calculate the permeability and permeability thickness of the zones, the fracture half-length, skin factor, mobility ratios, and the approximate distance to the high mobility zone using standard well test analyses (Horne, 2000).

2.2.4 INJECTED TRACER STUDIES

Tracer tests can take many different forms. One test has already been carried out, termed the Overthrust Tensleep Nitrogen Test (La Pointe and Hermanson, 2001). During this project period, a second tracer test was initiated to examine the flow properties of the Phosphoria Formation and any linkage to the Tensleep. The tracer used was an aqueous sodium-bromide (NaBr) tracer.

This Subthrust Block 6 tracer test was delayed due to permitting issues until November 2001. Permission to inject the tracer was requested from the United States EPA in mid-July 2001, but was not obtained until late October. The tracer test began November 15th at the Phosphoria injector, Shoshone 65-20, and surrounding producers in Block 6. The test is expected to conclude in mid-December, 2001.

Background water samples from eleven producing wells, offsetting Shoshone 65-20, were collected during late October and early November. Analysis, using a high-pressure liquid chromatograph, indicated background bromide concentrations of less than 1 ppm at all offsets. Eight of the wells, Shoshone 65-6, Shoshone 65-37, Shoshone 65-45, Shoshone 65-53, Shoshone 65-54, Shoshone 65-61, Shoshone 65-67, Shoshone 65-73, were completed in the Subthrust Phosphoria. The four additional wells were only open in the Subthrust Block 6 Tensleep or and/or Amsden Formations.

On November 15, 2001, 41 barrels of 24% NaBr aqueous solution were injected into the Subthrust Block 6 Phosphoria Formation at Shoshone 65-20. This aqueous solution contained 3,339 pounds (1,517.7 kg) of bromine and was gravity fed into the well at a rate of 2,300 barrels per day (365.7 m^3/day). Following injection of the tracer slug, the well was returned to water injection at approximately 175 barrels (27.8 m^3) water injected per day (BWIPD). Monitoring wells were sampled on an approximately daily basis.

2.2.5 ANALYSIS OF WELL TESTS USING DFN MODELS

Analysis of well tests involves both calculations based on the well test data itself, and also on simulations of these tests using DFN models. There are two broad types of well test simulations: those involving only pressure and flow, such as the single well pressure build-up or multiwell pressure interference tests; and those involving mass transport, such as the NaBr tracer experiment. The tracer tests may also offer the opportunity to simulate

the pressure and flow without regard to mass transport. During the current project phase, simulations have involved only pressure and flow analyses, rather than mass transport, due to the 3-month delay in the permitting of the NaBr test.

The key parameter to simulate in transient pressure tests in fractured reservoirs is the pressure derivative. The analysis of the pressure derivative (Horne, 2000) was originally used to identify the radial-cylindrical, infinite-acting portion of the well test curve. The pressure derivative is calculated for each pair of time and pressure values in the well test as:

$$Derivative = t\frac{\partial p}{\partial t} \qquad \text{Equation 1}$$

which produces a zero-slope line when the semi-log straight line condition of infinite-acting, radial-cylindrical flow is satisfied.

The pressure derivative is closely linked to transmissivity calculations. The permeability-thickness product (*kh*) defines the flow capacity of a conducting feature. The pressure derivative (e.g. Horne) is a method that was originally intended to identify the radial-cylindrical, infinite-acting portion of the well test curve. The pressure derivative is calculated for each pair of time and pressure values in the well test as $t\frac{\partial p}{\partial t}$ which produces a zero-slope line when the semi-log straight line condition of infinite-acting, radial-cylindrical flow is satisfied.

The pressure derivative is closely linked to transmissivity calculations. The permeability-thickness product (*kh*) defines the flow capacity of a conducting feature. The values of the pressure derivative are semi-log slope of the well test, hence the derivative can be related to transmissivity by

$$\frac{\partial p}{\partial t} \equiv derivative = \frac{162.6(qB)\mu}{kh} \qquad \text{Equation 2}$$

(Horne 1995). Where *kh* is the permeability thickness, *q* is the flow volume, *B* is the formation volume factor and μ is the viscosity. By this simple transformation one can re-plot the derivative as a map of the transmissivity versus time during the well test. The permeability-thickness product *kh* can be represented in units of m^2-*m* (i.e. m^3) (SI) or *mD-m* (oil field).

By this simple transformation, the derivative essentially expresses how transmissivity varies with time during the well test.

Although the single well simulation will help calibrate the fracture geometry and permeability necessary to match reservoir *kh*, simulating pressure response in the

pumping wells is necessary to determine the relative permeability of one set to other sets. Multiwell pressure simulation was carried out by creating a multiwell-scale model using the calibrated parameters from the local, single well scale DFN model (Section 3.3.4).

Simulating the pressure response in tracer tests with a DFN model for the nitrogen injection test presents some additional difficulties as there are potentially four phases acting: (1) Oil (2) Water (3) Natural Gas and (4) Nitrogen. However nitrogen dominates in the injector well and the fall off test can be used to calculate permeability thickness, *kh*. The initial simulation was carried out with a dual porosity Eclipse™ (Schlumberger) simulation to calculate permeability thickness. Next, a single-phase DFN model of the well was run, and the derivative of the pressure curve was used to determine the appropriate permeability and storage values for the individual fractures in the fracture system surrounding the wellbore.

2.3 Experimental Techniques for Comparison of Strain Values Calculated from 3D Palinspastic Reconstruction with Fracture Orientations and Intensity in Outcrop

The construction of the field-wide DFN model for the Tensleep and Phosphoria Formations requires some way of specifying fracture properties away from well control. There are three possible alternatives for interpolating fracturing between wells:

1) Condition the fracture pattern to seismic attributes;
2) Interpolate from well data using statistical methods such as Geostatistics; or
3) Establish a model that relates fracture geometry to structural and/or lithological parameters.

There is no modern seismic data for the Circle Ridge Field, so the first option is not possible without the acquisition and processing of new, 3D seismic data. The second option is likely to lead to substantial errors, since statistical interpolation techniques assume that the rock behaves as a continuum between wells. Matrix properties often behave in this manner, but it is highly unlikely that variations in fracture properties vary in such a simple manner, especially when the fractures may have been produced by faulting and folding, which is inherently local and discontinuous in nature. Thus, the third alternative was adopted for this project.

In the Circle Ridge Field, fracture information is very sparse in the subsurface, coming from unoriented core and a few image logs. The methodology adopted in this project requires the comparison of the strain field in various structural positions relative to the fracture orientations, intensity and size. Subsurface data is not adequate as spatial coverage is very low and there is no direct information on fracture size. On the other hand, the top of the field is only a few hundred meters below the surface near the crest, so that the abundant outcrops above the field should reflect a similar deformation history, at least in the units below the detachment zone afforded by the Gypsum Springs Formation (La Pointe and Hermanson, 2001). Thus the fracture parameters necessary for

ascertaining the structural controls on fracturing and developing input statistical distributions has been based upon studies of fracturing in outcrop.

As documented in previous reports (La Pointe and others, 2000; La Pointe and Hermanson, 2001), fracture data was obtained for this project along eleven different scanlines (Figure 2-1) in the Triassic Red Peak and Crow Mountain Members of the Triassic Chugwater Formation.

Figure 2-1. Scanline used to measured fractures. Outcrop is of the Triassic Red Peak Member of the Chugwater Formation.

The fracture data obtained in this manner represents the fracture pattern in several different structural positions and two different rock types. Although neither of these Members are reservoir units, field mapping and the structural reconstruction indicate that they should have deformed in a manner analogous to the Tensleep and Phosphoria Formation reservoir units. Of particular interest are the orientation and intensity of fracturing along these scanlines.

The structural reconstruction of the Circle Ridge Field (La Pointe and Hermanson, 2001) suggested a sequence of folding and faulting events that likely produced the present-day structure. They found that the initially undeformed rock was first folded. Of the two algorithms tested, inclined shear folding produced better results than flexural slip folding. Following the folding, a series of faulting events occurred. The first large faulting is movement on the Gray Wash Fault that is the lowest structurally of all major faults. Upon encountering some obstacle or reaching the stress limit of strain release, the stress field then broke higher in the sequence, creating the Blue Draw Fault. Towards the south both these faults merge into the Red Gully Fault system, which at this time continued to move along an earlier established thrust plane. The imbrication process in the northern end of the field is repeated once again with the formation of the Yellow Flats Fault higher in the section. The final thrust displacement was focused on the Red Gully Fault that is structurally highest.

The Orange Canyon Fault obliquely cuts all these faults and was formed last of the large faults through the Circle Ridge anticline.

At each stage in the reconstruction, it is possible to calculate various types of volumetric strain and directional strain. For a complete description of these strain parameters and how they are calculated, see La Pointe and Hermanson (2001).

Only directional strain parameters can be assessed as to their correspondence to fracture orientations, as volumetric strain measures have no associated directionality. The dominant joint (extension fracture) set should form orthogonal to the principal extension strain vector. Due to local stress redistribution, a second joint set orthogonal to the first and parallel to the principal pre-fracturing maximum extension direction might also occur.

Both the individual magnitudes of the directional strain components, as well as the volumetric strain measures, may relate to variations in fracture intensity (Jamison, 1997).

There are some uncertainties regarding the comparison of the calculated strains and the outcrop fracturing.

The structural reconstruction was carried out for the three principal reservoir formations, with particular emphasis on the Tensleep Formation, as described in La Pointe and Hermanson (2001). However, outcrop fracture data was obtained from the Crow Mountain and Red Peak Members, which are stratigraphically younger. Since there are no detachment horizons, such as the Gypsum Springs, intervening between the Crow Mountain and Red Peak units and the reservoir units, the principal directions of strain and relative strain magnitude variation of the Crow Mountain and Red Peak are likely to be very similar to that calculated for the Tensleep and Phosphoria Formations.

A greater source of uncertainty arises in the way that the outcrop data is spatially situated within the palinspastic modeling results. Ideally, the scanline site occurs in a structural position that should be compared to the strains in an equivalent structural position in the Tensleep Formation, for example. However, it is not possible to track equivalent structural positions in the reconstruction software. Thus it is assumed that two regions that occupy the same horizontal location occur in the same structural position. If the beds are flat lying, no error is made using this assumption. If the beds are steeply dipping, then some error will occur. In the restoration of structurally complex areas of the Field, strains may vary over a few tens of meters, or alternate between two common directions. The error introduced by assuming that horizontal equivalence equals structural equivalence might be on the order of a few tens of meters in some locations of the Field. Thus, the comparison of scanline fracture data with the strain in the reservoir formations should consider not only the strain at the equivalent horizontal position, but also in the general few tens of meters around the position.

With the exception of the rock in the area adjacent to the major faults, the strain produced by faulting is probably low. At some distance from the faults, the rock and any pre-existing fractures would be “translated” according to the fault geometry and slip vector,

but the orientations of the fractures would be little changed unless there was significant block rotation. Fracture intensities, other than in areas adjacent to the fault, would also likely be unaffected. On the other hand, folding may produce significant rock strain, leading to the formation of fractures throughout the reservoir units.

Since the initial folding is the dominant strain event in the model, and it is the earliest significant event, it should have the highest probability of producing the fractures. If the fracture pattern does relate consistently to a major structural event, particularly the initial folding of the reservoir units, then the sensible geological explanation for the present-day fracture pattern lends confidence to the DFN model. It would be hard to have confidence in using the palinspastic model for predicting fracture patterns if only a minor, low-strain event seemed to correspond with the fracture patterns.

For these reasons, the correspondence between the fracture orientations and intensity with the various strain components calculated due to folding were closely evaluated.

2.4 Experimental Techniques For Validation of DFN Model Geometry and Connectivity Using Subsurface Fracture Geometry and Flow Data

There are two levels or types of validation that can be used to assess the quality and usefulness of the palinspastic reconstruction. The first type of validation essentially evaluates the internal consistency of the restoration, and is based on whether various aspects of the model "balance". This type of self-consistency checking guides the sequence and geometrical parameters governing the unfolding and unfaulting of the model. La Pointe and Hermanson (2001) have previously documented the sequence of structural events that provide an internally consistent model.

During this project period, the DFN model was validated not for its internal consistency, but for its usefulness in predicting fracture geometry and flow behavior in the reservoir formations. This was carried out through two series of comparisons:

1) Comparison of predicted fracture orientations and intensity of subsurface image log data; and
2) Comparison of predicted fracture pattern connectivity with subsurface flow results.

Comparison of the predicted and measured fracture geometry relies upon the model developed between strain components and fracturing. This strain/fracture model is applied to the reservoir at the locations where subsurface image log data has been collected. These locations are Shoshone 66-07, a predominantly Overthrust Tensleep section, and Shoshone 65-37, a predominantly subthrust section including both the Tensleep and Phosphoria Formations.

The comparison of subsurface flow data with the connectivity properties of the fracture pattern inferred from the strain pattern is less quantitative. The data that provides the

most independent check on the flow properties of the fracture network are the tracer tests. The reason for this is that:

1) Tracer tests involve a number of wells covering a larger area than any single well test, and so reflect the larger scale heterogeneity important for reservoir engineering optimization design involving secondary or tertiary recovery schemes;
2) Tracer tests not only identify areas with very high or low pressure communication, but also identify zones of higher or lower mass transport, which is of importance when designing surfactant injection processes or heat injection processes; and
3) Simulation of single well tests requires specification of fracture permeability and storativity, which can only be derived through calibration against the well tests, and so are not independent checks on the DFN model.

Thus, additional validation is provided by comparing the pattern and timing of tracer breakthrough and pressure interference with the connectivity of the fracture network.

2.5 Integration of the Matrix and Fault Block Architecture Into a Single Numerical Reservoir Model

An important aspect of this project is the creation of an integrated matrix/fault block/fracture numerical model. This model will allow the visualization of the fractures in 3-D and their relation with other parameters, and will provide the numerical parameter values to reservoir simulations or other calculations to design and evaluate options to enhance production.

The Circle Ridge Field is encompassed within a complex structural sitting. The basic structure that defines the field is an anticline. The complexity enters due to the faulting of the anticline structure. This complexity is not just due to the number of the faults observed and modeled, but also the type of faulting in the Field. Many faults intersect other faults, cross other faults, or die out. The Circle Ridge Field has not only nearly vertical faulting which is fairly simple to model, but also shallowly dipping faults and in particular, shallowly dipping reverse faults. This last type of fault is difficult to incorporate in many 3D modeling software systems.

Of the modeling software packages that can handle the complex types of faulting that occur at Circle Ridge, further classification of the software can be made in their ability to upscale the geo-cellular model to reservoir simulation models. This process of upscaling has been addressed in some of the software so that directly readable grid files are written that can be read by the reservoir simulation software. This becomes important in order to allow the operator of the field a method of evaluating the best economic methods of extracting the most reserves from the field. The ability of geo-cellular models to easily output simulation modeling grids is an important point to consider in picking the geologic modeling software.

Initial experiments with importing the data into Roxar's RMS™ software showed that the current release of RMS cannot handle reverse faults without breaking the model into several pieces, which is cumbersome for use in later simulation or other types of calculation. Currently, modeling is being carried out using Technoguide's Petrel™ and Gocad™ to determine the best piece of software to be used for this project.

2.6 Plans to acquire remaining subsurface flow and fracture data

This section describes the experimental plan to acquire the remaining subsurface data.

2.6.1 TRACER TESTING:

Status: complete.

2.6.2 FMI AND SPINNER LOGGING

Marathon currently plans to run the final FMS log and high-resolution injection profile at Shoshone 66-14. The original plans to obtain this data at Shoshone 66-75, a proposed 2001 drill well, were aborted when a drilling rig could not be obtained. Shoshone 66-14 offsets the proposed 66-75 location and has openhole interval in the Overthrust Phosphoria, Tensleep, and Amsden. A modern log suite including FDC/CNL porosities and laterlog resistivities may also be performed. This work is scheduled for December 2001.

2.6.3 FALLOFF AND MULTI-WELL INTERFERENCE TESTING:

Multi-well interference testing will be performed using Shoshone 65-20 as a central observation well. This testing will indicate the maximum permeability direction for the Phosphoria in Subthrust Block 6. Plans include pulsing Shoshone 65-53, Shoshone 65-37, and Shoshone 65-38. This work will begin following the completion of the tracer test in mid-December, 2001

The acquisition of this data will fulfill Marathon’s in-kind commitment of the subsurface data to be provided to this project.

3 RESULTS AND DISCUSSION

3.1 Overview

This section discusses the results of the active subtasks within Task 2, Task 3 and Task 5 that were the focus of work during the 3rd six-month project period. These tasks comprise the development of a procedure to populate the reservoir model with fractures based upon the strain calculated in the 3D palinspastic reconstruction; the validation of this model; the derivation of flow parameters for the fracture model from the analyses of the subsurface tests; and the development of the integrated 3D fault block and matrix model.

3.2 Task 2.6 – Generation of the DFN Model

3.2.1 PURPOSE OF TASK

Task 2.6 involves the comparison of the strain field predicted by the successfully-balanced restoration with the fracture geometry measured in outcrop in the subsurface, in order to determine how the strain field relates to fracture pattern development, as well as to the parameter values necessary to utilize strain information for developing the discrete fracture network (DFN) model.

In order to evaluate alternative improved oil recovery processes in fractured reservoirs, and to design these processes, it is important to understand the development of fractures throughout the reservoirs, not only in the vicinity of the wells.

To date, there has been no seismic data acquired at the Circle Ridge Field that could be processed to yield the types of attributes that may correspond to fracture intensity or orientation. Moreover, the steep dips of the strata in some areas of the Field could make processing problematic, and the shallowness of the reservoirs would require a closely-spaced 3D survey, which would greatly increase the per-acre acquisition cost.

Fortunately, the Circle Ridge Field's fracturing most likely originated in response to the folding and faulting that has produced the present-day structure. Because of the excellent well control on key horizons, and due to the successful acquisition of additional cross section data and successful cross-section balancing (Tasks 2.3 and 2.4, respectively; La Pointe and Hermanson, 2001), it is possible to determine whether and how the strains developed during folding and faulting have produced the current fracture pattern.. Thus, the two goals of this Task are to:

1) Determine if the strains related to folding and faulting are likely to have produced the observed fracture patterns in the Tensleep and Phosphoria Formations; and

2) If there does appear to be a causal relation between the strain history and the fracture pattern, to quantify how the strain magnitudes, orientations and possibly other parameters relate to fracture intensity, orientation and other parameters.

Several of the key pieces of information for developing the DFN conceptual model have been completed. It has been determined that the scale of fracture intensity does not appear to depend upon scale for scales on the order of a few meters to some tens of meters, but may vary at scales greater than hundreds of meters. This variation is, fortunately, at the horizontal scale typical of many reservoir simulation discretizations, which suggests that the reservoir simulator input calculated from the DFN model should accurately reflect the in inherent scale of fracture variability.

Moreover, the intensity studies do not show variation as a function of whether the scanline was located in the Crow Mountain member or the Red Peak member. While this does not rule out variations as a function of lithology for other formations or members, it does indicate that the strain differences associated with deformation may play a greater role in controlling fracture intensity than the mechanical property variations attendant to different lithologies. This implies that the intensity variation of the fracturing in the DFN model may be controlled primarily or completely by the strain differences inferred from the palinspastic reconstructions.

While the complete comparisons between the intensity and orientation of strain derived from the structural reconstructions and the scanline data have not been completed, the values do show orientations and intensity variations that are consistent with the fracturing having been generated by the folding and faulting. This suggests that the palinspastic reconstruction of the field will provide very useful and important controls on the development of the reservoir model.

3.2.2 RESULTS OF COMPARISON

3.2.2.1 Fracture Orientations

Figure 3-1 shows a contour map of the magnitude of principal extensional strain resulting from the early folding of the Tensleep Formation. The strains have been mapped to the present-day structural configuration of the Field. The black dots show the scanline sites.

This contour plot shows that the magnitude of extension varies throughout the Field. There is a northwesterly-trending belt of greater extension immediately southwest of the Red Gully Fault system. Scanlines 1 through 4 lie in the tightly folded nose of the fault. Scanlines 10 and 11 are on opposite sides of the Red Gully Fault.

Figure 3-1 shows that the magnitude of the extensional strain varies among the scanline sites. Scanlines 7, 8 and 9 are in the areas of the lowest extension strain, while Scanlines 1 through 4 are in the highest.

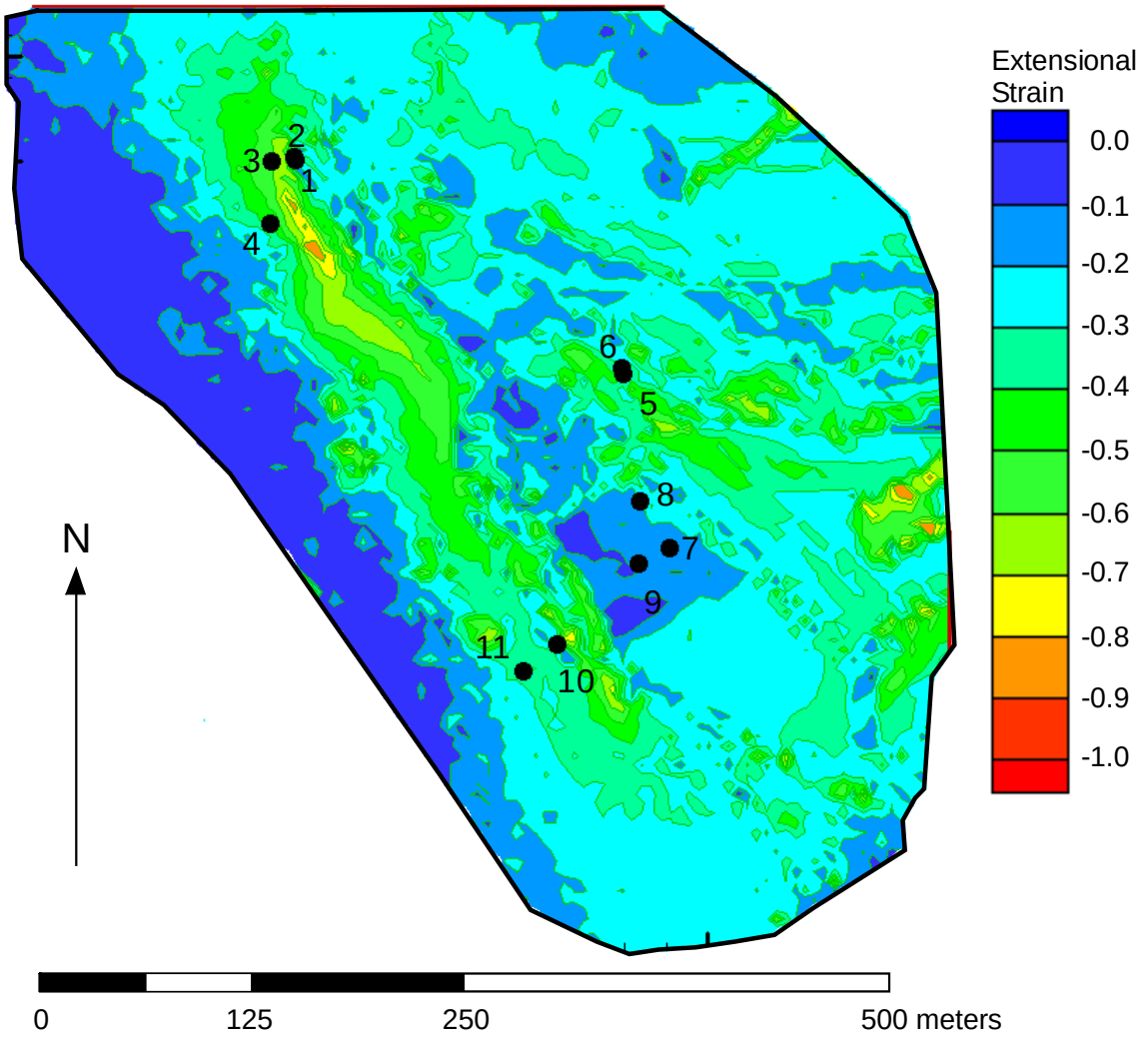

Figure 3-1. Map of principal extensional strain magnitude produced by folding. The contour map shows the approximate horizontal limits of the fault blocks used in the reconstruction. The location of the eleven scanline sites are shown on the map. The strains shown have been mapped on the present-day structural configuration of the Circle Ridge Field, and represent deformation in the Tensleep Formation.

Most of the production in the Circle Ridge Field comes from the structural block termed the Overthrust Block (La Pointe and others, 2000), and was designated as Block 1 in the structural model of the Field. There are six scanline sites in Block 1. This abundance of scanline data in an individual block makes it possible to test out preliminary comparisons among strain and joint patterns that other blocks do not afford because of more limited data.

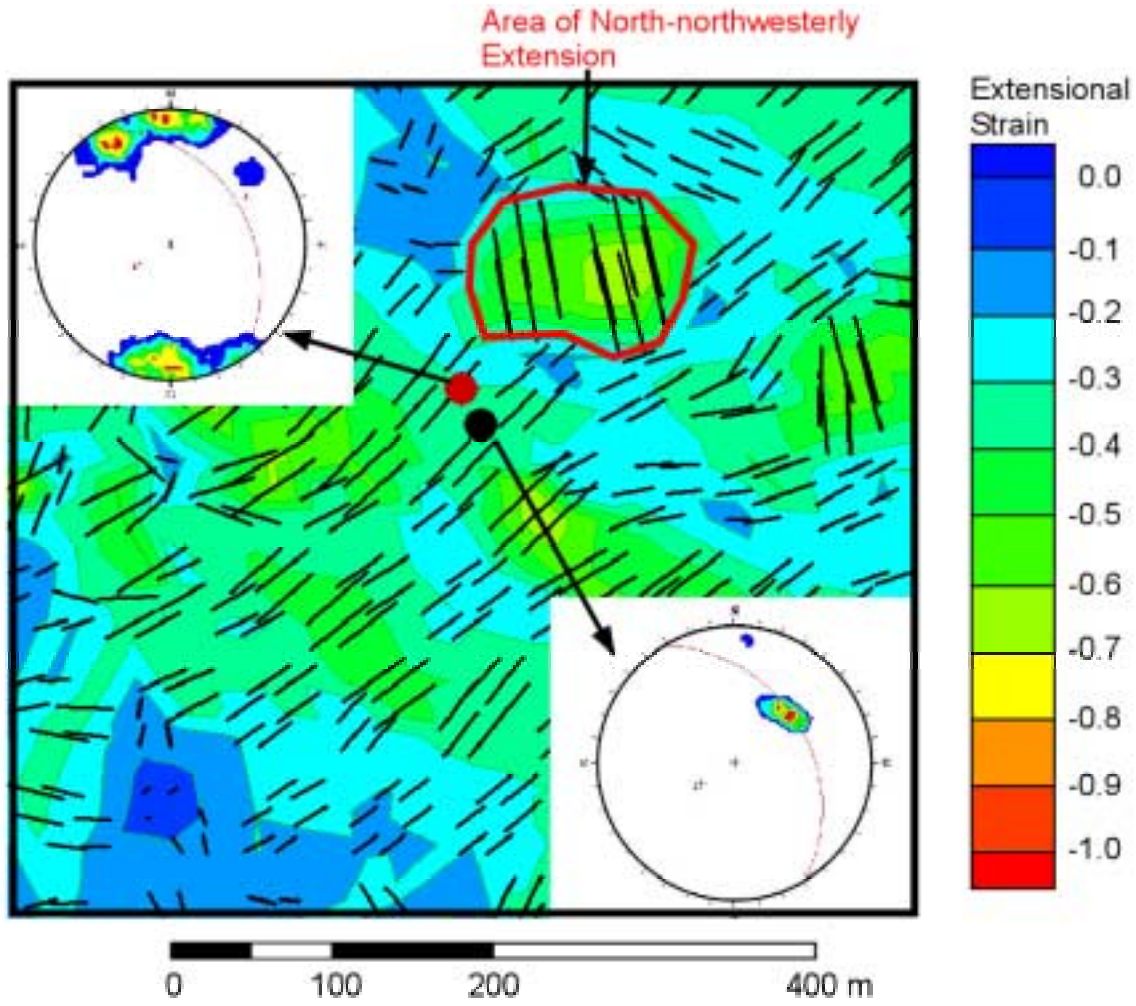

Figure 3-2. Fracture orientations measured at scanlines 6 (red circle) and 5 (black circle). Black lines indicate trend of principal extension. Lines lengths are proportional to the magnitude of extension.

The prevalent northeasterly direction of strain (Figure 3-2) is consistent with the fracture orientations shown at Scanline 5, and is also possibly evident in a minor set at Scanline 6. The north to north-northwesterly strain in the area immediately to the northeast of Scanline 6 is consistent with the dominant orientations shown in the joint stereoplot for Scanline 6. Both stereoplots suggest that the principal direction of extensional strain in the vicinity of the scanlines is perpendicular to the strike of the joint sets found in outcrop along the scanlines.

The direction of greatest extension in the vicinity of Scanline 5 plunges 50^{o} to 60^{o} to the northeast (Figure 3-3), which makes it almost exactly perpendicular to the dominant joint set shown in the stereoplot. The northeasterly extension near Scanline 6 plunges 20^{o} to 50^{o} to the northeast, which is nearly orthogonal to the secondary set. To the northeast of Scanline 6, the north-northwesterly extension in this region dips over a large range from 20^{o} to about 70^{o} in a south-southeasterly direction. The shallower dips are consistent with the dominant joint set dip, but the steeper dips are not.

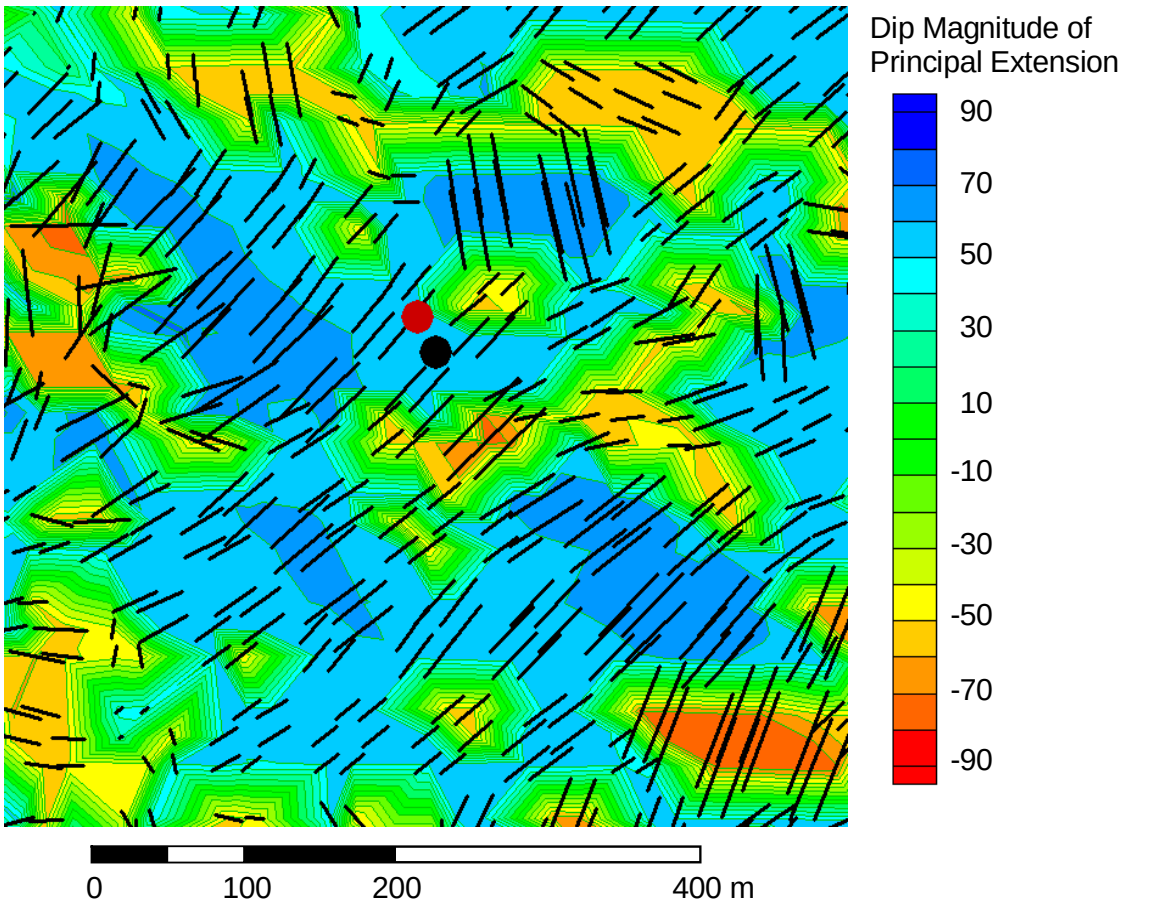

Figure 3-3. Plunge of principal direction of extension (contours) and trend of maximum extension direction. Plunge at Scanline 6 (red circle) is about 50° to the northeast. Plunge at Scanline 5 (black circle) is similar. Black lines indicate trend of principal extension. Lines lengths are proportional to the magnitude of extension.

Figure 3-4 shows the trend of the principal extensional strain for the region around Scanlines 7,8 and 9. At Scanline 7, the principal direction of extension is to the northeast or north-northeast. This is nearly perpendicular to the strike of the dominant joint set, which strikes northwesterly and dips steeply to the southwest. Some nearly north-south extension occurs just to the east of Scanline 7, which is nearly perpendicular to the strike of the other prominent joint set. Scanline 8 has a dominant west-northwesterly striking subvertical joint set, and a secondary set orthogonal to it that strikes north-northeasterly. The dominant direction of extension is nearly perpendicular to the west-northwesterly striking primary set. Scanline 9 exhibits a very similar joint orientation pattern, however, the azimuth of the direction of principal extension is northeast-southwest, some ten to fifteen degrees from being perpendicular, although the extension direction just to the west of the scanline is nearly exactly perpendicular.

Figure 3-5 shows the plunge of the principal extension vector. The three scanlines generally are in the vicinity of very shallow plunges, varying from -30° to +30°. This is consistent with the steep dips shown by all of the major joint sets in Scanlines 7, 8 and 9.

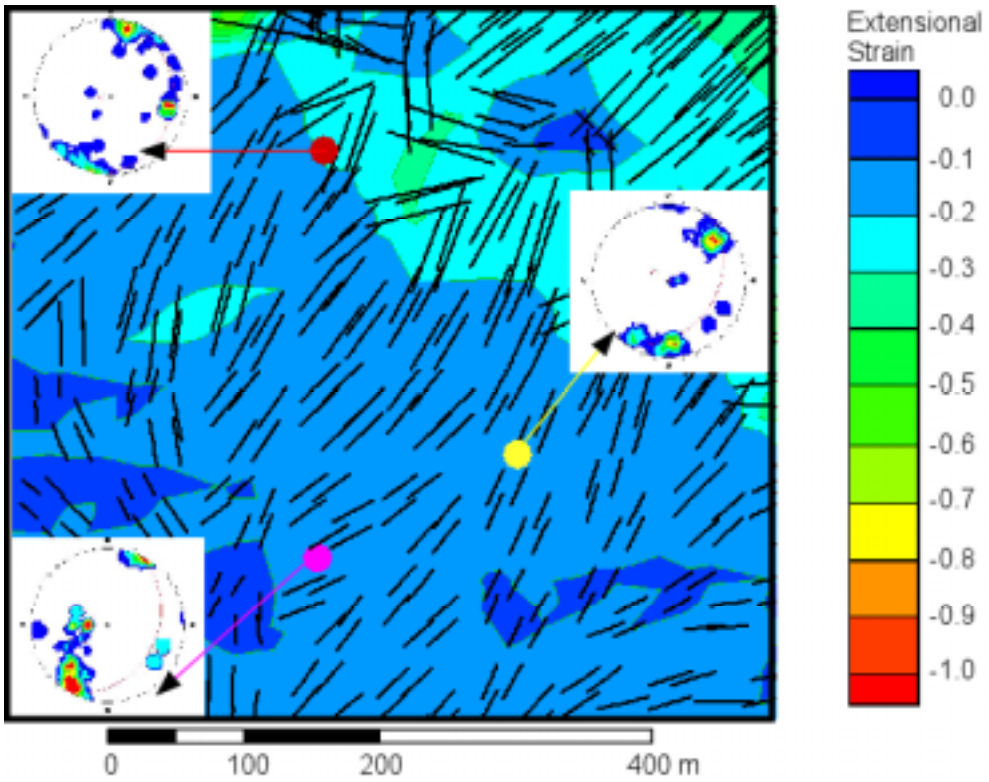

Figure 3-4. Comparison of extensional strain and fracture orientations measured at scanlines 7 (yellow circle), 8 (red circle) and 9 (violet circle). Black lines indicate trend of principal extension. Lines lengths are proportional to the magnitude of extension.

The final scanline in Block 1 is Scanline 10. The trend of the principal extension (Figure 3-6) is nearly perpendicular to the strike of the dominant joint set. There is some evidence in the stereoplot of another joint set nearly orthogonal to the first. The plunge of the principal extension vector (Figure 3-7) show that the plunges of the principal direction of extension are on the order of 10^{o} in the vicinity of Scanline 10 (red circle) to the southeast.

Overall, the joint pattern for the six scanline sites in Block 1 indicate a very consistent relation to the trend and plunge of the principal extension vector. The dominant set is generally very close to being orthogonal to the extension vector, and occasionally there is a secondary joint set that is approximately orthogonal to the primary set and striking parallel to the trend of the extension vector.

At least in Block 1, it seems as if the joint sets measured along scanlines in are consistently orthogonal to the direction of principal extension during the folding event.

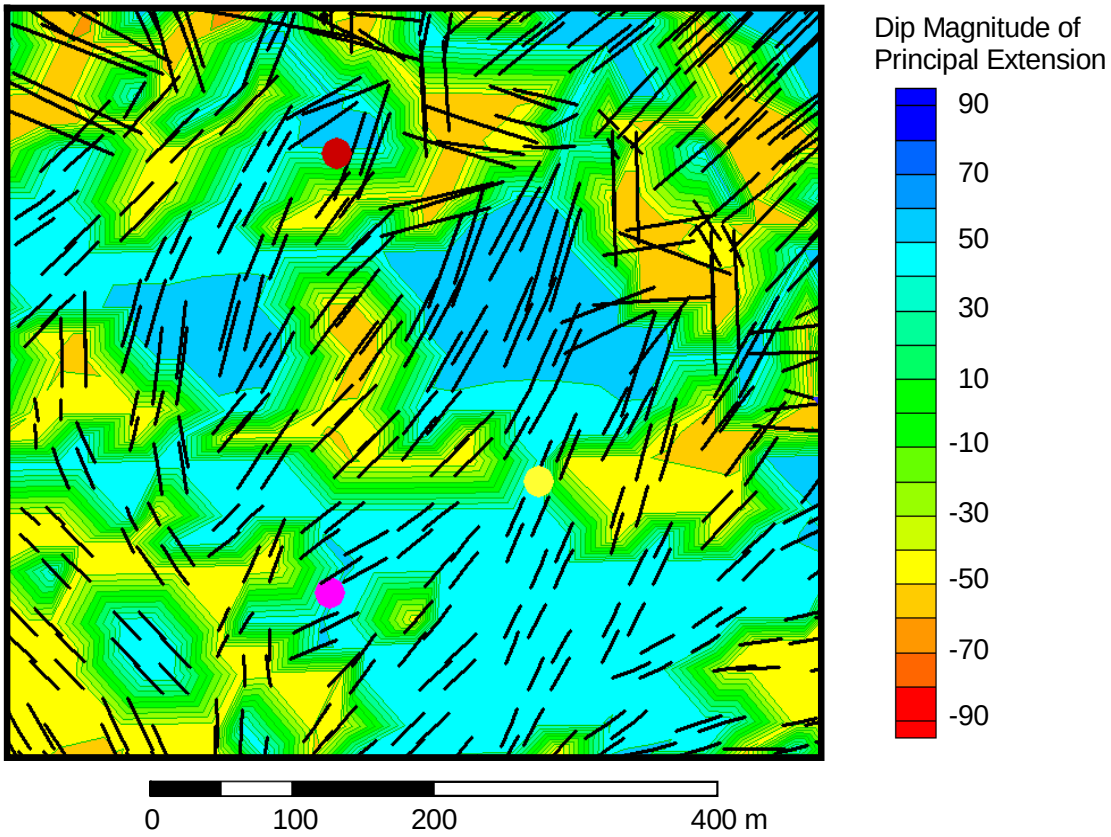

Figure 3-5. Plunge of principal direction of extension (contours) and trend of maximum extension direction. Green shading indicates very shallow plunges. The three scanlines generally are in the vicinity of very shallow plunges, varying from -30° to +30°. This is consistent with the steep dips shown by all of the major joint sets in Scanlines 7, 8 and 9.Black lines indicate trend of principal extension. Lines lengths are proportional to the magnitude of extension.

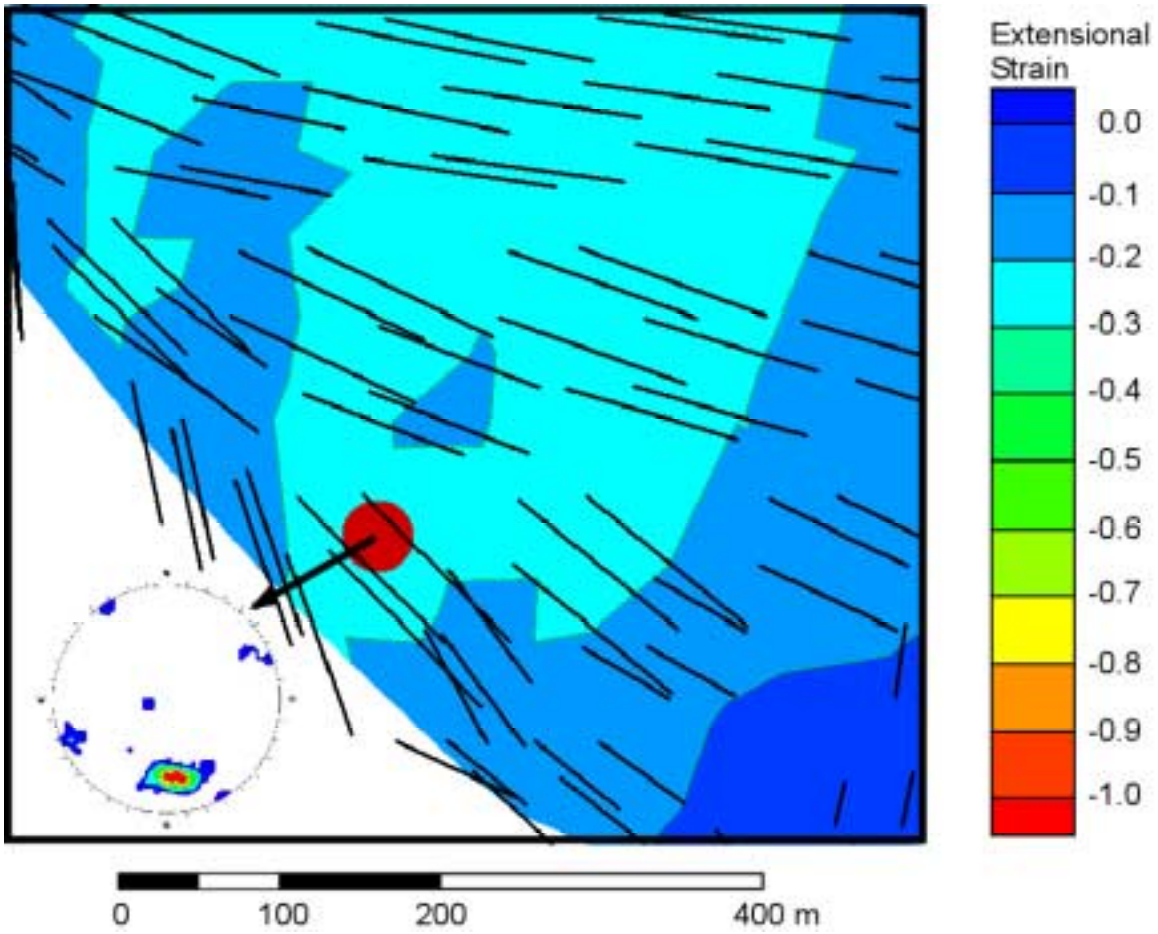

Figure 3-6. Orientation of joints and principal extensional strain for Scanline 10 (Red Peak). The direction of strain is perpendicular to the dominant northeasterly-striking joint set. Black lines indicate trend of principal extension. Lines lengths are proportional to the magnitude of extension.

The remaining scanlines are in other blocks, including subthrust blocks to the southwest of the Red Gully Fault.

Scanline 11 lies a few hundred meters to the southwest of Scanline 10 (Figure 3-1), but is on the opposite of the Red Gully Fault in the footwall block. Unlike the Scanline data from Block 1, the trend of the direction of principal extension (Figure 3-8) is not perpendicular to the strike of the dominant joint set. Rather, the strike is sub-parallel to slightly oblique to the trend of the principal extension vector. It is not clear why this might be the case, although the rock becomes increasingly tightly folded in the southeastern end of the field, in some cases leading to overturned beds and abundant minor faulting. It is possible that the joint pattern measured in outcrop reflects these local structures, which due to their small scale, were not incorporated into the field-wide reconstruction. In general, the joint pattern in outcrop strikes sub-perpendicular to the trend of the Red Gully Fault near the scanline location, which is the extension fracture orientation that would be expected due to compression from the northeast. Why the strains from the palinspastic reconstruction do not trend in a direction subparallel to the Red Gully Fault is not clear.

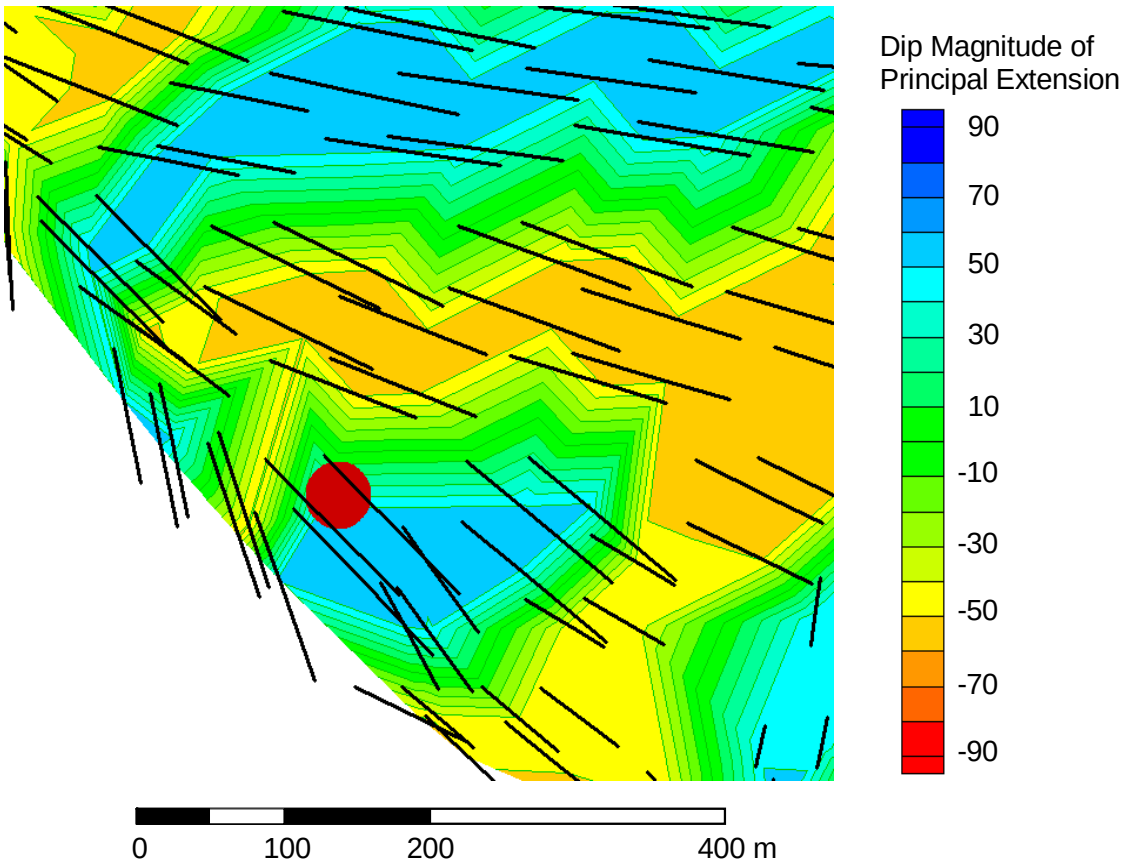

Figure 3-7. Plunge of principal direction of extension (contours) and trend of maximum extension direction. The contours show the amount of plunge of the principal direction of extension. Green shading indicates very shallow plunges. Black lines indicate trend of principal extension. Lines lengths are proportional to the magnitude of extension.

The trend of extension in the northern end of Block 16 (the major footwall block) is dominantly to the east-northeast in the vicinity of Scanlines 1 through 3, and northeasterly for Scanline 4 (Figure 3-10). Scanlines 1 and 2 are close together, and so are represented as a single circle on this plot (Scanline 2 is slightly to the north of Scanline 1). The dominant joint set at Scanline 1 strikes approximately parallel to the trend of principal extension, while the dominant joint set at Scanline 2 strikes approximately perpendicular to the trend of maximum extension. The plunge of the maximum extension vector in the vicinity of Scanlines 1 and 2 (Figure 3-11) is shallow, somewhere on the order of 10°. The dominant joint set at Scanline 2 is thus essentially orthogonal to the maximum extension vector, while the dominant joint set at Scanline 1 is sub-parallel to it. These are the same relations as seen in Block 1.

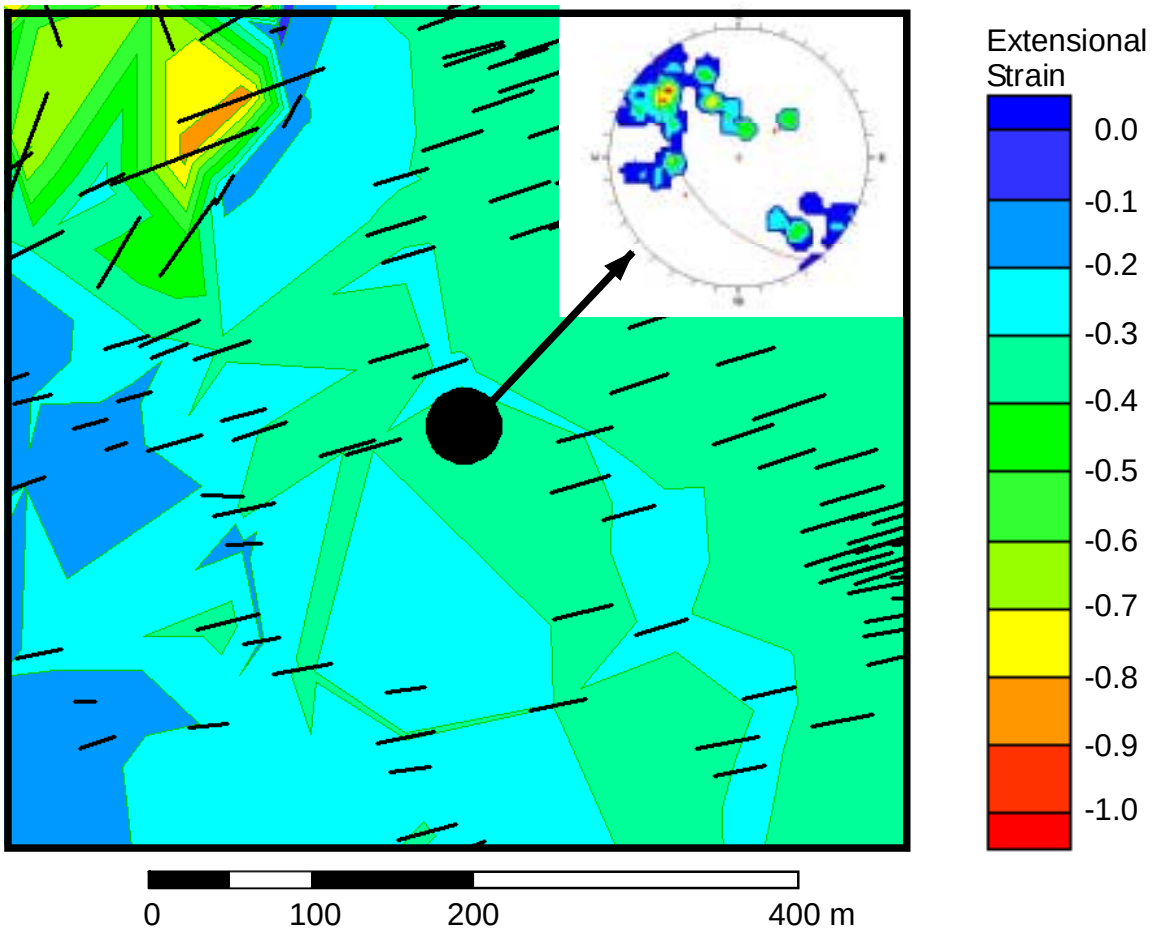

Figure 3-8. Orientation of joints and principal extensional strain for Scanline 11 (Red Peak). The direction of strain is perpendicular to the dominant northeasterly-striking joint set. Black lines indicate trend of principal extension. Lines lengths are proportional to the magnitude of extension.

Scanline 3 at first appears to have little relation to the direction of principal extension. The contour concentration at the center of the stereoplot indicates that the dominant joint set is subhorizontal with a slight southwesterly dip, although there is a small concentration of poles (blue contours) at the edge of the stereoplot that indicates a vertical joint set striking northeast to east-northeast.

However, the plunge of the extension vector in the vicinity of Scanline 3 (Figure 3-11) indicates very steep plunges, on the order of 60° to 70°. Thus, the shallowly dipping joint set in outcrop is with ten degrees or so of being orthogonal to the principal extension vector.

The dominant joint set at Scanline 4 strikes east-northeast and dips steeply. The principal extension vector trends more northeasterly, and dips steeply. The trend of the extension vector becomes more easterly to the east of the scanline location, becoming more nearly parallel.

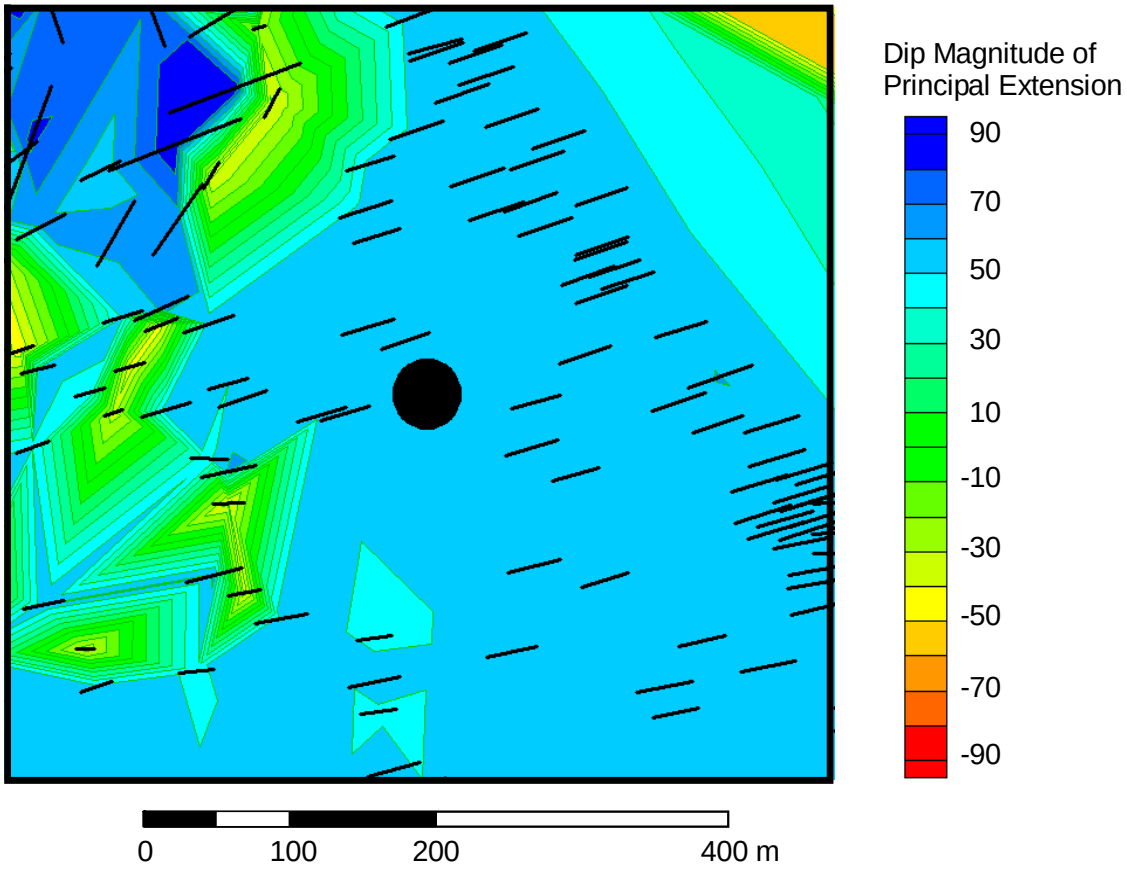

Figure 3-9. Plunge of principal direction of extension (contours) and trend of maximum extension direction around Scanline 11. The contours show the amount of plunge of the principal direction of extension. Light blue shading indicates shallow plunges. Black lines indicate trend of principal extension. Lines lengths are proportional to the magnitude of extension.

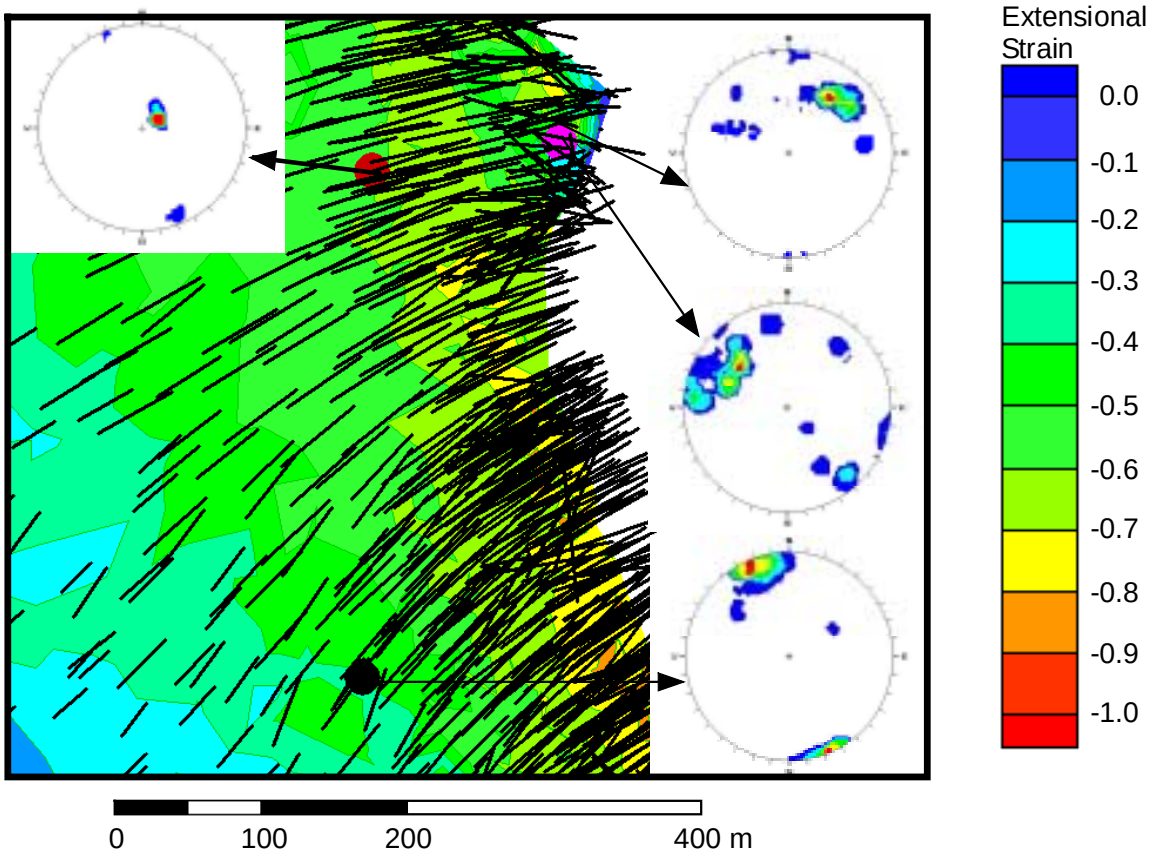

Figure 3-10. Orientation of joints and principal extensional strain for Scanlines 1 and 2 (pink circle), Scanline 3 (red circle) and Scanline 4 (black circle). Black lines indicate trend of principal extension. Lines lengths are proportional to the magnitude of extension.

In general, the relation between the dominant joint sets in outcrop and the principal extension vectors are more complex than they were in Block 1, but still show a consistent relation to the vector. The joint sets seen in Scanlines 1 through 4 and 11 typically strike either parallel to or perpendicular to the trend of the principal extension vector. If the joint set strikes perpendicular, it is generally orthogonal or close to orthogonal to this vector. If the joint set strikes subparallel, then it is often a subvertical set and has no relation with the plunge of the principal extension vector.

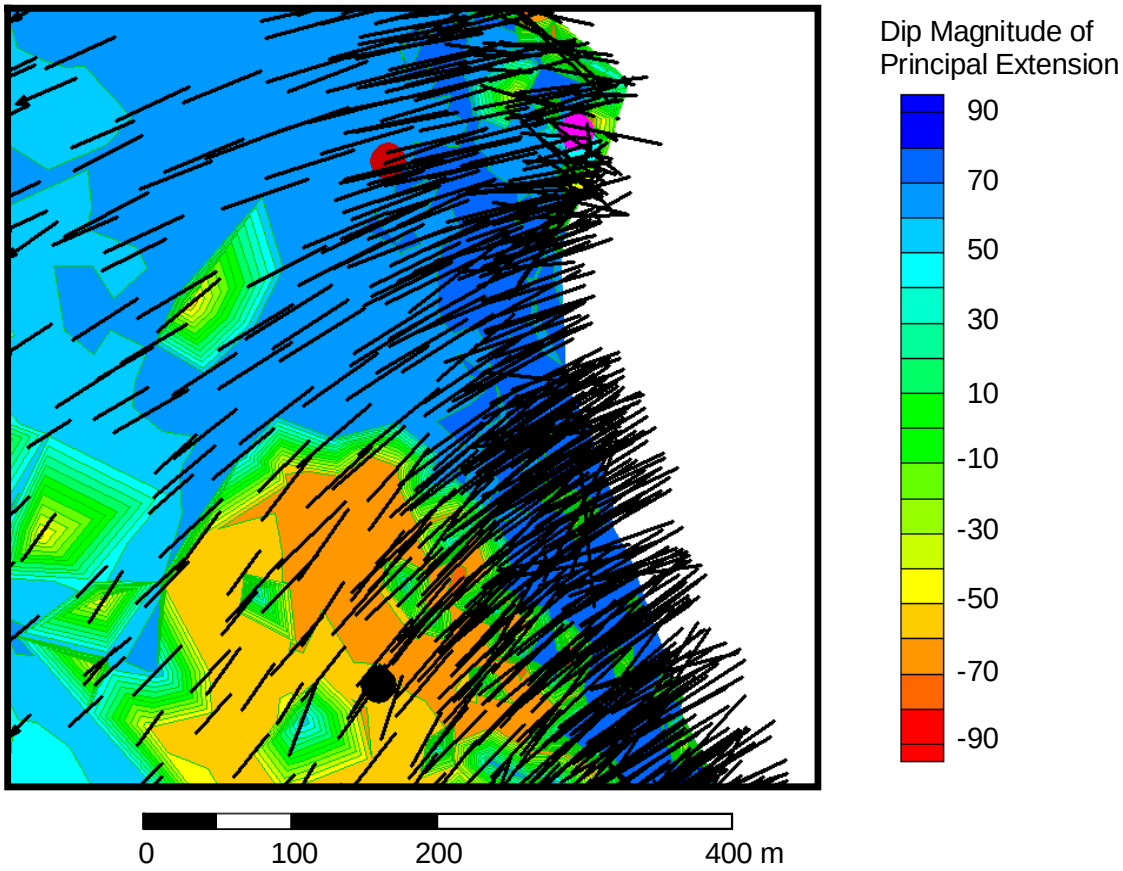

Figure 3-11. Plunge of principal direction of extension (contours) and trend of maximum extension direction around Scanlines 1, 2 (pink circle) 3 (red circle) and 4 (black circle). The contours show the amount of plunge of the principal direction of extension. Dark blue and orange/red shading indicates steep plunges. Black lines indicate trend of principal extension. Lines lengths are proportional to the magnitude of extension.

3.3 Task 3.1 – DFN Flow Model Validation

3.3.1.1 Analysis of the Fracture Image Log from Shoshone 65-37

3.3.2 PURPOSE OF TASK

The purpose of this task is to further validate the DFN model for its usefulness in modeling reservoir connectivity at the scale of many secondary and tertiary recovery processes. This Task has two components:

1) the derivation of flow properties of the reservoir-scale fractures through the analysis of single well and multiwell tests; and
2) an independent comparison of the DFN model to the subsurface flow information that does not incorporate the fluid flow properties derived from the well tests.

3.3.3 COMPARISON OF FRACTURE ORIENTATIONS AND INTENSITY WITH IMAGE LOG DATA

The first step in validating the DFN model is to assess whether the use of the model in which fractures form due to folding strain adequately predicts fracture orientations and variations in intensity. This comparison is carried out by using the strains calculated for the folding stage in the palinspastic reconstruction to predict fracture orientations, and then to compare this with the subsurface image log data.

3.3.3.1 Analysis of Fracturing and Bedding in Image Log from Shoshone 65-37

Figure 3-12 summarizes the dip and dip azimuth of the features identified in the image log for Shoshone 65-37. These features include bedding and fractures. The fractures are further subdivided by the number of pads on which they have been imaged. The size of a fracture is related to the number of pads on which it is imaged (La Pointe and others, 1993), and so the pad count serves as a surrogate for approximate fracture size. Various visual groupings of the fracture dips or dip azimuths are indicated in the figure.

There are three groups of data based on dip azimuth. Each group is outlined by an oval of a different color. The red group is restricted to fractures generally shallower than about 850 ft (259 m) MD. Two other groups, outlined in green and blue, occur below this depth.

There are also distinct differences in bedding dip in these groups. Dashed lines on the figure show the mean dip calculated for these bedding groups.

When the poles to bedding are plotted (Figure 3-13), three distinct sets are evident. The shallow set has a mean pole orientation of 231/18 (designated as Set 2 in the figure). The two deeper sets have mean pole orientations of 232/53 and 042/29, with the more shallowly dipping set (232/53) being more abundant in the data.

Fracture orientations also fall into distinct groups. Figure 3-12 shows the dip and dip azimuth of fractures as a function of pad intersection counts. The 4-pad fractures are probably larger than the 3-pad or the 2-pad, which is likely to be the smallest fracturing encountered by the well.

Both Figure 3-12 and Figure 3-14 suggest that fracturing in Shoshone 65-37 may be segregated by depth. The cumulative fracture count as a function of depth and fracture pad count is shown in Figure 3-14. There is a change in the slope of the cumulative fracture count curves for every pad count set somewhere in the vicinity of 820 ft (250 m) MD. The shallower or upper zone has greater fracture intensity than the lower zone. This plot also shows that 2-pad and 3-pad intersection fractures are almost exclusively restricted to the upper zone.

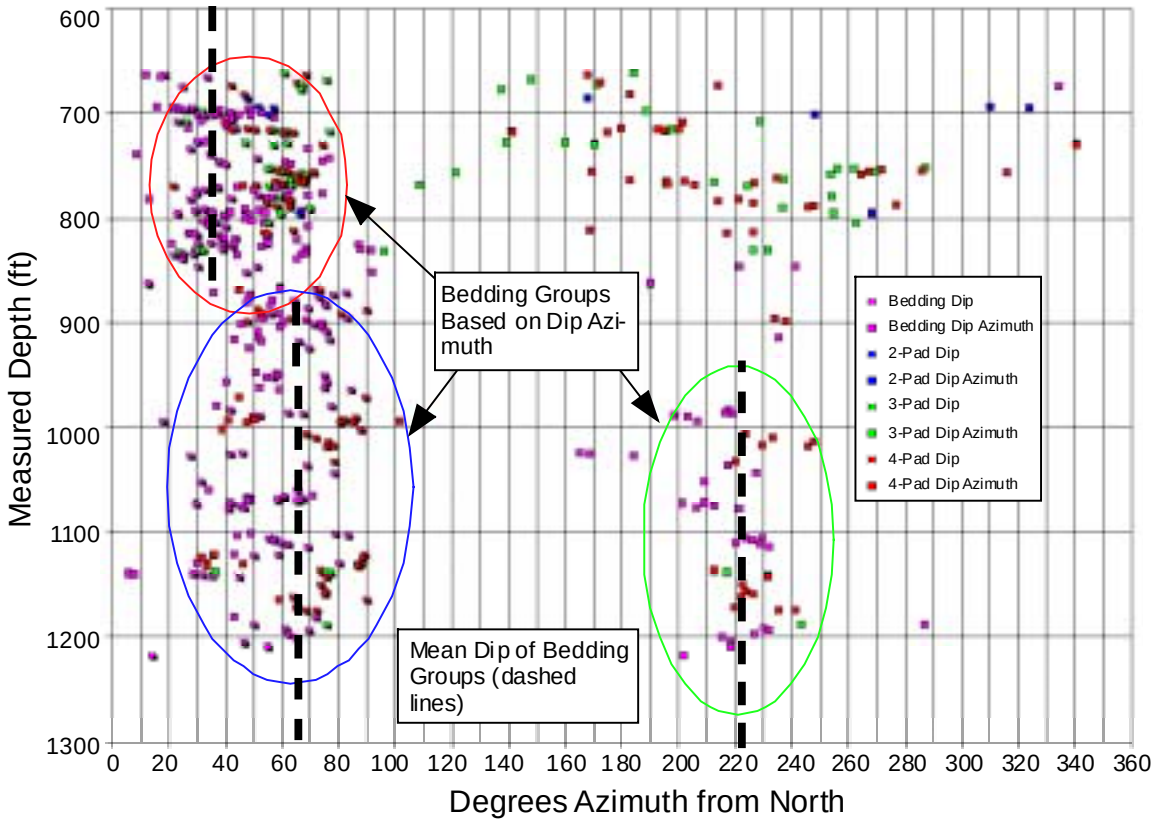

Figure 3-12. Dip and azimuth of fractures identified in image log from Shoshone 65-37.

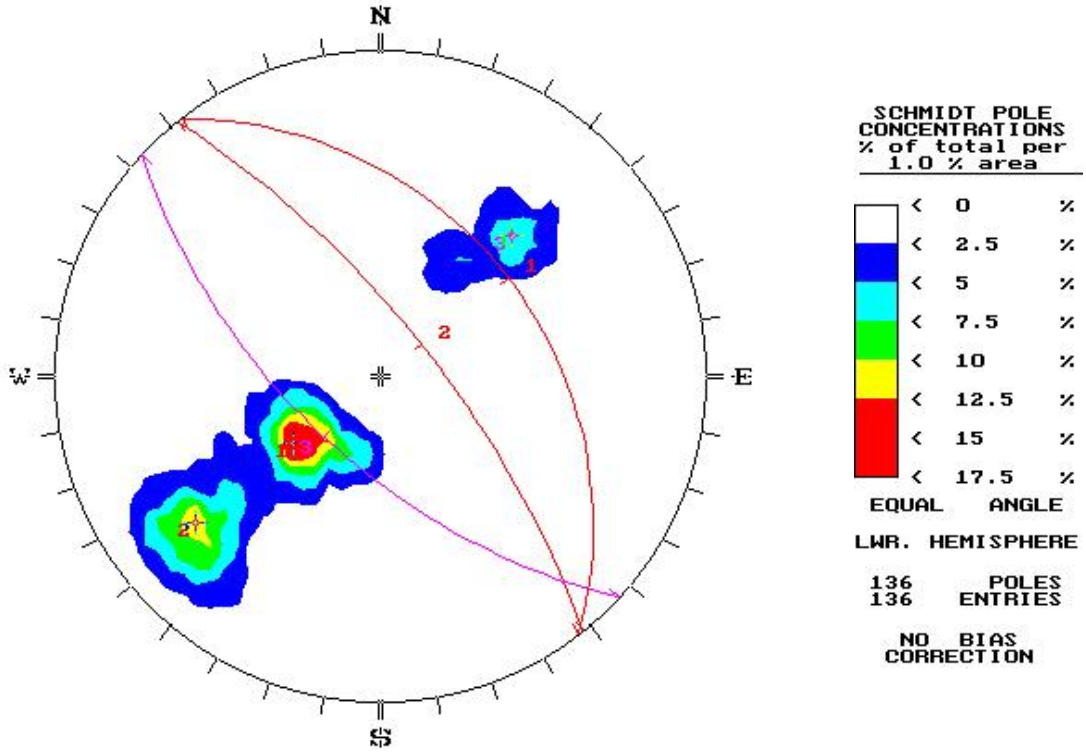

Figure 3-13. Stereoplot of bedding plane orientations in Shoshone 65-37.

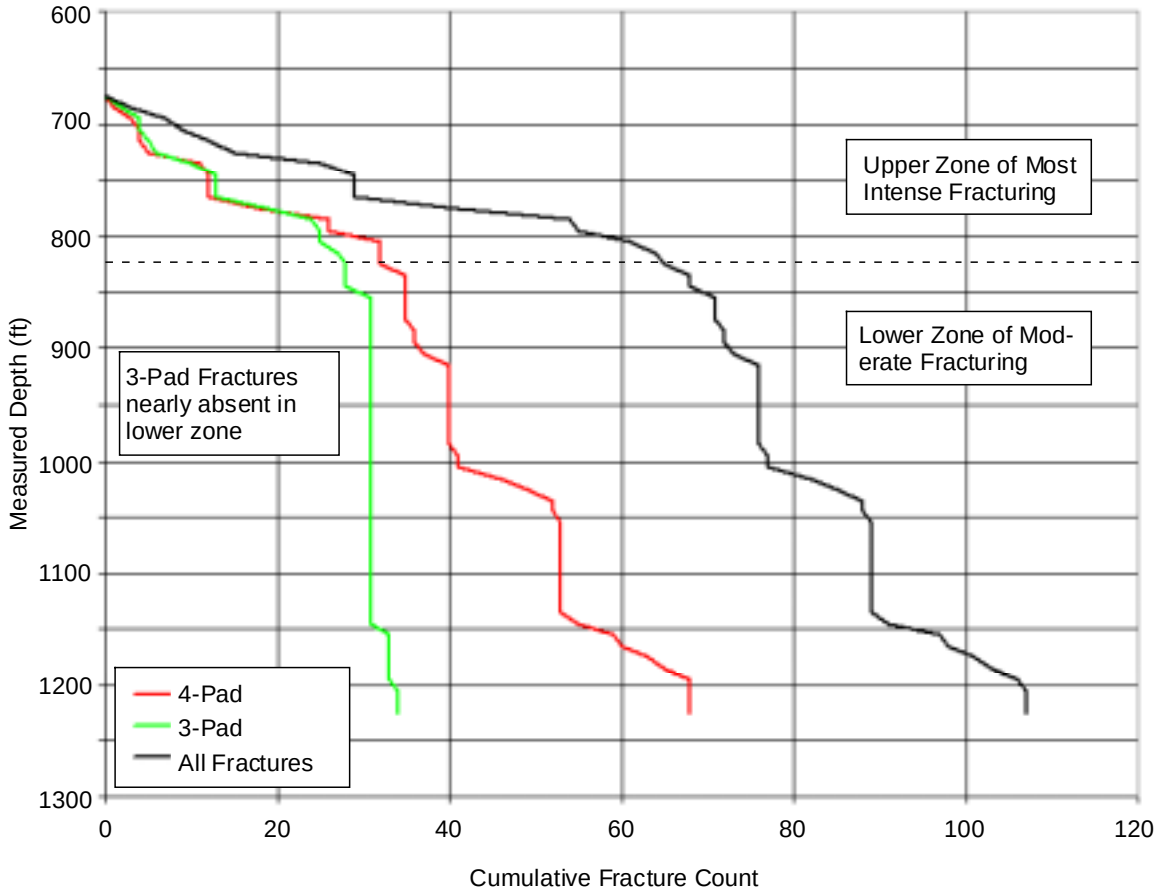

Figure 3-14. Cumulative fracture count with depth as a function of fracture type, Shoshone 65-37.

Figure 3-15 shows the orientations of fractures in the upper and lower zones. The stereoplots do not distinguish sets by pad count. It is clear from this figure that the orientations of fractures in the lower zone differ from those in the upper zone.

The Tensleep marker in this well occurs at around 890 ft. (271.3 m). While not exactly coincident with the boundary between the upper and lower zone, there may be some reworking of the Tensleep Formation in the lower Phosphoria, so that the more characteristic Phosphoria fracture pattern develops some distance above the Tensleep-Phosphoria boundary.

Fractures in the lower zone dip very steeply, and strike N40°W to N50°W. Fractures in the upper zone show a much different pattern, nearly following the great circle (shown on the figure) that describes the bedding in the upper section (232/53). The fact that fracture poles in the upper zone nearly conform to the great circle defined by bedding indicates that they are all nearly orthogonal to bedding. Figure 3-16 further shows that the 2-pad and 3-pad fractures follow a similar pattern, regardless of depth zone.

Moreover, the 4-pad fractures have orientations very similar to the deeper zone. The two pole concentrations for the 4-pad fractures are 227/06 and 048/18, while the deep fractures are 237/07 and 045/15.

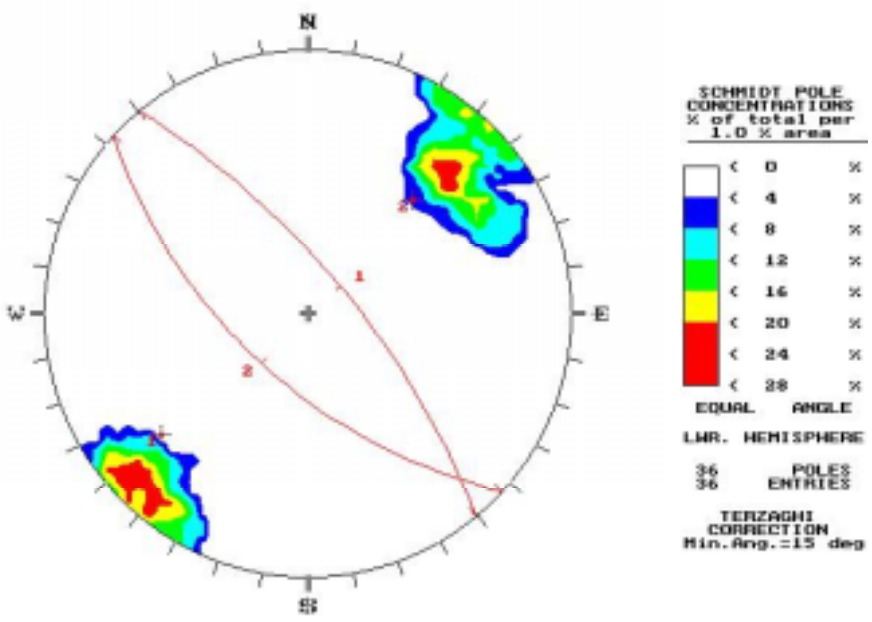

Fractures Below 850ft MD

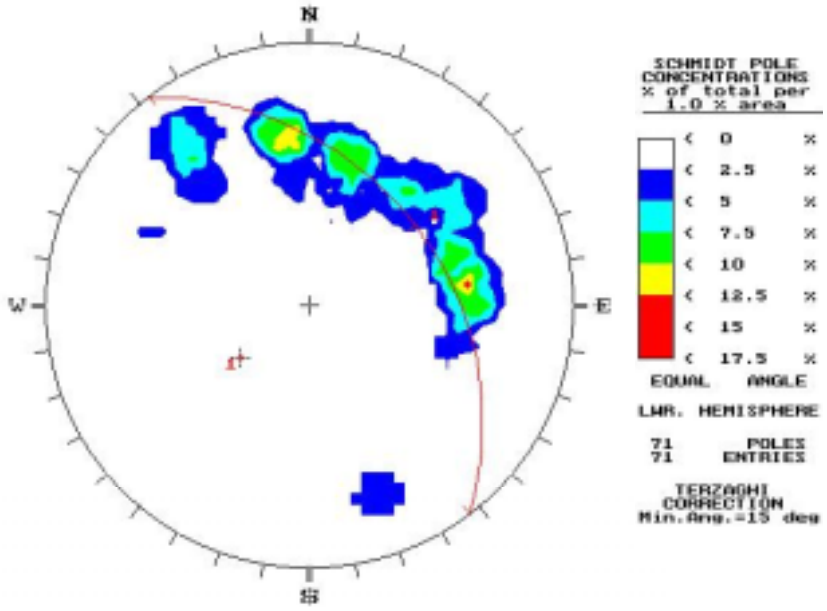

Fractures Above 850 ft (MD)

Figure 3-15. Stereoplots of fractures above and below 850 ft (259 m) measured depth in Shoshone 65-37.

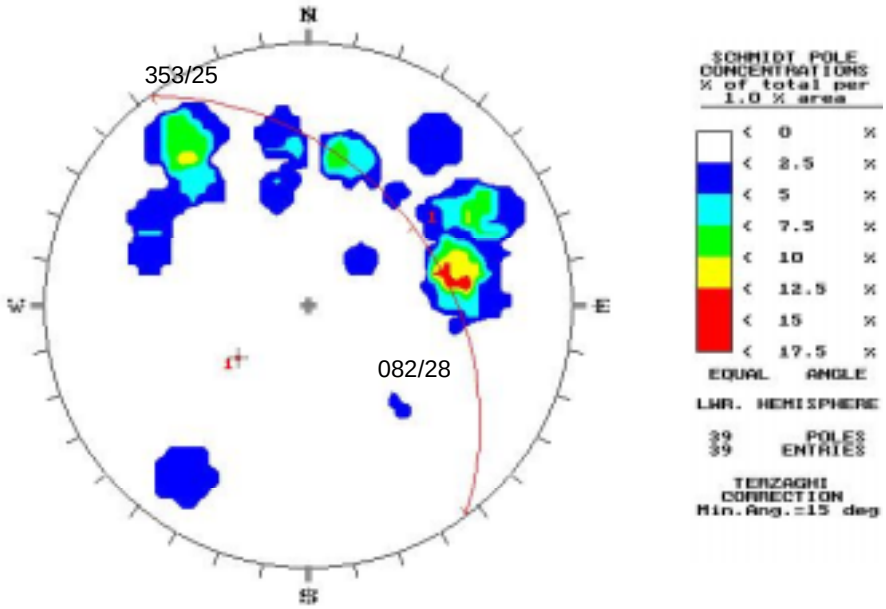

Small fractures (2,3 pad)

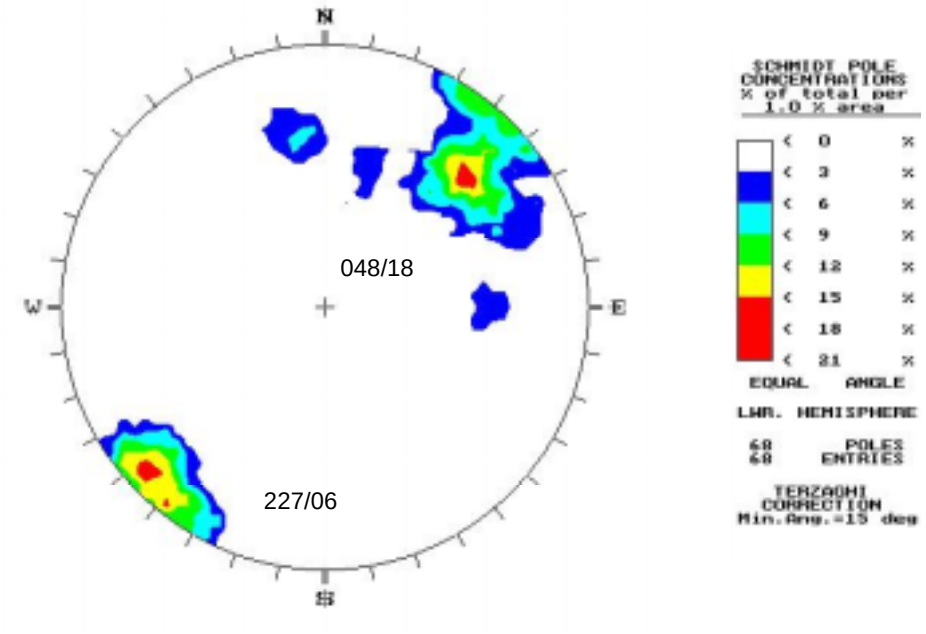

Large Fractures (4 pad)

Figure 3-16. Stereoplot of fractures as a function of pad count, Shoshone 65-37.

These deeper and larger fractures strike parallel to bedding strike, but are not orthogonal to bedding. They make a solid angle on the order of 45° to 60°, unlike the 2-pad and 3-pad fracture sets.

It turns out that when the fracture orientations are compared to the maximum extension vector (Figure 3-17 and Figure 3-18), the large set is orthogonal to the extension vector.

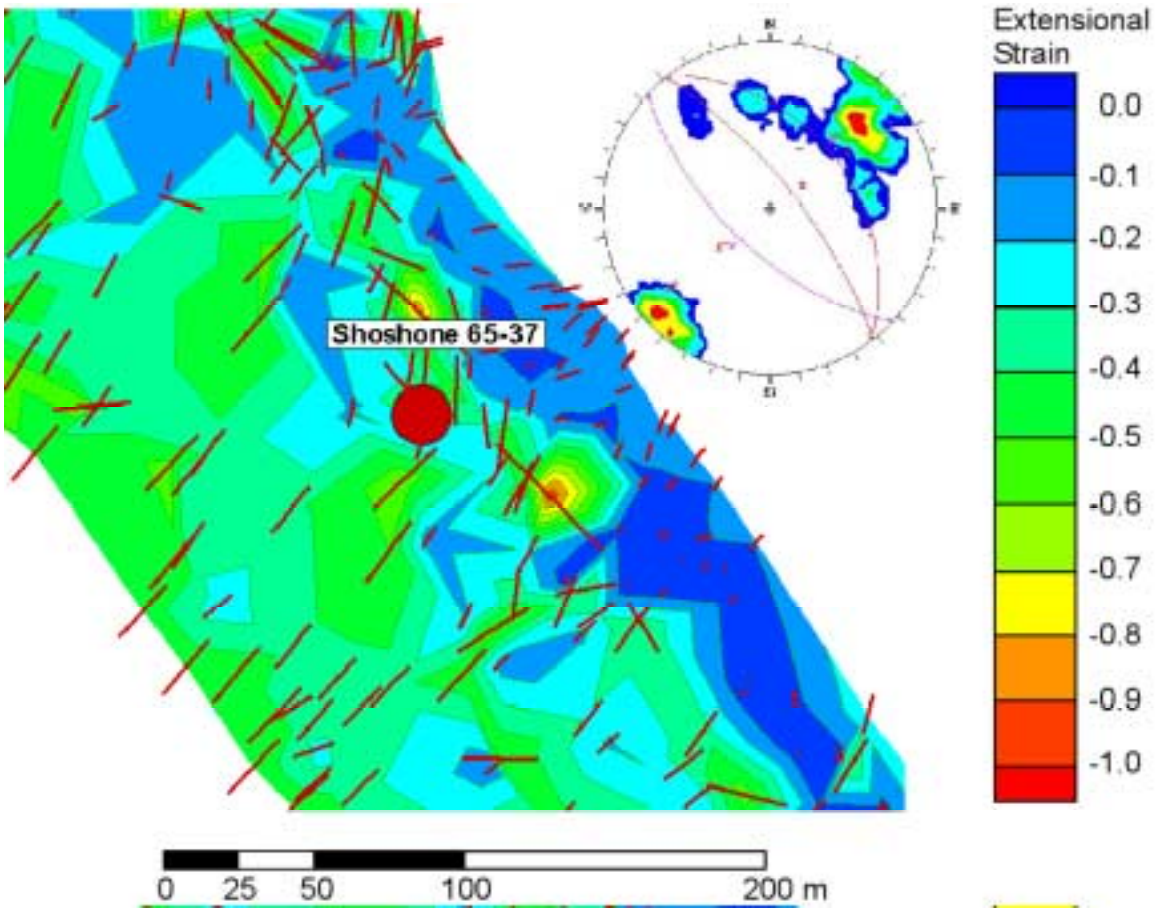

Figure 3-17. Comparison of principal extension trends and strain magnitudes with fractures interpreted from image logs in Shoshone 65-37. The principal extension vector typically plunges about 16°, making it almost perfectly orthogonal with the two, 4-pad sets. Also shown on the inset stereoplot are the three bedding planes.

When the trends of the vectors shown in Figure 3-17 in the vicinity of Shoshone 65-37 are plotted (Figure 3-18), it is clear that the dominant orientation is perpendicular to the strikes of the larger, deeper fractures, as predicted by the strain model.

Overall, the fracturing in the image logs suggests that the Phosphoria, while having a higher fracture intensity, has many more 2-pad and 3-pad fractures, suggesting that the increase in intensity is in part due to the increase in small fracture intensity, although the

4-pad fracture intensity in the upper zone is still somewhat greater than the 4-pad intensity in the lower zone.

Figure 3-18. Rosette of trend vectors of the direction of maximum extension due to folding in vicinity of Shoshone 65-37 based on palinspastic restoration.

3.3.3.2 Analysis of Fracturing and Bedding in Image Log from Shoshone 66-07

The orientations of fractures in Shoshone 66-07 has been previously described by La Pointe and Hermanson (2001). The relation between the extensional strain and the fractures identified in the image log taken from this well is somewhat compromised by the very small (6) number of open fractures interpreted from the image log and the lack of any single trend to the maximum extension vector. However, the very low magnitude of extensional strain is consistent with the small number of open and partially open fractures. The image log data shows that of the six open fractures, three strike approximately east-west, two strike northwest, and one strikes north-northwest. The partially open fractures show a much greater variety of strikes, including the orientations seen for the open fractures, and a northeasterly striking set not seen in the open fracture population.

There appear to be about three common trends of the extension vector in the vicinity of Shoshone 66-07: northeast, northwest and north-south (Figure 3-19). This would suggest joint orientations with strikes of northwest, northeast and east-west, respectively. Thus, the strikes of the three fracture sets interpreted from the image logs and the trends of the maximum extension vectors are approximately perpendicular. In general, the fracture strike orientations, and the small number of fractures, are consistent with the trend of the principal extension vector and the small magnitude of the extensional strain.

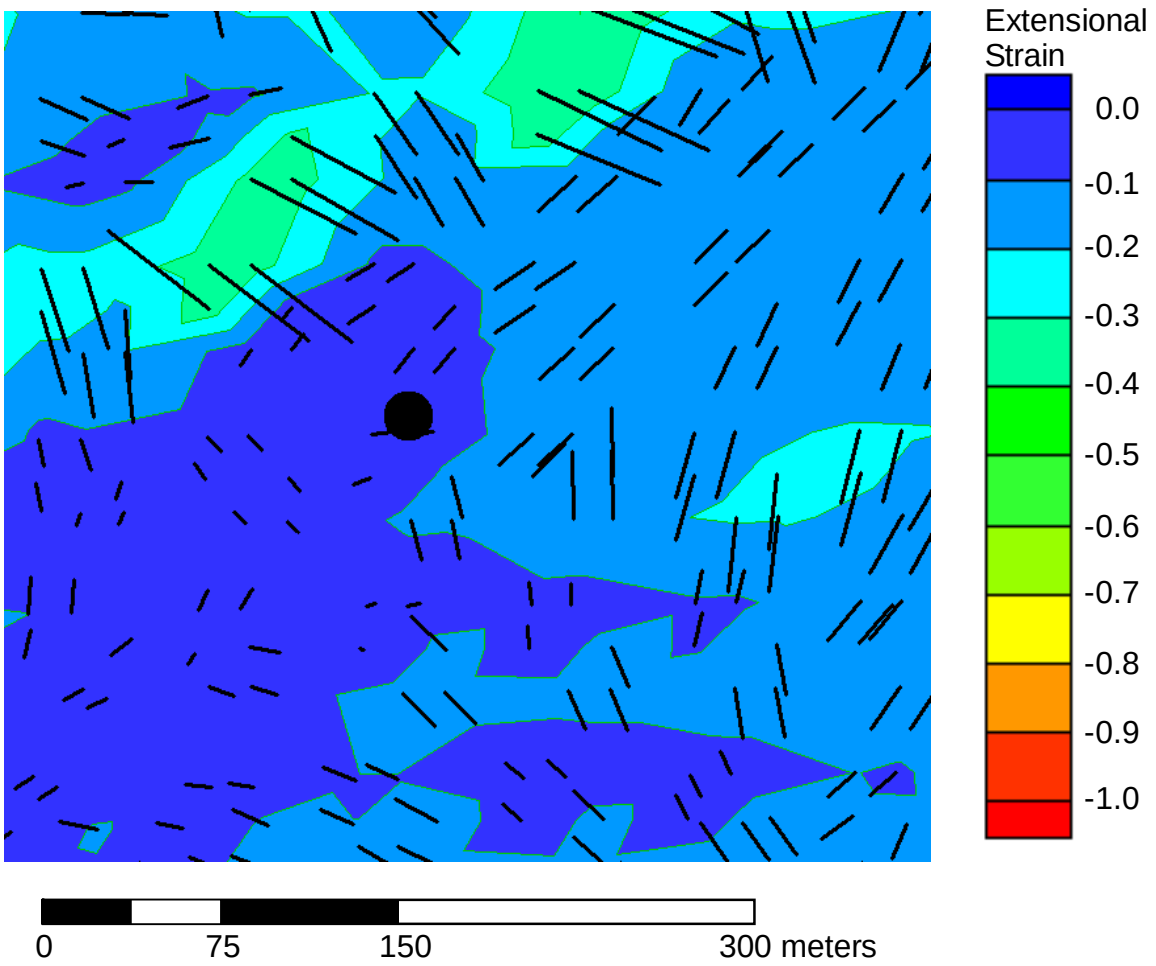

Figure 3-19. Trend of principal extensional strain in the vicinity of Shoshone 66-07. Black lines indicate the trend of the extensional strain, while contours and line length indicate the magnitude.

Overall, the fracture intensity difference between Shoshone 66-07 and Shoshone 65-37 is consistent with the difference in extensional strain magnitude. Figure 3-19 shows that Shoshone 66-07 lies in an area of low strain, on the order of –0.1 to –0.2. Shoshone 65-37, on the other hand, lies in a region where strains vary from –0.3 to over –0.5 (Figure 3-17).

Thus, not only do the fracture orientations for Shoshone 66-07 and the large fractures for Shoshone 65-37 appear to conform well to the folding strain calculated from the palinspastic reconstruction, the variation in extensional strain magnitude corresponds to the fracture intensity differences seen in the image logs. This good correspondence suggests that the fracture geometry can be usefully predicted by the folding strain maps calculated from the structural reconstruction.

3.3.4 DERIVATION OF FRACTURE FLOW PARAMETER VALUES FROM WELL TESTS

3.3.4.1 Local model

In order to simulate the single well injection/fall-off test a small DFN model was constructed around well Shoshone 65-02. The locations of key wells are shown in Figure 3-20. Two sub-vertical fracture sets were generated based on the orientation of the strain field in the vicinity of Shoshone 65-02 with one set sub-parallel (L) and one set sub-perpendicular (T) to the regional strain field near this well. Geometric parameters for these two sets are given in Table 3-1. A single 250 m x 260 m x 100m realization of this fracture network is presented in Figure 3-21. For the local scale simulation both fracture sets are given the same aperture size and permeability in order to calibrate the network and reservoir *kh*, while in the following section the relative permeabilities of the two sets is varied to calibrate to the relative breakthrough times of each of the wells.

Parameters for the local scale DFN model were based on the orientation of the strain field in the vicinity of the injection well Shoshone 65-02. Fracture size and fracture intensity were initially chosen to be consistent with reservoir and the expected intensity of major conductive features. The effect of varying length and the relative intensity of the two fracture sets are analyzed in the next section.

The network that results from these input parameters is well-connected network composed primarily of sub-vertical fractures. Six sided fractures are used with an aspect ratio of one, and these fractures are large enough that most reach from the top to the bottom of the reservoir. In order to calibrate the effective network permeability, a constant permeability was applied to each fracture within both the T and L fracture sets. The permeability thickness of the reservoir depends on both the permeability of the individual fractures within each set, and the overall connectivity of the network. The connectivity of the network for the local model depends on the fracture intensity and fracture length. The effects of applying different permeabilities for each fracture set are discussed further below, and the impact of changing the relative intensities of each of the fractures sets, and the size of the fractures is also examined.

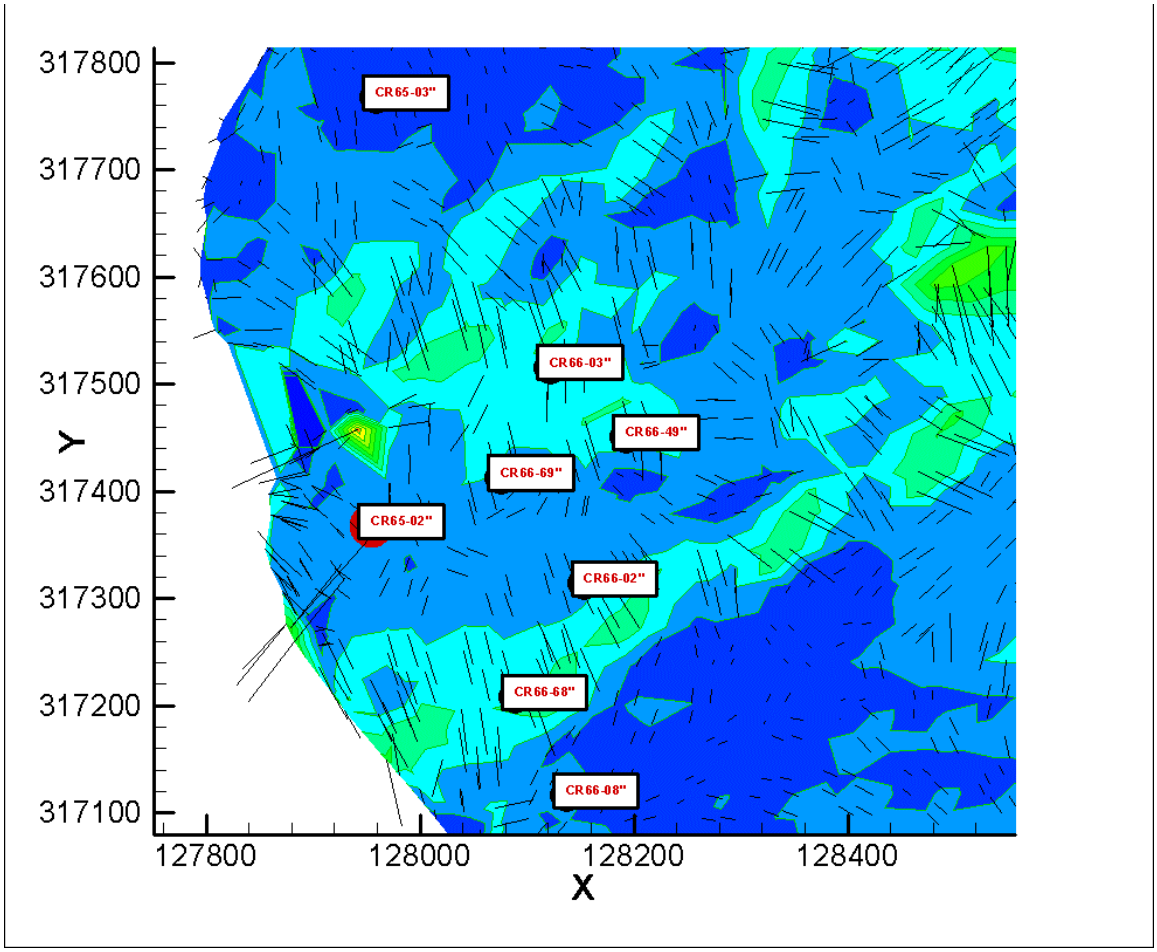

Figure 3-20. Key well locations for nitrogen injection test.

A snapshot of the pressure differential due to nitrogen injection at Shoshone 65-02 is presented in Figure 3-22. Close to the well the pressure distribution is strongly affected by local discrete features. As the pressure field moves away from the injector, the effect of the individual features is averaged out so that an almost circular radius of influence appears. The circular radius of influence is not expected in the field and is likely a consequence of the two fracture sets being assigned equal permeability. The pressure tends to migrate along the T-set direction faster than along the L-set direction because of the higher fracture intensity in the T-set.

A series of simulations were run in which individual fractures were assigned permeabilities averaging from 1 to 1000 millidarcies (Figure 3-23). Each of these pressure curves has a similar response character other than an increase in effective permeability for an increase in fracture permeability. Each derivative shows a positive half-slope at early times indicating a restriction in the immediate vicinity of the well. After this early period the derivative drops off as the pressure field expands out of the "entry feature" and into the fracture network. Once the pressure field expands to the

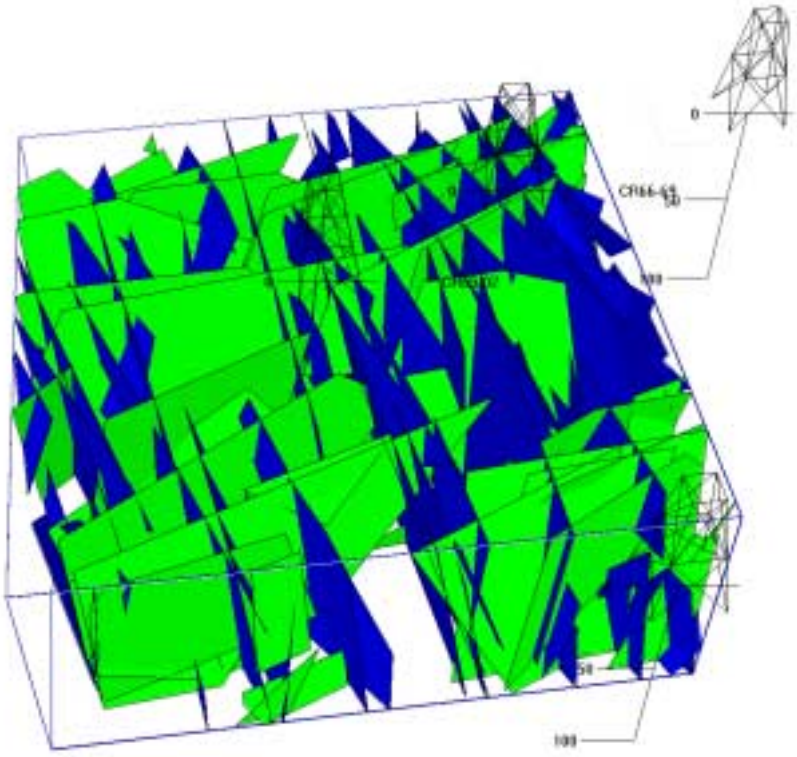

Figure 3-21. Local scale DFN model for Shoshone 65-02.

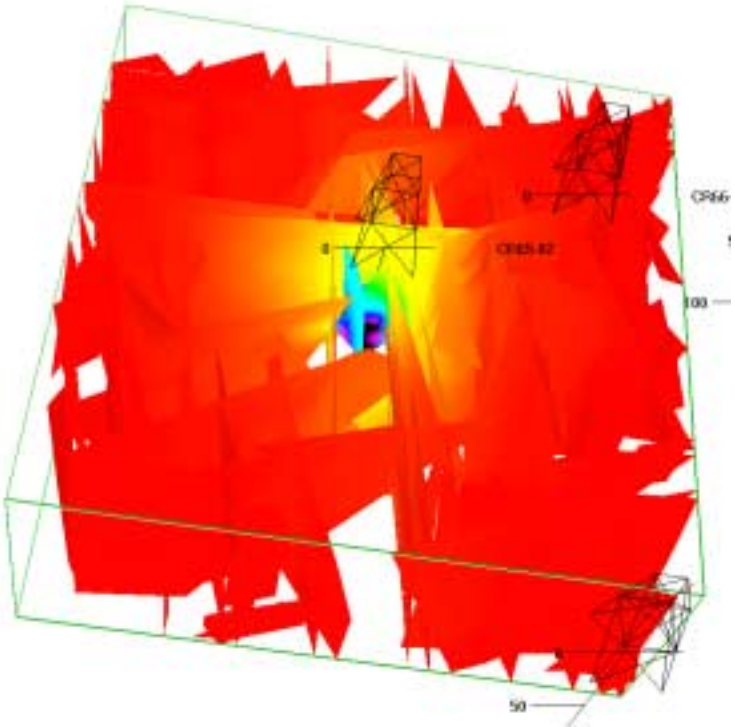

Figure 3-22. Pressure snap shot at 100 hours. Color indicates change from initial reservoir conditions in red.

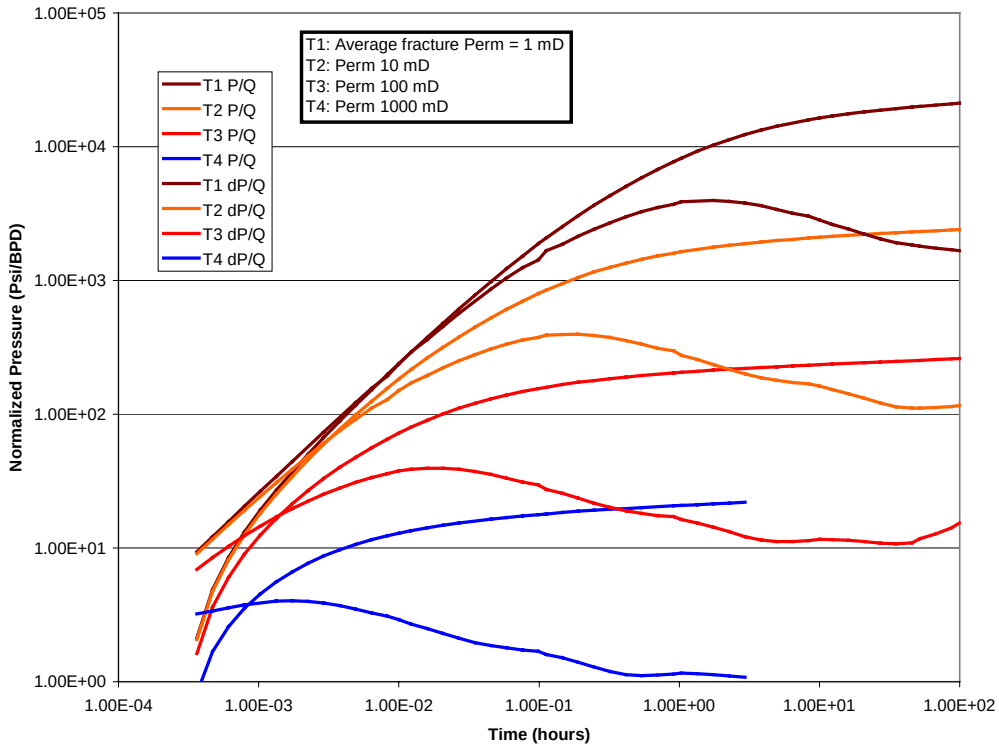

Figure 3-23. Build up test simulations for average fracture permeabilities of 1 to 1000 mD

point where it is constrained by the upper and lower boundaries of the reservoir, the derivative goes to a slope of zero, similar to classic radial flow. The value at which the derivative levels off is a function of the permeability of the fracture system, with smaller derivative values consistent with higher reservoir permeabilities. Conversely the derivatives can be plotted as a function of permeability thickness (Figure 3-24), and the value of the calibrated fracture permeability can be determined.

Fracture Set	**Orientation**			**Size: Log Normal Distribution**				**Intensity**
	Mean Pole	Mean Plunge	Fischer Dispersion	Mean	St.Dev	Min	Max	P_{32}
Strain Perpendicular	73	0	30	50	30	20	200	0.05
Strain Parallel	163	0	30	50	30	20	200	0.03

Table 3-1. Geometric inputs for local DFN model

There appears to be a linear relationship between assigned fracture permeability and the corresponding effective *kh* of the reservoir. Based on this it appears that the average fracture permeability must be approximately 40 mD to obtain a reservoir *kh* of 408 mD-m. The 40-mD value can be compared to spinner log data in order to calibrate the model to observed values of flowing features. This value of 40mD is consistent with the order of magnitude of flowing features observed in similar reservoirs. The 40 mD represents an average value for an individual fracture. When a network is formed by a number of fractures, the network permeability is much greater.

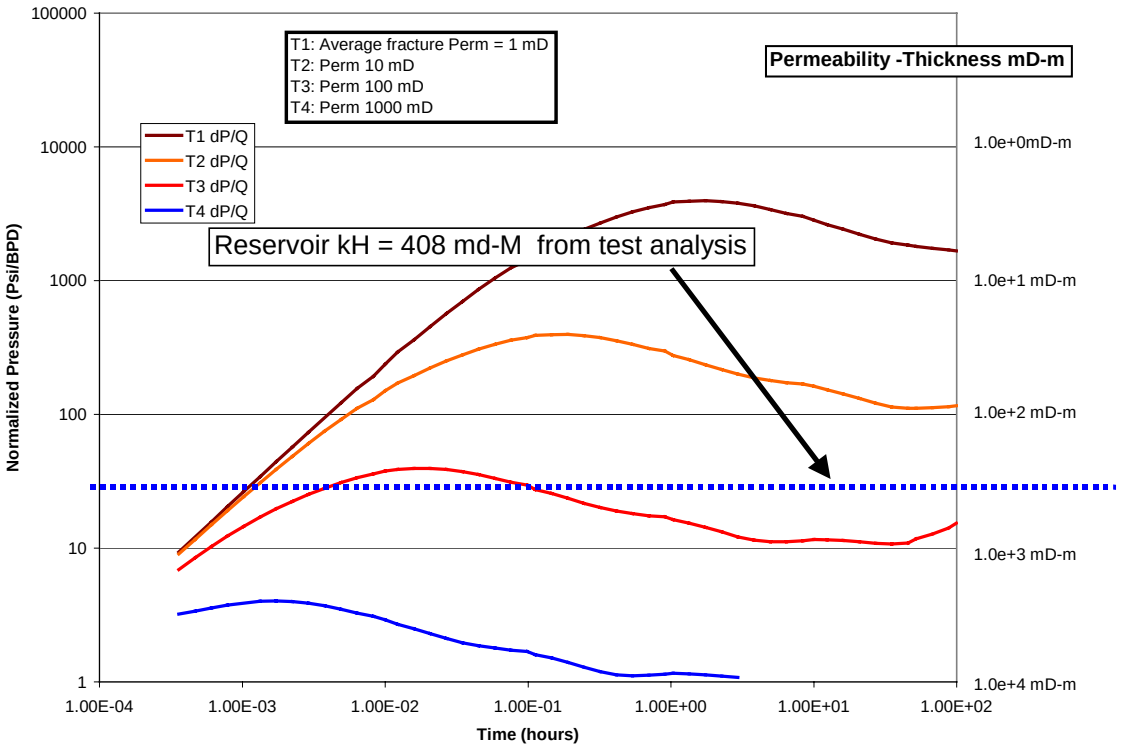

Figure 3-24. Permeability thickness values based on late-time derivative curves

3.3.4.2 Breakthrough match

Although the single well simulation will help calibrate the fracture geometry and permeability necessary to match reservoir *kh*, simulating pressure response in the pumping wells is necessary to determine the relative permeability of one set to the next. For this reason a regional scale model was simulated using the calibrated parameters from the local scale model (Table 3-1) over the entire test area (Figure 3-20). The underlying control grid geometry is shown in Figure 3-25. Additionally, the strain field from the palinspastic reconstruction was used to control both fracture intensity and fracture orientation. Two sets were generated: (1) A T-set perpendicular to the local strain field orientation; and (2) an L-set sub-parallel to the local strain field vector. One realization of this network is presented in Figure 3-26. The regional model encompasses

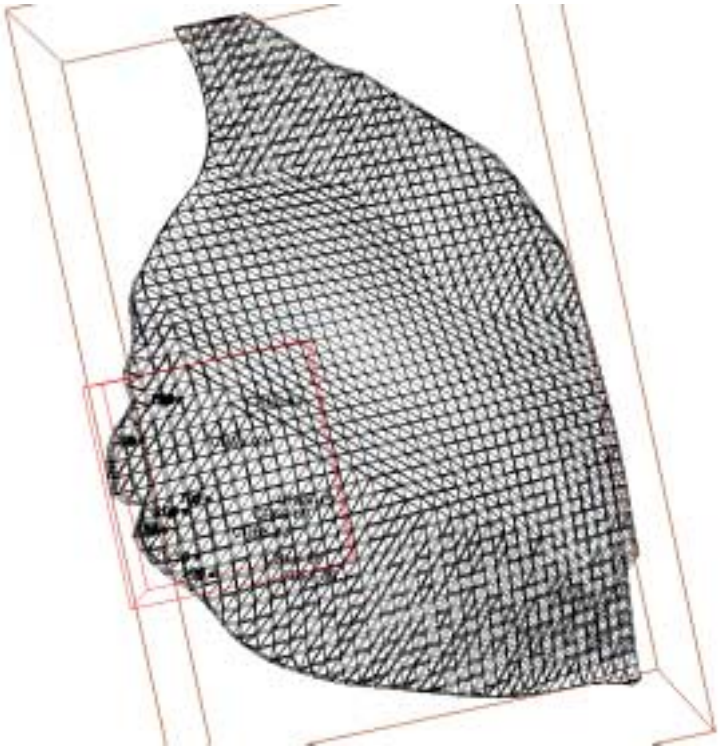

Figure 3-25. Strain grid for development of regional scale model

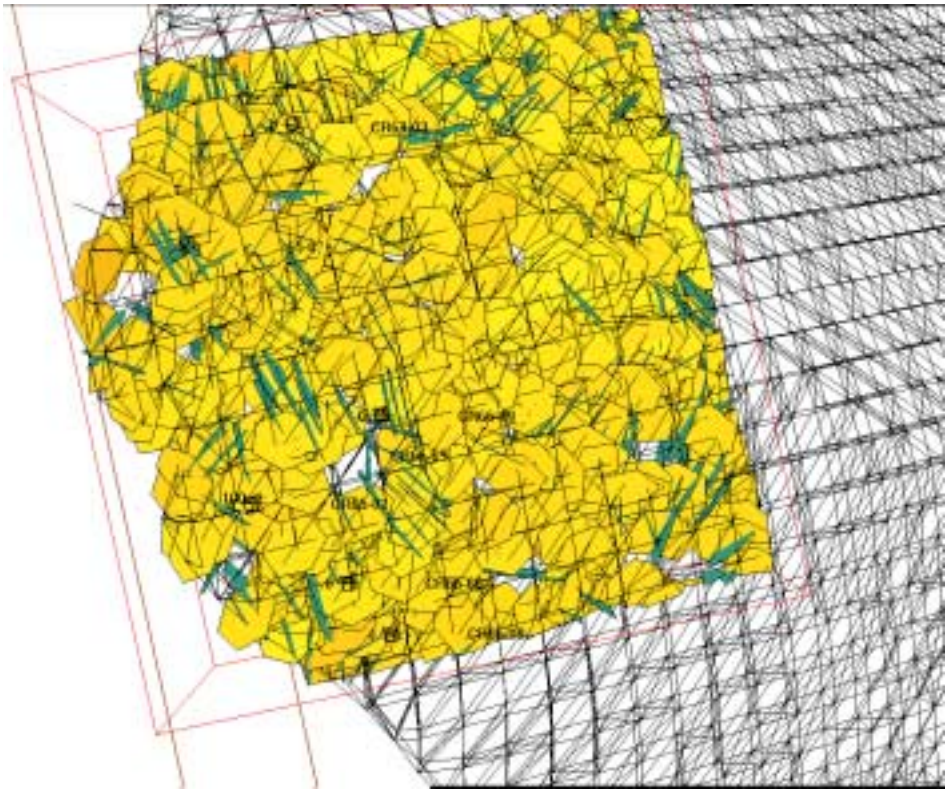

Figure 3-26. Regional scale DFN model populated by strain perpendicular and strain parallel fracture sets.

a 1 km x 1km region of the strain grid. This includes the test well and 6 production wells in which pressure values were monitored. Fracture intensity varies within the model according to the extensional strain values in each of the grid cells. These strain values were determined during the palinspastic reconstruction work described previously. The extensional strain is summed throughout the grid region, and then a normalized strain is calculated for each grid cell. An average fracture intensity or P_{32} is assigned to the fracture system, and then the normalized strain is used to calculate an individual P_{32} value for each grid cell. In this manner the fracture intensity is varies throughout the model domain while the average fracture intensity of each fracture set, averaged over the entire grid, can be scaled up or down.

In addition to the magnitude of the strain field, the orientation is used to determine the orientation of the T and L fracture sets. For the early realizations the T-set is exactly perpendicular to the local strain field and the L set is sub-parallel to the strain field.

In the resulting DFN model the T-set has a 25% higher fracture intensity than the L-set, and tends to dip at shallower angles than the L-set. As a result of the varying strain grid the fracture intensity varies throughout the model.

An average value 0.09 m2/m3 was used for the fracture intensity, with a linear correlation between strain magnitude and local intensity. A plot of the resulting P_{32} values is given in Figure 3-27. Fracture intensity in the model region is dominated by cells with a calculated fracture intensity of 0.1 m2/m3 and slightly higher. A few scattered grid cells have P_{32} values higher than 0.015 m2/m3. Cells with fracture intensities below 0.025 tend to appear in clusters. One of these low permeability clusters occurs immediately to the north-east of Shoshone 65-02, the injection well. As a result there tend not to be connecting fractures immediately to the north-east of Shoshone 65-02. This becomes important, as this direction has been identified by the nitrogen break-through as a direction of preferential permeability.

As had been seen in the breakthroughs during the nitrogen injection there is some directional trends suggested in the permeability. The time before the pressure field travels from the injector to the producer is a function of both the distance between the two wells, and the direction from one to the other.

Three simulations of the regional model were run, in order to evaluate the relative permeabilities of the T and L- fracture sets. In the first simulation the ratio of the T to L set permeabilities was set to 1, i.e. the permeability assigned to all fractures was identical. In the second simulation the permeability assigned to fractures in the T-set was 10 times that assigned to fractures in the L-set (ratio of 10:1). In the third simulation the ratio was reversed (0.1) with fractures in the L-set assigned a permeability value 10 x the permeability assigned to fractures in the T-set.

One of the key features of the injection experiment was that breakthrough times for well Shoshone 66-49 were earlier than for well Shoshone 66-69, although Shoshone 66-68 is closer to the injector. The low intensity of the fracture network between the injection

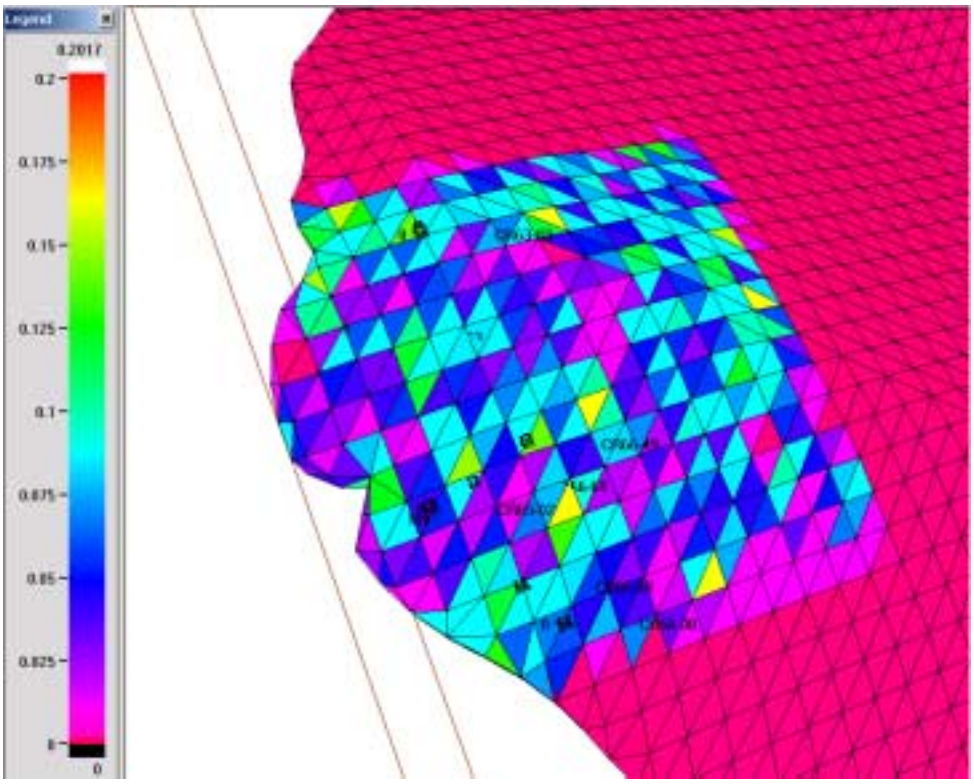

Figure 3-27. Fracture intensity values (P_{32}) resulting from an average P_{32} value of 0.08

well and Shoshone 66-49 suggests that a large permeability difference must occur between the T and L fracture sets. When the permeability ratio is set so that the permeability of the L-set is 10 times the permeability of the T-set the pressure evolve in a north east direction more quickly than in the north-west/south-east direction, consistent with the fast arrival time at Shoshone 66-49.

When the permeability assigned to each of the two sets is equal breakthrough occurs in the following order: well 66-69, 66-68, 66-49, 66-8, 65-03 and finally 63-03. These pressure breakthroughs are generally a function of distance from the injector, notably that 66-68 breaks through before 66-49.

Three pressure snap-shots are presented to illustrate the effect of changing the relative permeabilities of the strain-perpendicular and strain-parallel sets. In Figure 3-28 the regional model is presented with the average fracture permeability in both sets identical (ratio of Set1 k: Set2 k =1). In Figure 3-29, a permeability ratio of 10:1 is presented and a 1:10 ratio is presented in Figure 3-30. As is apparent from these plots the second fracture set must have a lower permeability in order to explain the high NE permeability trend, and the low SE permeability trend.

In Figure 3-31 the change in pressure for wells Shoshone 65-02, Shoshone 65-49 and Shoshone 66-68 is plotted for the regional model where the permeability of each fracture set is equal (i.e. ratio of Set1 k: Set2 k =1). The breakthroughs for Shoshone 65-49 and

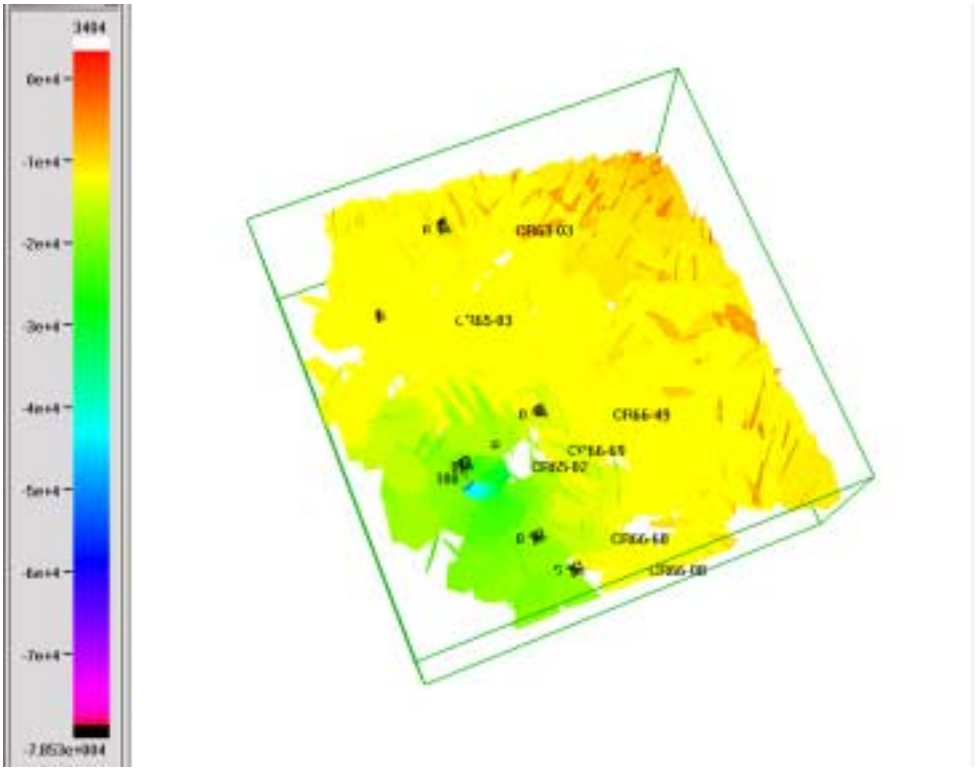

Figure 3-28. Pressure snapshot of injection in regional model with permeability ratio Set1:S

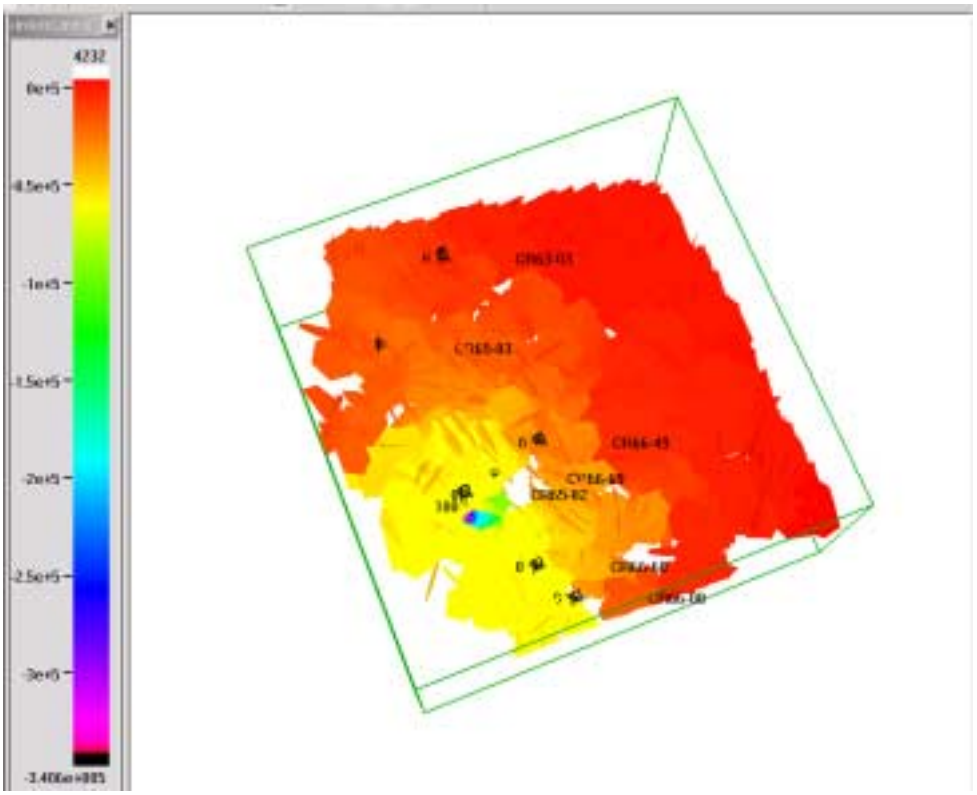

Figure 3-29. Pressure snapshot of injection in regional model permeability ratio Set1:Set2 = 10. This simulation shows earlier pressure breakthrough to the north-west and south-east rather than to the north-east set2 = 1

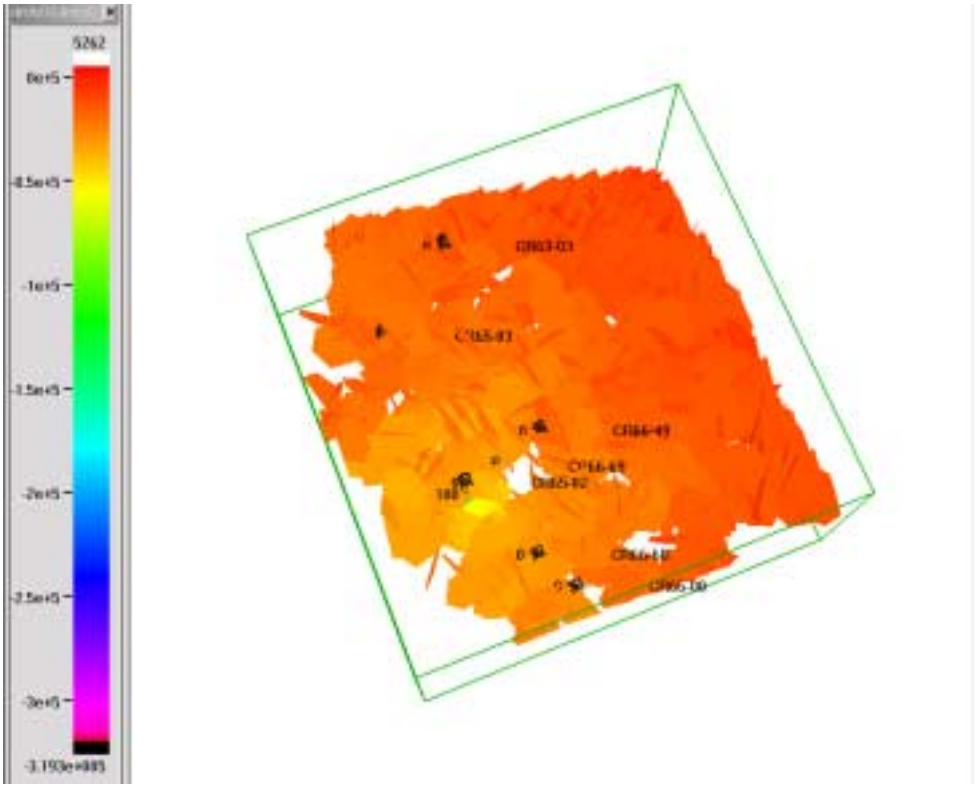

Figure 3-30. Permeability ratio Set1:Set2 = 0.1.

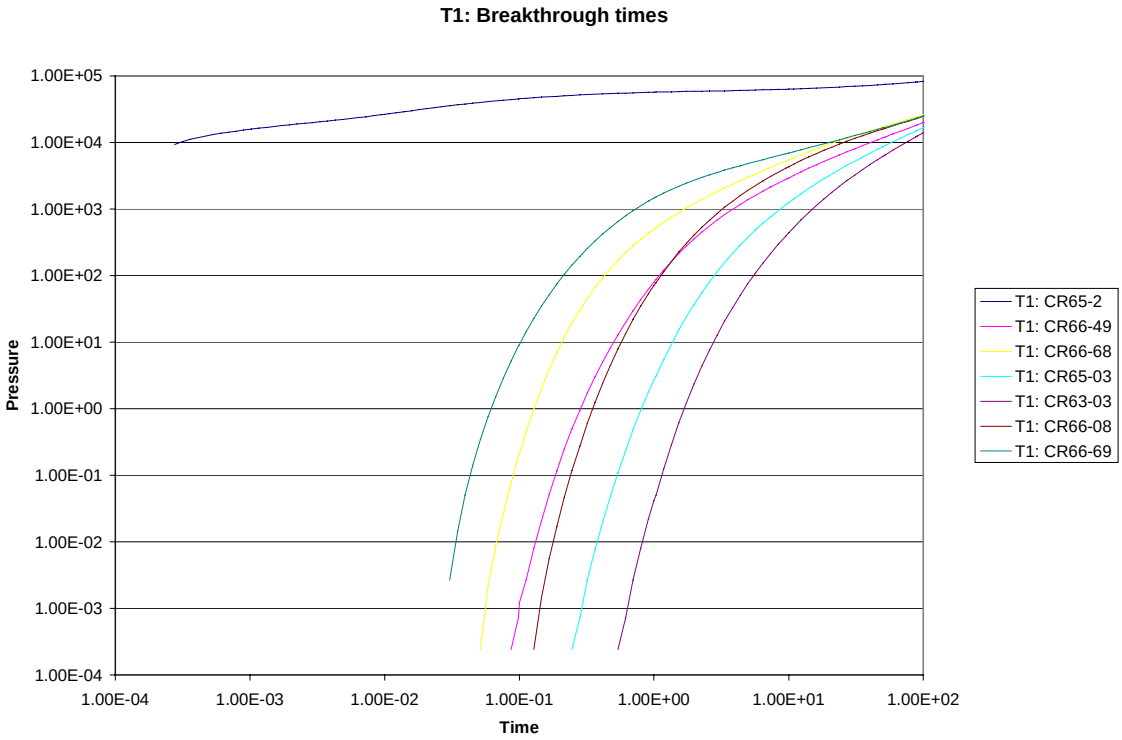

Figure 3-31. Change in pressure for wells 52, 49 and 68. Pressure response is quicker for Shoshone 66-68 because it is closer to the injection in Shoshone 65-2

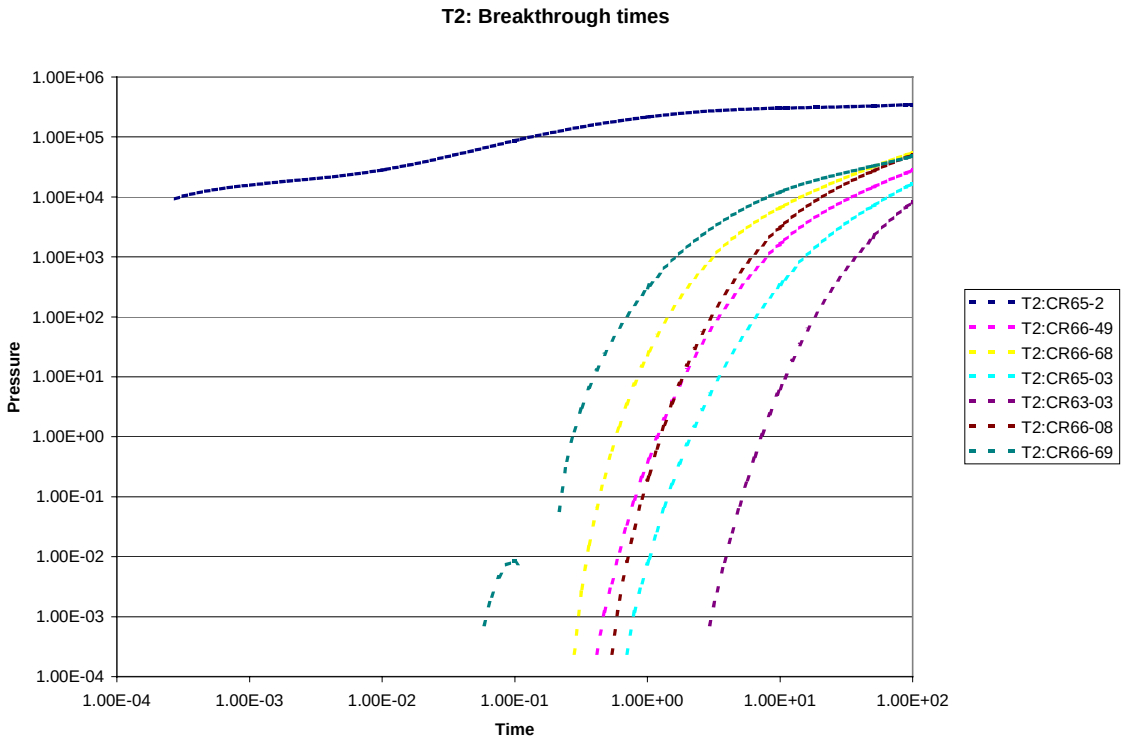

Figure 3-32. Change in pressure for wells 65-52, 66-49 and 66-68. Pressure response is quicker for Shoshone 66-49 although Shoshone 66-68 is closer to the injection in Shoshone 65-2.

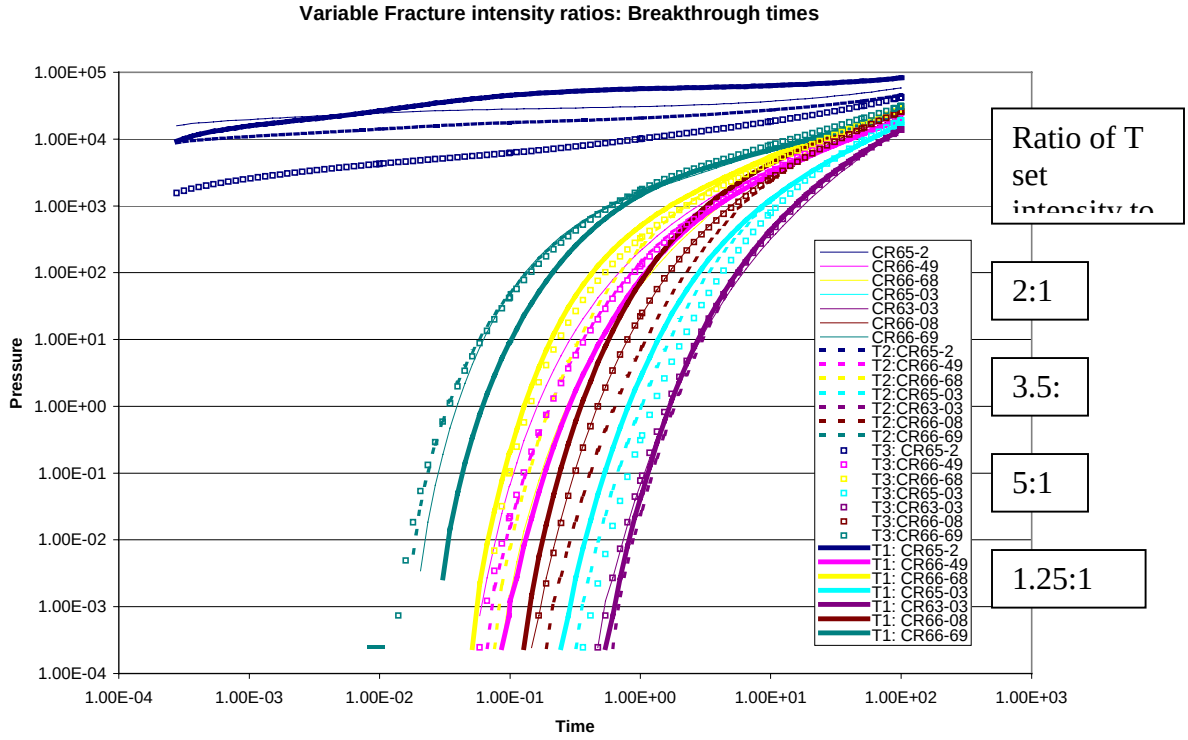

Figure 3-33. Breakthrough curves for all wells for varying the ratio of the fracture intensities between the T and L sets.

Fracture intensity for T and L sets				
Run	T-set	L-set	Ratio	Total
1	0.05	0.04	1.25	0.09
2	0.06	0.03	2	0.09
3	0.07	0.02	3.5	0.09
4	0.075	0.015	5	0.09
5	0.0819	0.0081	10.11111	0.09

Table 3-2. Input parameters for varying fracture intensities in T and L sets

Fracture set intensity (P_{32})			
Run	T-set	L-set	Fracture Length
1	0.06	0.03	50
2	0.06	0.03	75
3	0.06	0.03	100

Table 3-3. Input parameters for breakthrough test with variable fracture length

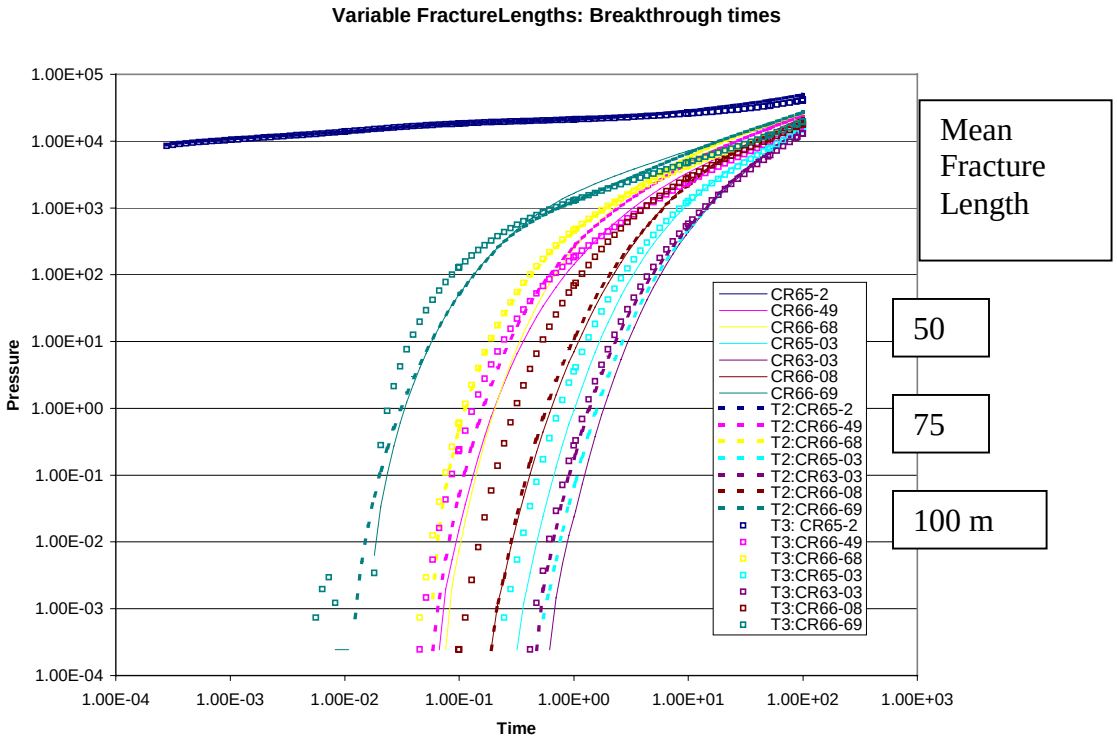

Figure 3-34. Relative breakthrough curves as a function of fracture length.

Shoshone 66-68 occur within minutes of each other, and the closer well (Shoshone 66-68) breaks through earlier.

In Figure 3-32 the same changes are plotted but for the case in which the ratio of Set1 to Set 2 permeabilities is 0.1. The Shoshone 65-49 well now breaks through earlier, consistent with the measured breakthroughs.

3.3.4.3 Conclusions

The true relative intensity of the T and L fracture sets is not known, but the ratio of T-set is thought to range between 2 and 5 times the intensity of the L-set. The effect of changing the relative fracture intensity of the two fracture sets, while keeping the overall intensity, and fracture length consistent is shown in Figure 3-33. The input parameters for the fracture intensity for each of the two fracture sets is given in Table 3-3, with the simulations ranging from intensity ratios of 1.25: 1 to 5:1 with the T-set having the higher fracture intensity. Results are varied depending upon the location of the well relative to the injector. For example, for the Shoshone 66-69 well that is closest to the injector, as the T fracture set intensity increases, the breakthrough time decreases. For Shoshone 65-03, the opposite occurs: as the T-fracture set intensity increase, there is an increased delay in the arrival of the pressure field. For the Shoshone 66-49, and Shoshone 66-68, as the T-fracture intensity increases, the breakthrough time decreases for Shoshone 66-49, but increases for Shoshone 66-68. For a fracture intensity ratio of 3.5:1, the pressure response is seen earlier in Shoshone 66-49 than in Shoshone 66-68, which is consistent with the field observations.

A second model experiment was to maintain the fracture intensity but vary the equivalent radius of the fractures in both sets. Using a relative fracture intensity of 2:1, the fracture radius was varied from 50 m to 75 m to 100m. The resulting breakthrough curves are shown in Figure 3-34. Generally, as the fracture radius increases the time to breakthrough decrease for almost all wells. However, this is not uniformly true. Interestingly as the fracture radius increase to 75 the breakthrough times for Shoshone 66-49 and Shoshone 66-68 become almost identical. The breakthrough time for well Shoshone 65-08 is unchanged from 50 to 75m, but is substantially reduced for a fracture radius of 100 m. Shoshone 65-03, as there was no consistent correlation between increased fracture length and decreased arrival time.

Pressure transient modeling has demonstrated that the DFN models generated for the Circle Ridge field are consistent with permeability values calculated from fall-off tests. Differences in pressure breakthrough times in the producing wells can also be introduced by the discrete nature of the flow-fields within the DFN model. Calibration has suggested that individual fractures have permeability around 40 mD and a radius on the order of 50 to 75 m. Model results also suggest a 2:1 ratio of T-set to L-set fracture intensities will produce breakthrough times consistent with field observation.

Pressure breakthrough times at production wells are strongly influenced by local heterogeneity in the DFN model, for this fracture intensity. A further step will be to use simulated tracer tests to refine the calibration of the DFN model to field measurements.

3.3.5 HIGH RESOLUTION INJECTION PROFILE, SHOSHONE 65-37

A Schlumberger FMS log was obtained in the open hole at Shoshone 65-37, as described previously in Section 3.3.1.1. The open hole interval in this well contains Subthrust Block 6 Phosphoria, Subthrust Block 6 Tensleep, and Subthrust Block 6 basal Phosphoria and Tensleep.

In order to further understand which features provide the flow paths for fluid flow, a high-resolution injection profile was obtained for the well (Figure 3-35). This profile was obtained using a Baker-Atlas spinner tool. This high-resolution profile indicated that all water was exiting the wellbore in the Subthrust Block 6 Phosphoria. Approximately 16.2% of the 7250 BWIPD was exiting in the interval from 630 ft to 650 ft (192 m to 198 m), 18.3% was exiting from 680 ft to 700 ft (207 m to 213 m), 56% was exiting from 750 ft to 773 ft (229 m to 236 m), and 8.3 % from 782 ft to 799 ft (238 m to 244 m). A graphical depiction of the high-resolution profile is shown in Figure 3-35.

3.3.6 SINGLE WELL PRESSURE TRANSIENT TESTING

A 44-hour Subthrust Block 6 Phosphoria falloff test was performed at Shoshone 65-20. This test was matched using commercial software and a uniform flux fractured well model in a radial composite reservoir. Late time data indicated a constant pressure boundary. The inner zone may reflect a region of wellbore damage, or may be due to a situation where only a few fractures are directly connected to the wellbore. As the distance from the wellbore increases, these fractures become part of a more well-connected fracture network, thereby increasing the network permeability. Results from the this test are as follows:

Inner zone kh= 444 millidarcy-ft (k=17.8 md, h=25 ft)
Fracture half length = 315 feet
Skin=0.1
Inner/Outer Mobility Ratio= 0.13
Radius to high mobility zone= 321 feet
Constant Pressure Outer Boundary= 210 psi

A plot of the falloff type-curve match is presented in Figure 3-36.

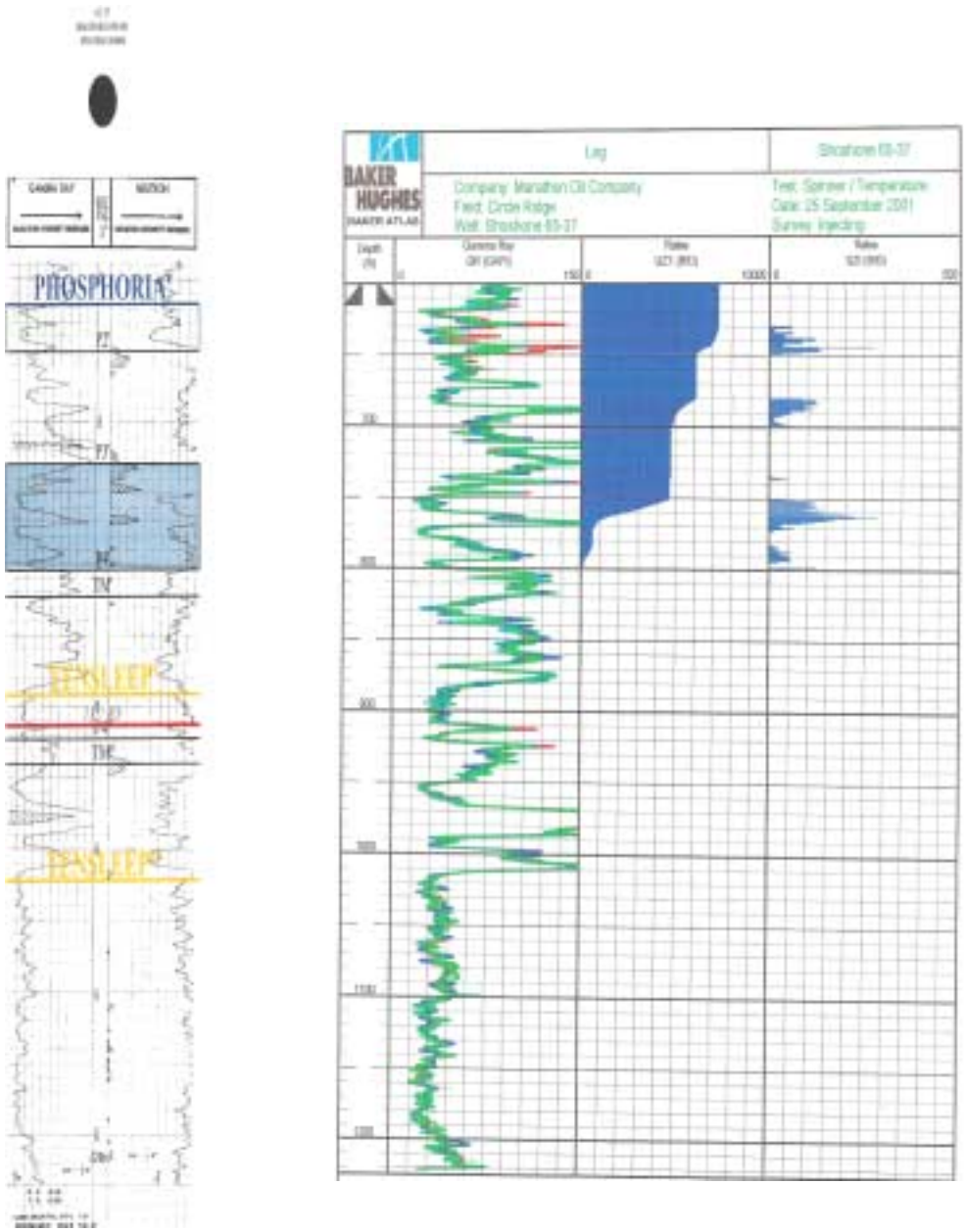

Figure 3-35. High-resolution spinner profile for Shoshone 65-37.

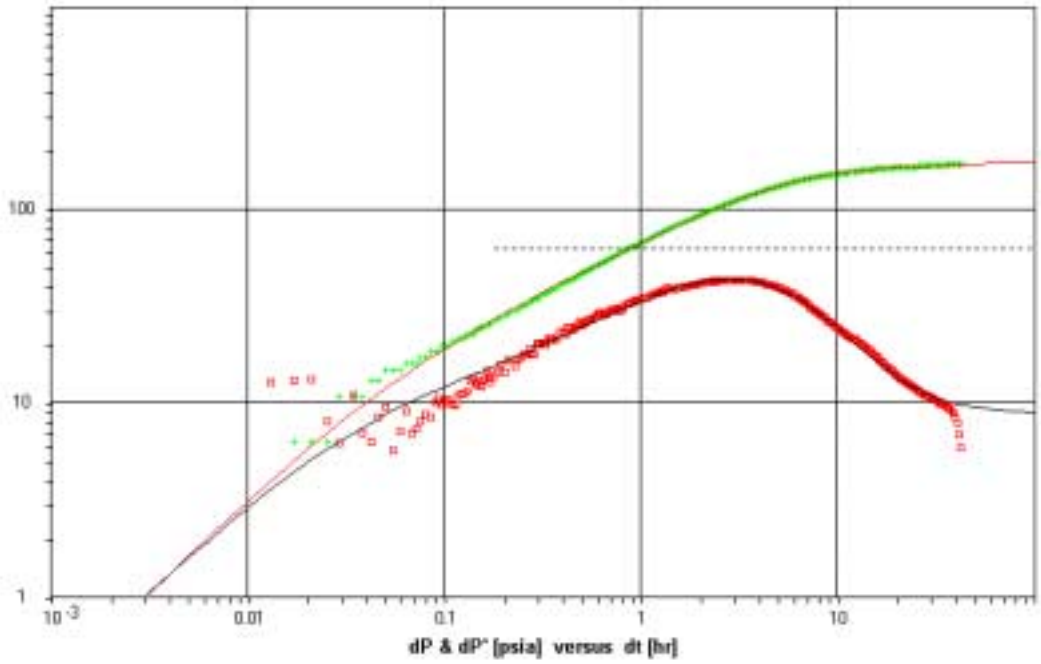

Figure 3-36. Fall-off curve for Shoshone 65-20.

3.3.7 COMPARISON OF TRACER TESTS AND FRACTURE NETWORK CONNECTIVITY

3.3.7.1 Nitrogen Injection Test

One of the uses of the data from the tracer tests is to see whether monitoring wells where tracer was detected and/or where there were strong pressure responses also correspond to fracture pathways inferred from the extensional strain patterns predicted from the palinspastic reconstruction. Figure 3-37 shows the area around the nitrogen injection well, Shoshone 65-02, and several of the monitoring wells. Approximately 17.9 MMCF of nitrogen gas was injected into the Tensleep Formation lying in the overthrust block (structural block 1). Bottom hole pressures (BHP) were monitored in seven offset wells out of a total of 66 total wells monitored for gas breakthrough. These seven wells are listed below:

Shoshone 65-03: Overthrust Tensleep
Shoshone 65-03: Overthrust Phosphoria
Shoshone 66-03: Overthrust Tensleep (Lost BHP data)
Shoshone 66-08: Overthrust Tensleep
Shoshone 66-49: Overthrust Tensleep
Shoshone 66-68: Overthrust Tensleep
Shoshone 66-69: Overthrust Tensleep

All of these wells showed pressure response, although the response was minor in the Shoshone 65-03 Phosphoria interval. In addition, there was a BHP response in Shoshone 66-68, but no gas breakthrough was observed.

The nitrogen was injected at rates ranging from 1.6 to 2.1 MMCFPD over a 9.3-day period. Surface injection pressure at Shoshone 65-02 rose to 240 psi by the end of the test. Overthrust Tensleep gas cap pressure increased from approximately 3 psi to over 140 psi, as monitored in Shoshone 66-69, an offsetting observation well.

The gas initially broke through down structure to the east at Shoshone 66-69 and 66-49. This breakthrough was along a high directional permeability trend, which had previously been determined from multi-well pressure interference testing. The down structure gas coning occurred prior to gas breakthrough at Shoshone 65-03, an observation well to the north. Shoshone 65-03's open hole completion interval included Overthrust Tensleep at approximately the same structural elevation as the nitrogen injector.

Gas breakthrough was noted at over twenty monitor wells during and following gas injection. Times for breakthrough were noted whenever possible. Gas breakthrough occurred in both the Overthrust Tensleep and Overthrust Phosphoria reservoirs. The communication between the Overthrust Tensleep and the Overthrust Phosphoria may have occurred through reservoir pathways or at individual wellbores.

A block of Overthrust Tensleep with apparently little or no effective fracturing was also highlighted by the nitrogen test. This block surrounds Shoshone 66-68. While liquid pressure response was observed at this well, no gas breakthrough occurred. Shoshone 66-68 is located up structure of other gas breakthrough wells (Shoshone 66-08 and Shoshone 66-55; not shown) and down structure of the gas injector, Shoshone 65-02.

Nitrogen breakthrough occurred in about 20 of the 60 monitored wells. Figure 3-37 shows the pattern of nitrogen breakthrough. Red filled circles indicate the locations of wells that had evidence of nitrogen breakthrough, while black filled circles indicate locations of wells with no evidence of breakthrough. Most of the wells in which breakthrough occurred can be linked together by two fairways that parallel the dominant local extensional fracture trend (black lines on figure), and lie in or connect regions of higher extensional strain. Many of the wells in which breakthrough was not noted are in regions of very low extensional strain, or lie in regions of higher strain that are separated from the injector by regions of low strain. A notable exception to this general pattern are the two wells at the south end (bottom) of the region shown, which had breakthrough, but are not obviously connected to the injector by corridors of high extensional strain.

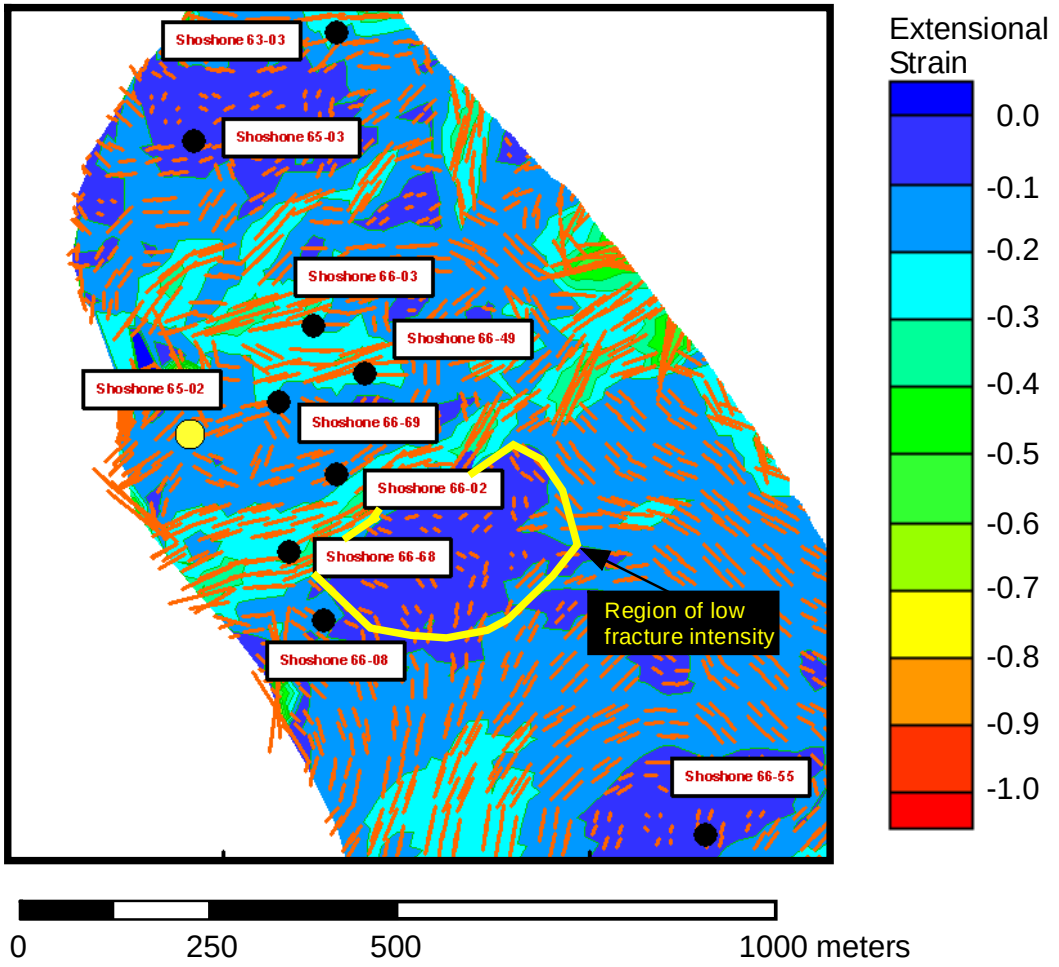

Figure 3-37. Inferred dominant conductive fracture orientations and intensity throughout the region of the nitrogen injection test. Wells with bottom hole pressure data include 65-03, 66-08, 66-49, 66-68, 66-69 and 65-02, the injector (shown as a yellow filled circle).

Overall, the pattern of nitrogen breakthrough is consistent with the dominant extensional fracture directions and intensity inferred from the strain maps calculated from the palinspastic reconstruction. These results suggest that the use of the strain pattern to control fracture orientations and intensity in the DFN model should lead to useful reservoir-scale flow predictions.

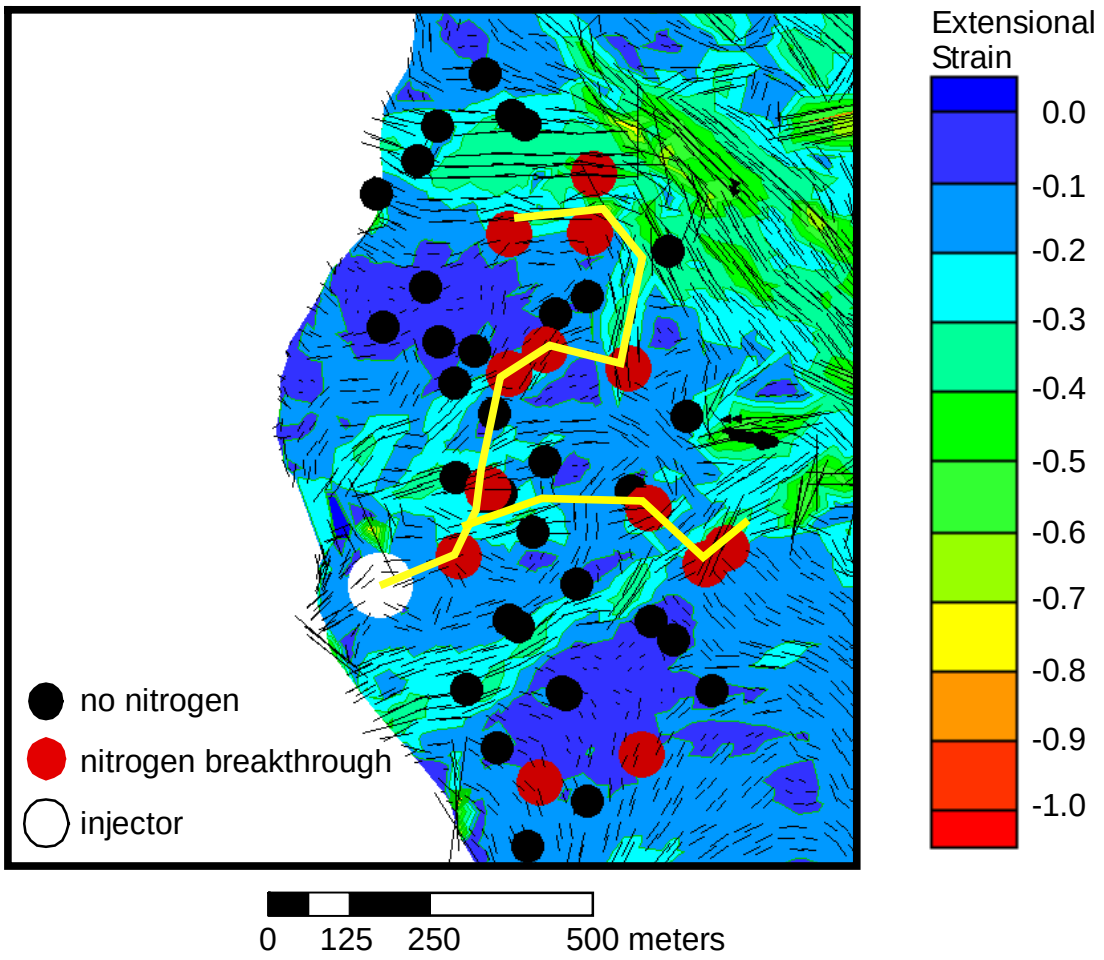

Figure 3-38. Pattern of nitrogen breakthrough during nitrogen injection test. Yellow line on figure shows possible migration pathways for nitrogen. The two pathways generally parallel the dominant fracture trend (black lines) and follow or connect regions of ghier extensional strain. The two wells at the bottom of the diagram are not easily connected by any obvious fracture pathway leading from the injector.

3.3.7.2 NaBr Tracer Test

The first offset water samples were obtained after a period of approximately 6 hours and after displacing the tracer slug with only 40 barrels of water. These samples indicated that strong breakthrough (704 ppm Br) had occurred at Shoshone 65-53. Shoshone 65-53 is 410 feet southeast of Shoshone 65-20. Falloff testing at Shoshone 65-20 has indicated fractured well behavior with a fracture half-length of approximately 300 feet (see Falloff Testing discussion below). Subsequent water sampling at Shoshone 65-53 has shown declining tracer concentrations (142 ppm Br after 6 days and tracer slug displacement of 2170 barrels). Approximately 29.6% of the original Bromine slug has been recovered at Shoshone 65-53 in the six days following injection. The rapid breakthrough and high percentage recovery indicates significant fracture communication

between the injector and Shoshone 65-53. Tracer breakthrough data for Shoshone 65-53 is presented graphically below.

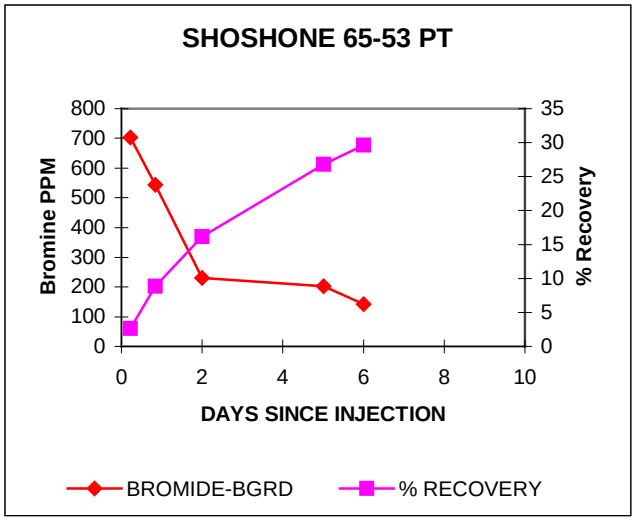

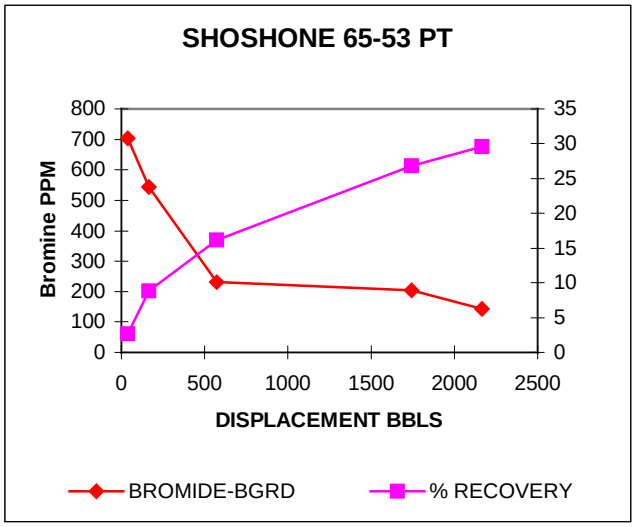

Definitive breakthrough at a second well, Shoshone 65-37, occurred five days after the tracer slug was injected. This breakthrough might have been even sooner, had this well not been shut-in due to down-hole pump problems for the first 24 hours of the test. Approximately 106 ppm of bromine was noted in this well following displacement of the tracer slug with 1740 barrels of water. Shoshone 65-37 is located 1020 feet to the south-southeast of Shoshone 65-20.

Minor tracer breakthrough (less than 5 ppm Br) may be occurring at Shoshone 65-73. This well is located 1450 feet northwest of Shoshone 65-20. Due to the extreme breakthrough at Shoshone 65-53 and subsequent recycle of low concentration tracer to other Fault Block 1 injectors, this breakthrough is not yet deemed definitive. Also, no definitive tracer breakthrough has been noted to date at any offsets not completed in the Subthrust Block 6 Phosphoria.

Attempts to match the tracer data will be performed following the completion of data gathering. Pulse testing utilizing 65-20 as a central observation well will also help define the direction of maximum permeability in the Subthrust Block 6 Phosphoria.

3.4 Task 3.2 – Fault Block and Matrix Model Development

3.4.1 INPUT DATA

The input data for the geo-cellular modeling consisted of point set files describing the surfaces of nine fault blocks for three horizons. These horizons are the Phosphoria, Tensleep and Amsden. Point set files for seven faults were also a part of the input data. The faults are the Red Gully, Green Valley, Yellow Flats, Blue Draw, Gray Wash, Purple Sage and Orange Canyon. Other data includes various log traces for over 100 wells.

Figure 3-39 shows the point sets for the Fault Block 1 of the Phosphoria (in red) and for the Red Gully fault (in blue):

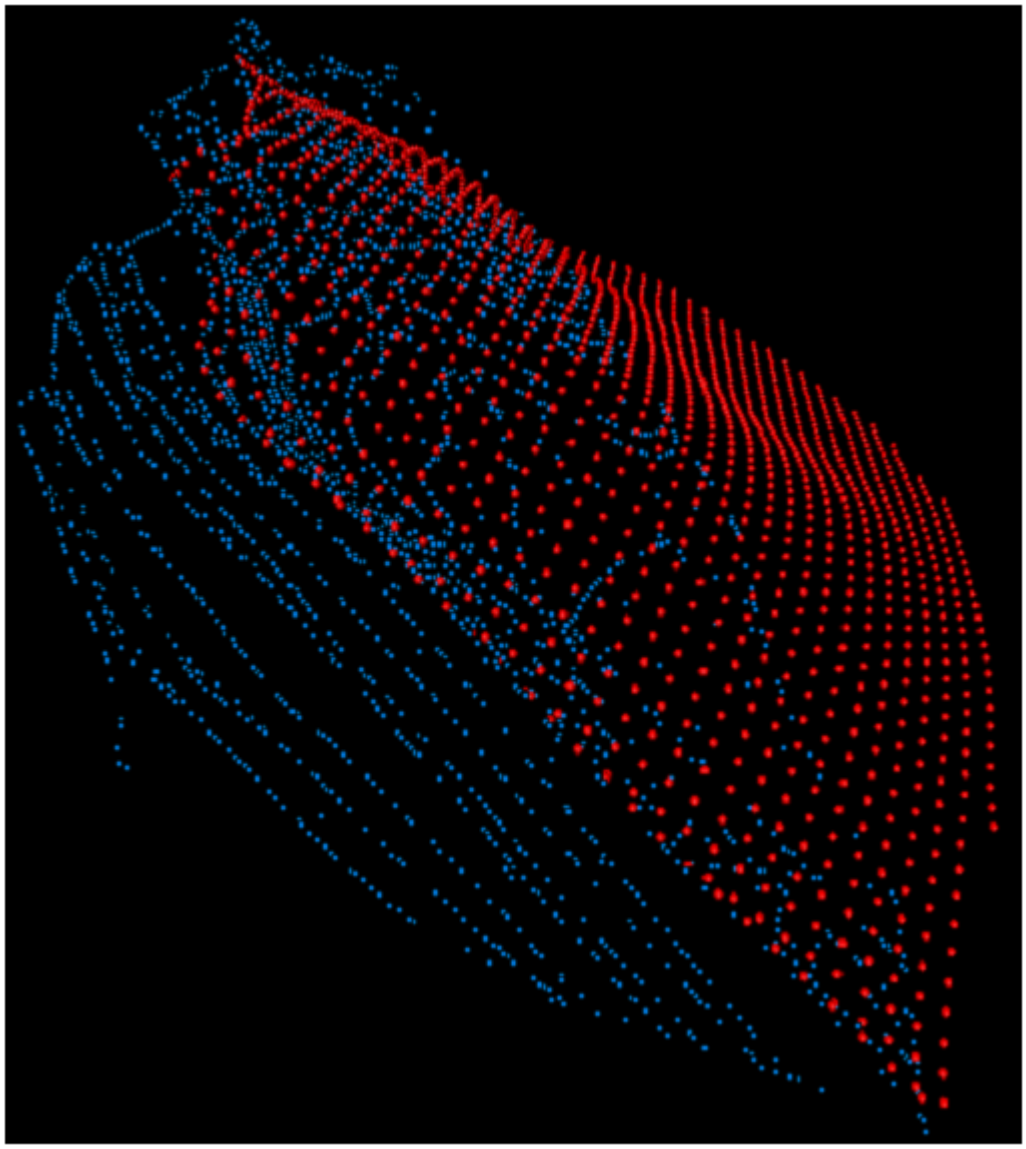

Figure 3-39. Geo-Cellular Modeling Construction

The process of creating the geo-cellular model has encompassed many steps. The first step taken was to edit the horizon and fault point sets to a format readable by the geo-cellular modeling software. Once in the software, surfaces were created from the point sets. The following two figures shows these surfaces. The first figure (Figure 3-40) shows the Phosphoria horizon surfaces for each of the fault blocks (shown with different colors). Figure 3-41 shows the fault surfaces (colors correspond to the fault names).

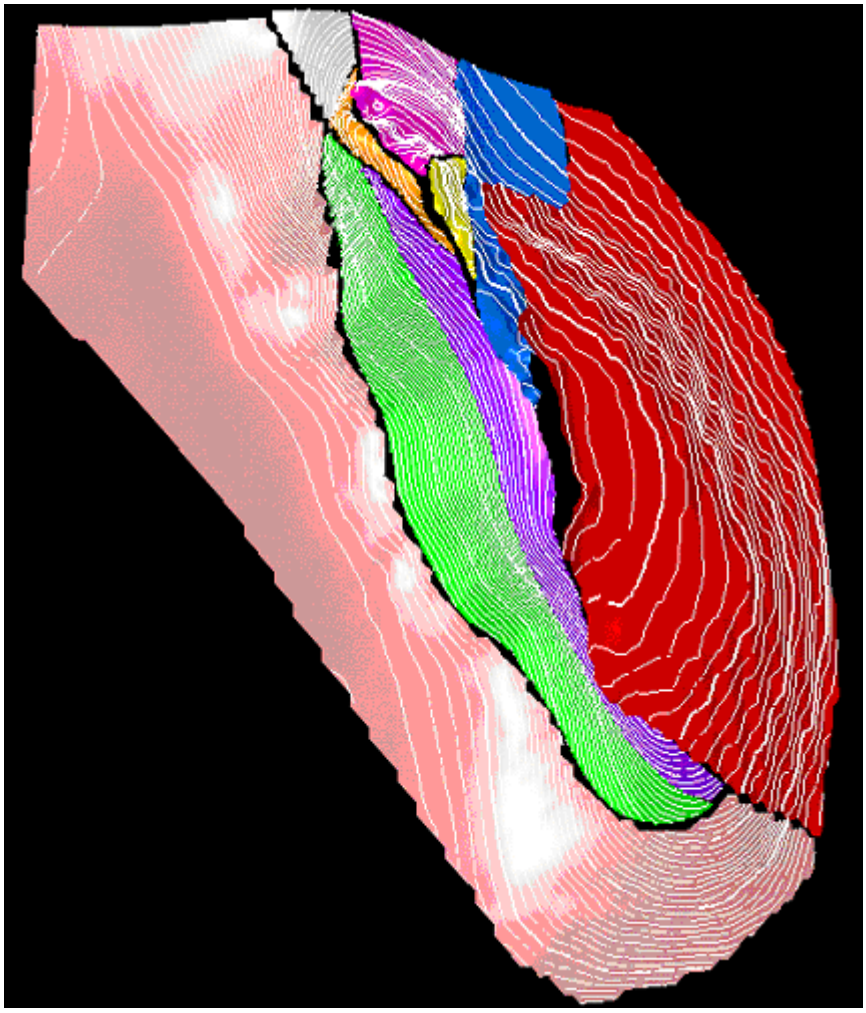

Figure 3-40. Phosphoria horizon surfaces modeling using Petrel™ software.

The faults required a different procedure after the point sets were imported. This procedure is needed to establish the connections not only with the related surfaces of the horizons, but also the interaction of the faults with each other. This interaction included the intersection and crossing of the faults. This requires establishing in the program which fault in an intersecting pair ends at the intersection with the other fault.

The above steps have been taken. Future steps will include the creation of the geo-cellular 3-D modeling grid, the import of the well data, the distribution of the well data into the 3-D modeling grid and the incorporation of the fracture distribution.

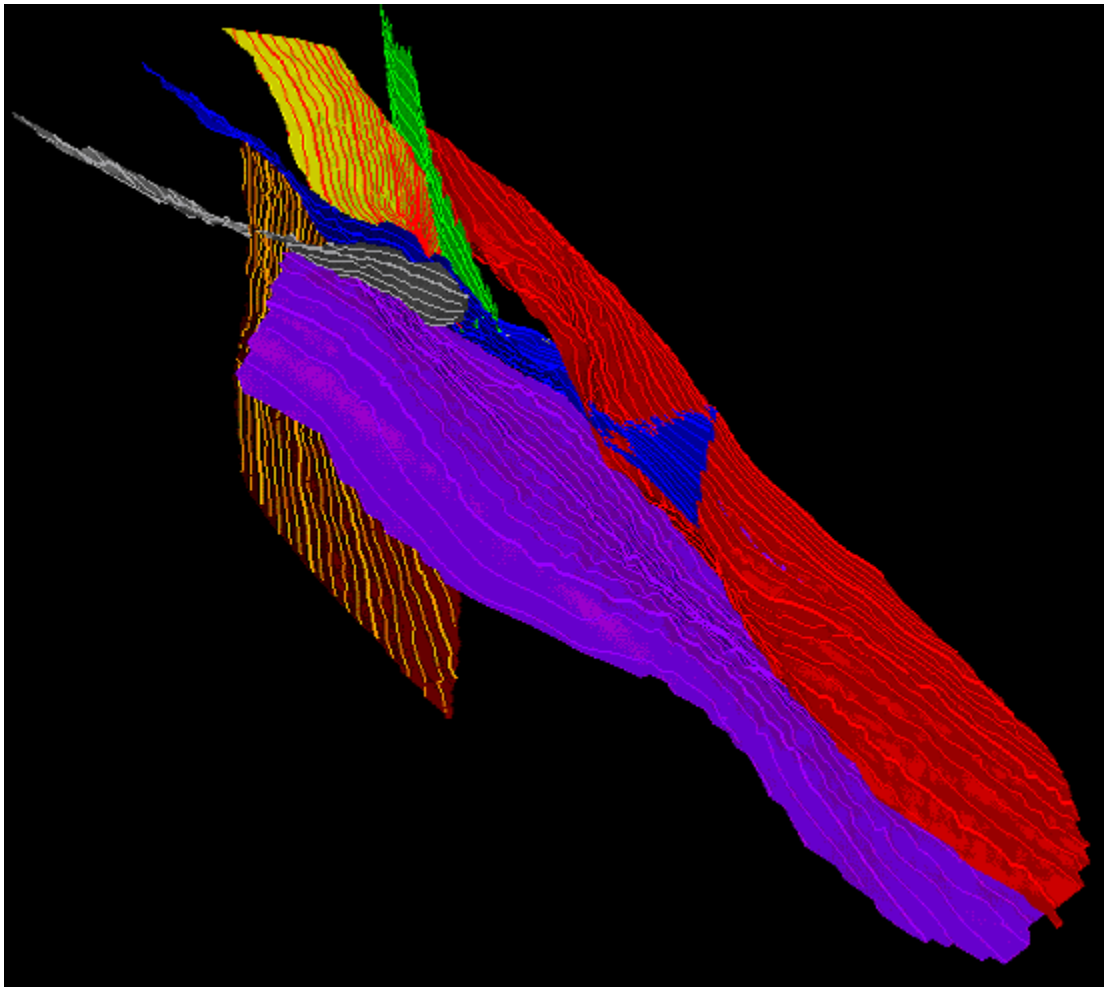

Figure 3-41. Representation of fault surfaces.

3.5 Task 5.1 – Project Web Site

3.5.1 WEB SITE DEVELOPMENT

During the third six-month project period, additional data was added to the website, and new first-level options were added. The new first-level options are shown in *blue* italic type in Table 3-4.

Background	General information about the Circle Ridge project
History	Brief description of the history of the Circle Ridge Oil Field
Data	Project Data Warehouse
Workflow	*This section describes the process followed to carry out a particular task, the data used, the results, and how it is used to further project goals*
Results	*This section presents the results from a major project activity, including explanatory material, plots, data tables and maps.*
Documents	Progress Reports and Papers related to the Circle Ridge project
Presentations	Presentations given during the Circle Ridge project
Feedback	Form to provide feedback to the project team
Links	Links to related sites on the World Wide Web

Table 3-4. First-level organization of project web site content.

The new Workflow option (Figure 3-42) shows the two topics that are currently implemented in the project website. These are: Scanline Sampling and Well Log Analysis. The text and figures for each of these options provide a description and examples of the process to carry out these tasks. For example, the scanline sampling item describes why the scanline sampling was done, how it was done, the data required, the results produced, and how it is used to meet project goals. The technology transfer goal that this option strives to accomplish is to provide a description of the workflow for key project activities, rather than to emphasize the results themselves.

The other new first-level option is Results (Figure 3-43). Results currently implemented include the petrophysical analyses, the scanline analyses and the 3D palinspastic reconstruction. The purpose of this new option is provide a cogent summary of the results obtained in key project areas.

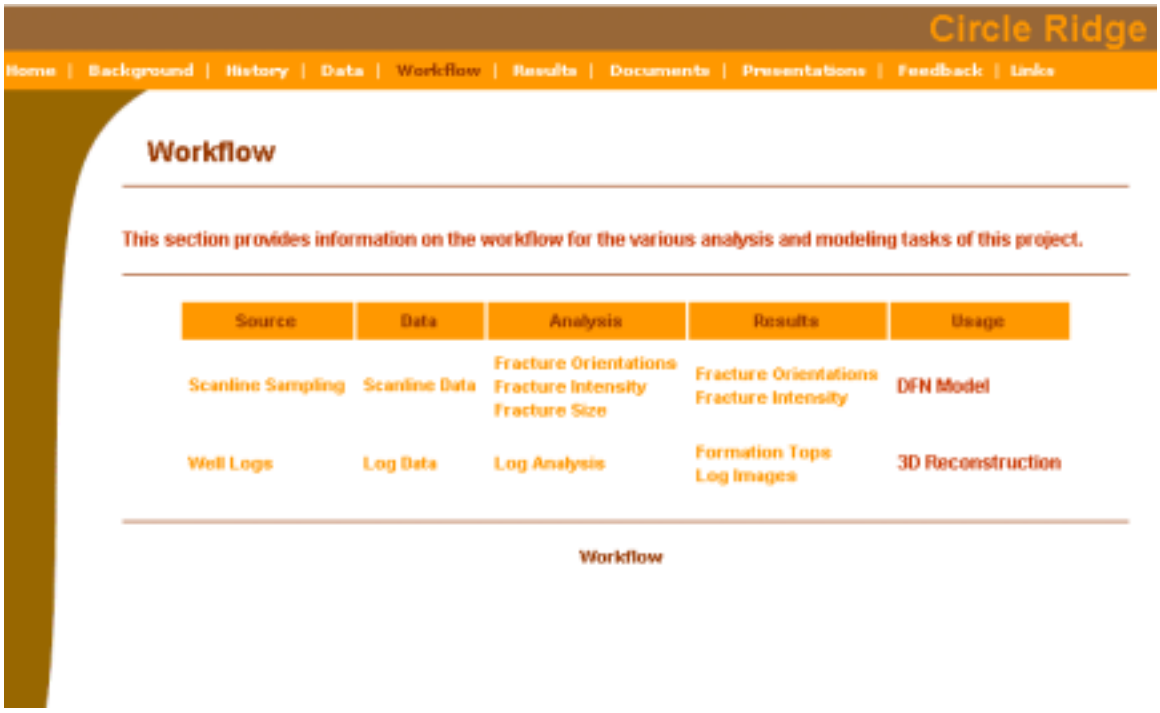

Figure 3-42. Example of new first level option, WORKFLOW, added to project website.

Figure 3-43. Example of new first level option, RESULTS, added to project website.

Figure 3-44 shows the type of information that is available for the 3D Palinspastic Reconstruction option.

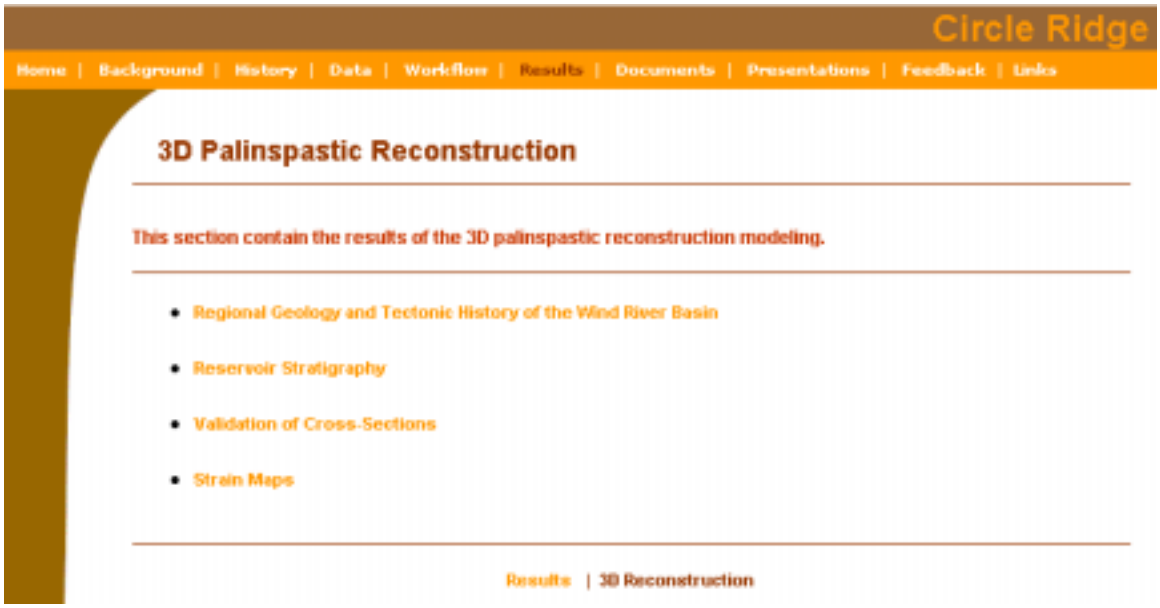

Figure 3-44. Example of results available for the palinspastic reconstruction.

Table 3-5 lists the additions to the data made accessible to the public during the project's second six-month period.

Website Category	Item Description(s)
Background	no new updates
History	no new updates
Data	image log data and spinner data from well Shoshone 65-37; five structural cross-sections; nitrogen test; NaBr tracer test
Documents	2nd Progress Report, November 1, 2000 – April 30, 2001. 3rd Progress Report, May 1, 2001 – October 31, 2001.
Presentations	no new updates

Table 3-5. Updates to website content during period Nov. 1, 2000 to April 31, 2001.

3.5.2 WEB SITE STATISTICS

From May 1, 2001 to October 31, 2001, there have been 533 hits on the project website. This translates into between two and three external visits a day. Figure 3-45 provides an overview of website activity, spanning the period August 17, 2000 through December 4, 2001 in order to provide context for the 3rd semi-annual project period. This figure shows

that the level of website activity has remained nearly constant since late November, 2000, the time when the first project report was released. There also appears to have been a slight increase in activity immediately following the release of the 2nd semiannual report in June, 2001.

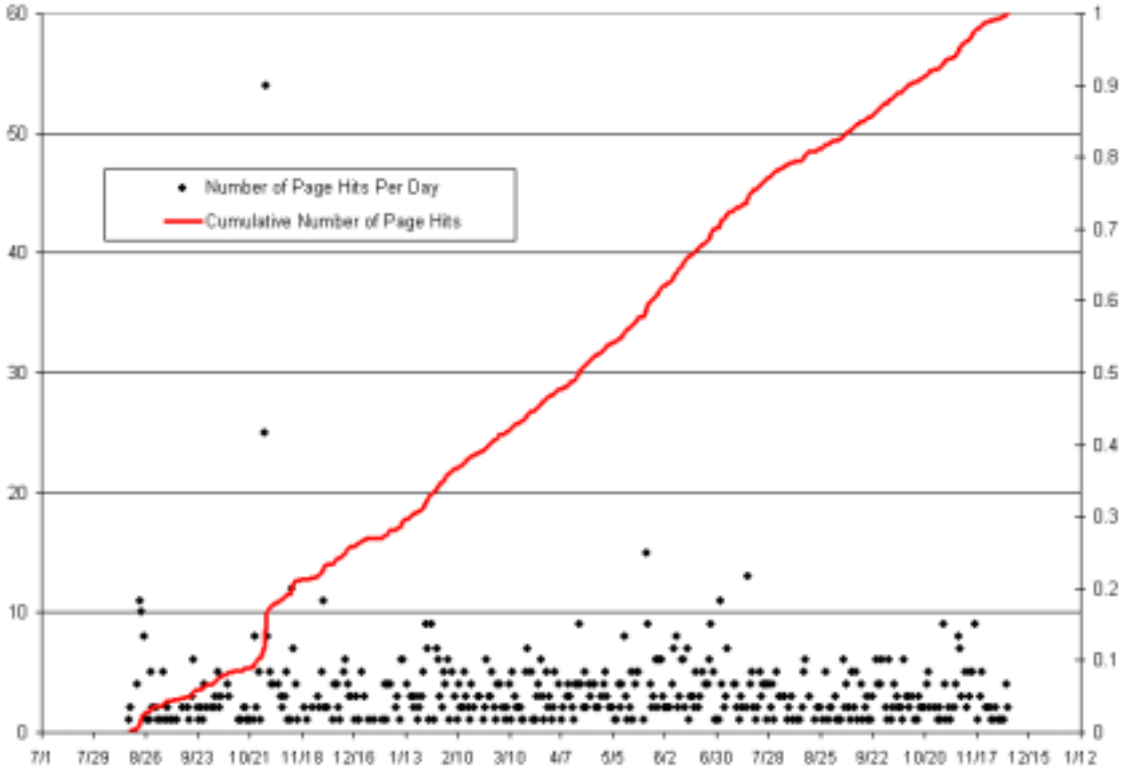

Figure 3-45. Web site activity, August 17, 2000 through December 4, 2001

3.6 Marathons Contribution to this project to Date

A summary of Marathon's in-kind contributions to date and associated costs are as follows:

ITEM	DESCRIPTION	COST
Fracture Image Logs	2 (Shoshone 66-7 and Shoshone 65-37)	$23,600
Dynamic Flow Logs	2 (Shoshone 66-7 and Shoshone 65-37)	$14,000
Interwell Pressure Interference Test	1 (Overthrust Phosphoria and Tensleep)	$122,500
Injected Tracer Studies	2 (65-2 N2, 65-20 NaBr)	$122,500
Single Well Falloff Tests	2 (Shoshone 66-2 and Shoshone 65-20)	$10,000
FMI Processing	6 man-days	$7,500

Construct 3-D Structure Model	15 man days	$18,500
Usage of MOC 3-DMove software	7 man-days	$5,000
Tech transfer, meetings reports	3 man days	$3,800
Total (to date)		**$327,400**

This amount already considerably exceeds the $205,000 originally committed to this project by Marathon Oil Company.

4 CONCLUSIONS

4.1 Overview

This section summarizes the most important results obtained in the project during the six-month reporting period, and discusses what implications they have both for their influence on future project activities, and more importantly, on the goal of recovering additional oil from the Circle Ridge Field. The two key areas where significant technical results have been obtained concern the palinspastic reconstruction and the scanline fracture data analysis.

4.2 Structural Controls on Reservoir Fracture Pattern

The palinspastic reconstruction made it possible to calculate strains in the reservoir formations after several folding and faulting events. Comparison of the strain pattern to orientations and intensity of fracturing in outcrop indicates that the initial folding event probably produced an extensional joint set perpendicular to the vector of maximum extension. An additional set, orthogonal to this dominant joint set and parallel to the strain vector, also is seen in outcrop and may represent a cross-set formed at the same time.

4.3 Validation of DFN Model

The fractures inferred from the strain pattern were compared to image log data from two wells. The orientation of large fractures in the image logs was approximately orthogonal to the vector of maximum extension.

The relative intensity of extensional strain predicted at the two well locations was substantially different; Shoshone 65-37 showed a much higher strain than Shoshone 66-07. This corresponded to the much reduced number of fractures in Shoshone 66-07 relative to Shoshone 65-37.

Thus, comparison of the fracture pattern predicted from the extensional strain due to the initial folding event corresponded well with measured fracture orientations and intensity variations in the subsurface. This implies that the extensional strain caculating for the folding event is a useful predictor of fracture orientations and intensity in the reservoir units.

The fracture network connectivity inferred from the strain pattern was compared to the breakthrough pattern measured from the nitrogen injection test. Most wells in which nitrogen breakthrough was detected lie in fairways defined by fracture trends and regions of higher fracture intensity. Wells in which breakthrough was not detected generally were in areas of low fracture intensity or in areas of high intensity separated from the injector by regions of low intensity.

Thus, the nitrogen injection experiment further suggests that the DFN model based on extensional folding strain should be a useful predictor of subsurface reservoir-scale fracture connectivity and flow.

4.4 Determination of Properties for DFN Model

Pressure transient modeling has demonstrated that the DFN models generated for the Circle Ridge field are consistent with permeability values calculated from fall-off tests. Differences in pressure breakthrough times in the producing wells can also be introduced by the discrete nature of the flow-fields within the DFN model. Calibration has suggested that individual fractures have a permeability around 40 mD and a radius on the order of 50 to 75 m. Model results also suggest a 2:1 ratio of T-set to L-set fracture intensities will produce breakthrough times consistent with field observation.

Pressure breakthrough times at production wells are strongly influenced by local heterogeneity in the DFN model, for this fracture intensity. A further step will be to use simulated tracer tests to refine the calibration of the DFN model to field measurements

4.5 Construction of Integrated Matrix/Fault-Block/Fracture Model

Although the original software package selected for creation of the combined matrix/fault block/reservoir scale fracture model has proven difficult to use due to the nature of the faulting in the Circle Ridge Field, other software was identified and evaluated, and appears to meet the needs of the project.

REFERENCES

Horne, R. N., 2000. Modern Well Test Analysis (4th Printing). Petroway, Inc., Palo Alto, CA. 257p.

Jamison, W. R., 1997. Quantitative evaluation of fractures on Monkshood anticline, a detachment fold in the foothills of western Canada.. Bulletin of the American Association of Petroleum Geologists, vol. 81, no. 7, p. 1110-1132.

La Pointe, P. R. and J. A. Hudson (1985). Characterization and Interpretation of Rock Mass Joint Patterns. Geological Society of America, Special Paper 199, 37p.

La Pointe, P. R., P. C. Wallmann and W. S. Dershowitz, 1993. Stochastic estimation of fracture size through simulated sampling. International Journal of Rock Mechanics, Mining Sciences & Geomechanics Abstracts, vol. 30, no. 7, 1611-1617.

La Pointe, P. R., J. Hermanson and T. Eiben (2000). 3-D reservoir and stochastic fracture network modeling for enhanced oil recovery, Circle r\Ridge Phosphoria/Tensleep reservoir, Wind River Reservation, Arapaho and Shoshone tribes, Wyoming. Semi-Annual Technical Report – May 1, 2000 through October 31, 2000. DOE Award Number: DE-FG26-00BC15190

La Pointe, P. R., and J. Hermanson (2001). 3-D reservoir and stochastic fracture network modeling for enhanced oil recovery, Circle r\Ridge Phosphoria/Tensleep reservoir, Wind River Reservation, Arapaho and Shoshone tribes, Wyoming. Semi-Annual Technical Report – November 1, 2000 through April 31, 2001. DOE Award Number: DE-FG26-00BC15190

Smith, V. (2000). Surface Geologic Map of the Circle Ridge Oil Field, Wyoming. B. S. Thesis, Baylor University, Waco, TX.